ISSN: 1545-0740

Nature and Science

Volume 2, Number1, 2004

Nature and Science

The **Nature and Science** is an international journal to enhance our natural and scientific knowledge spreading in the world under the free publication principle. Any valuable paper to describe natural phenomena/existence or report scientific researches/pursuits will be acceptable, including both natural and social sciences. Papers submitted could be reviews, objective descriptions, research reports, opinions/debates, news, letters, and all other information nature and science related. The journal is calling for papers and looking for more co-operators and editors.

Introductions to Authors

1. General Information

(1) Goals: As an international journal published in print and on the web, the Nature and Science is dedicating to the dissemination of fundamental knowledge in all areas of nature and science. The main purpose of the Nature and Science is to enhance our knowledge spreading in the world under the free opinion publishing principle. It publishes full-length papers (original contributions), reviews, rapid communications, and especially it publishes any debate and opinion in all the fields of nature and science.

(2) What to Do: The Nature and Science provides a place for discussion of the scientific news, research, theory, philosophy, profession and technology - that drive scientific progress. Research reports and regular manuscripts that contain new and significant information of general interest are welcome.

(3) Who: All people are welcome to submit manuscripts in any fields of nature and science.

(4) Publication Costs: US$20 per printed page of an article to defray costs of the publication will be paid by the authors when the submission or after the acceptance. Extra expense for color reproduction of figures will by paid by authors (estimate of cost will be provided by the publisher for the author's approval).

(5) Journal Copies to Authors: One hard copy of the journal will be provided free of charge for each author, and 20 offprints (reprints) of each article will be provided free of charge for the article's correspondence author (or the first author).

(6) Additional Copies Bought by Authors: Additional hard copies and offprints could be purchased with the price of US$4/issue and US$0.2/page-offprint (mailing and handling cost included). The offprints must be ordered prior to printing of the journal.

(7) Distributions: Web version of the journal is freely opened to the world without any payment or registration. The journal will be distributed to the selected libraries and institutions for free. US$5/issue is for the subscription of other readers.

(8) Advertisements: The price will be calculated as US$400/page, i.e. US$200/a half page, US$100/a quarter page, etc. Any size of the advertisement will be accepted.

2. Manuscripts Submission

(1) Submission Methods: Electronic submission through email is encouraged and hard copies plus an IBM formatted computer diskette would be also accepted.

(2) Software: The Microsoft Word file will be preferred.

(3) Font: Normal, Times New Roman, 10 pt, single space.

(4) Indent: Type 2 space in the beginning of each new paragraph.

(5) Manuscript: Don't use "Footnote" or "Header and Footer".

(6) Cover Page: Put detail information of authors and a short title in the cover page.

(7) Title: Use Title Case in the title and subtitles, e.g. "**Debt and Agency Costs".**

(8) Figure and Table: Use full word of figure and table, e.g. **"Figure 1.** Annul Income of Different Groups**", Table 1. Annual Increase of Investment".**

(9) References: Cite references by "last name, year", e.g. "(Smith, 2003)". References should include all the authors' last names and initials, title, journal, year, volume, issue, and pages etc.

Reference Examples:

Journal Article: Hacker J, Hentschel U, Dobrindt U. Prokaryotic chromosomes and disease. Science 2003;301(34):790-3.

Book: Berkowitz BA, Katzung BG. Basic and clinical evaluation of new drugs. In: Katzung BG, ed. Basic and clinical pharmacology. Appleton & Lance Publisher. Norwalk, Connecticut, USA. 1995:60-9.

(10) Submission Address: editor@sciencepub.net, Marsland Company, P.O. Box 753, East Lansing, Michigan 48826, The United States, 517-862-6881.

(11) Reviewers: Authors are encouraged to suggest 2-5 competent reviewers with their email and mailing addresses.

2. Manuscript Preparation

Each manuscript is suggested to include the following components but authors can do their ways:

(1) Title page: including the complete article title; each author's full name that family name appears with uppercase; institution(s) with which each author is affiliated, with city, state/province, and zip code; and the name, complete mailing address, telephone number, facsimile number (if available), and e-mail address for all correspondence.

(2) Abstract: including Background, Materials and Methods, Results, and Discussions.

(3) Key Words.

(4) Introduction.

(5) Materials and Methods.

(6) Results.

(7) Discussions.

(8) References.

(9) Acknowledgments.

Journal Address:

Marsland Company
P.O. Box 753
East Lansing, Michigan 48826
The United States
Telephone:(517)862-6881
E-mail: editor@sciencepub.net
Homepage: http://www.sciencepub.net

Nature and Science

(Quarterly, Started in 2003)

Vol. 2 No.1 (Cumulated No.2) March 2004

CONTENTS

1 **Assessment of the Biological Effects of a Natural Extract of *Equinacea Purpurea* : An *In Vitro* Analysis**
M. L. Gomes, G. F. Diré, E. A. C. Lima, et al.

6 **An *In Vivo* Evaluation of an Aqueous Extract of *Uncaria Tomentosa* on the Morphology on the Labeling of Blood Constituents with ^{99m} Technetium**
Gláucio F. Diré, Hayden P. Honeycutt, Maria L. Gomes, et al.

11 **Nanofiltration for Mixed Ion Systems with Commercial and Pore-Filled Membranes**
Wayne W. Jiang, Jesus Garcia-Aleman, James. M. Dickson, et al.

17 **Theoretical Analysis of Potential Runoff Energy from a Grid DEM**
Chuan Liang, Zhongbo Yu

24 **Ideal Interval Method Based Model for Water Quality Evaluation**
Juliang Jin, Shujuan Wang, Yiming Wei

29 **Technique of Animal Clone**
Hongbao Ma

36 **Self-Exciting Threshold Auto-Regressive Model (SETAR) to Forecast the Well Irrigation Rice Water Requirement**
Qiang Fu, Hong Fu, Yankun Sun

44 **Fuzzy Analysis on Water Resources of Heilongjiang State Farms**
Yongsheng Ma

48 **Application of a New Hybrid Model to Predicting Daily Runoff in a Week**
Beilei Qin, Wensheng Wang, Jing Ding, et al.

53 **A Novel H_∞ Output Feedback Controller Design for LPV Systems with a State-delay**
Junling Wang, Changhong Wang, Wei Yuan

61 **Study on the Mathematic Model of Product Modular System Orienting the Modular Design**
Shisheng Zhong, Jiang Li, Jin Liu, et al.

68 **L-THIA: A Useful Hydrologic Impact Assessment Model**
Yongsheng Ma

74 **Chaotic Analysis on Precipitation Time Series of Sichuan Middle Part in Upper Region of Yangtze**
Baohui Men, Chuan Liang, Xiejing Zhao

79 **Using RAGA for multi-objective planning of soil and water conservation in a small watershed**
Yankun Sun, Qiang Fu

85 **Characterization of a New Species of Taxol-producing Fungus**
Jingping Ge, Wenxiang Ping, Dongpo Zhou

89 **Optimization of Water Allocation in Canal Systems of Chengai Irrigation Area**
Zhiliang Wang, Zhenmin Zhou

Assessment of the Biological Effects of a Natural Extract of *Equinacea Purpurea*: An *In Vitro* Analysis

M. L. Gomes[1], G. F. Diré[1], E. A. C. Lima[1], S. Moreno[1], R. L. Jales[2], M.T. J. A. Catanho[3], M. Bernardo-Filho[1].

(1. Universidade do Estado do Rio de Janeiro, Instituto de Biologia Roberto Alcantara Gomes, Departamento de Biofísica e Biometria. Av. 28 de setembro, 87, Rio de Janeiro, RJ, Brasil 20551-030 (gdire@hotmail.com). Instituto Nacional do Câncer, Coordenadoria de Pesquisa, Praça Cruz Vermelha, 23, Rio de Janeiro, RJ, Brasil, 20230-130;
2. Universidade Federal do Rio Grande do nOrte, Faculdade de Farmácia, Natal, Rio Grande do Norte, Brazil;
3. Universidade Federal de Pernambuco, Departamento de Biofísica, Recife, PE, Brazil)

Abstract: Medicinal plants have been widely used by human beings. However, sometimes the biological effects of these plants are not fully known. It is concerned that many natural medicines may contain potentially toxic ingredients and contaminants such as heavy metals. Red blood cells (RBC) and plasma proteins labeled with technetium-99m (99mTc) have several clinical applications and it has been reported that some natural products are capable of reducing the efficiency of this radiolabeling. *Equinacea purpurea* is a plant with medicinal properties. It is indicated to treatment of the inflammation in the respiratory system and in the skin. The aim of this work was to assess the effects of *Echinacea purpurea* on the labeling of blood elements with 99mTc. A freshly extract of *E. purpurea* (300 mg/10 mL) was administered to the aliquots of blood withdraw from *Wistar* rats during 1 hour. After that, samples (0.5 mL) of blood were incubated with stannous chloride ($SnCl_2$) and 99mTc. The blood was centrifuged and plasma (P) and RBC were isolated. P and RBC were also precipitated with trichloroacetic acid and soluble (S) and insoluble (I) fraction (F) were determined. The results have shown that the referred extract was able to reduce the radiolabeling in BC to the concentrations of: 25% (from 93.09%±3.63 to 55.17%±7.85), 12.5% (from 93.09%±3.63 to 43.22%±3.92) and to the 6,25% (from 93.09%±3.63 to 35.15%±2.36). In the light of the results the referred extract has reduced the efficiency of.radiolabeling in the blood cells. We suggest that the extract may induce the generation of reactive oxygen species with oxidant properties with direct action on the labeling process. [Nature and Science, 2004,2(1):1-5].

Key words*:* *Echinacea purpurea*, red blood cells, plasma proteins, technetium-99m

1 Introduction

Natural products are widely used as food or food additives, or as a substance in medicinal treatment for humans. Medicinal plants are widely used worldwide for the treatment of many diseases. Aqueous extracts of many plants are widely used in therapy as complementary medicines (Oliveira, 2003). Traditional Chinese herbal medicines (TCHM) are increasingly used throughout the Earth, as they are considered to be effective and to have few side-effects. Contaminants of TCHM include heavy metals and undeclared drugs. Biological effects of metals have been reported as the effect of the transition metals, which catalyze free radical production that can be related to aging processes and neurodegenerative diseases such as Alzheimer's disease, Parkinson's disease, and others (Silva, 2002). The toxicity of these contaminants and additives, and the toxic effects of the herbal ingredients have important implications during the preoperative period. The anesthetist must consider the potential for drug interactions and systemic adverse effects of these natural products (Kam, 2002). Technetium-99m (99mTc) has been the most utilized radionuclide in nuclear medicine procedures and it has also been used in basic research. Many drugs and vegetable extracts have been reported to affect the biodistribution of different radiopharmaceuticals (Early, 1995; Braga, 2000). Natural and synthetic drugs can alter the labeling of red blood cells with technetium-99m (99mTc) (Braga, 2000; Oliveira, 2003). When a radionuclide has its capability to bind to blood elements altered by natural and therapy drugs, the process of labeled red blood cells may be repeated, resulting in an additional

radiation dose to the patient (Hesslewood, 1994; Sampson, 1996).

Preparations from *Echinacea purpurea* are among the most widely used herbal medicines. Most uses of *E. purpurea* are based on the reported immunological properties. A series of experiments have demonstrated that *E. purpurea* extracts do indeed demonstrate significant immunomodulatory activities. Among the many pharmacological properties reported, macrophage activation has been demonstrated most convincingly. Phagocytotic indices and macrophage-derived cytokine concentrations have been shown to be Echinacea-responsive in a variety of assays. Activation of polymorphonuclear leukocytes and natural killer cells has also been reasonably demonstrated. Changes in the numbers and activities of T- and B-cell leukocytes have been reported, but are less certain. Despite this cellular evidence of immunostimulation, pathways leading to enhanced resistance to infectious disease have not been described adequately. Several dozen human experiments including a number of blind randomized trials have reported health benefits. The most robust data come from trials testing *E. purpurea* extracts in the treatment for acute upper respiratory infection. Although suggestive of modest benefit, these trials are limited both in size and in methodological quality. Hence, while there is a great deal of moderately good-quality scientific data regarding *E. purpurea,* effectiveness in treating illness or in enhancing human health has not yet been proven beyond a reasonable doubt (Barret, 2003).

There are many applications of 99mTc-labeled red blood cells (99mTc-RBC), in cardiovascular nuclear medicine, in the detection of gastrointestinal bleeding, and in the determination of the RBC mass in patients. RBC have been labeled with 99mTc for *in vitro, in vivo* or *in vivo*/*in vitro* techniques (Srivastva, 1990; Bernardo-Filho, 1994; Early, 1995). Nevertheless, there is not a well established *in vitro* model to study the interaction of therapeutic drugs with radiopharmaceuticals. Then, we have evaluated the influence of a *E. purpurea* extract on the labeling of RBC and plasma proteins with 99mTc using *in vivo* and *in vitro* studies and the effect of this extract on the labeling of blood elements with 99mTc.

2 Material and Methods

To prepare the extract it was used 360 mg of *E. purpurea* dilute in 10 mL of saline solution 0.9%. It was used the natural product from Herbarium botanical laboratory (Brazil, Rio de Janeiro, Lot10932-01/01). The solution of the referred extract was centrifuged during 5 min (1,500 rpm) and after that the aqueous phase was separated and dilutions of 50% were performed to obtain five concentrations (100%; 50%; 25%; 12.5% and 6.25), which were used in this experimental.

Samples of 0.5 mL of blood from *Wistar* rats were incubated with 0.1 mL of the referred extract, after that these samples were incubated with 0.5 mL of stannous chloride (1.2 μg/mL), as $SnCl_2.2H_2O$ for 1 hour at room temperature. After this period of time, 99mTc (0.1 mL), as sodium pertechnetate, was added and the incubation continued for another 10 min. These samples were centrifuged and plasma (P) and blood cells (BC) were separated. Samples (20 μl) of P and BC were precipitated with 1 mL of trichloroacetic acid (TCA) 5% and soluble fraction (SF) and insoluble fractions (IF) were separated. The radioactivity in P, BC, IF-P, SF-P, IF-BC and SF-BC were determined in a well counter. After that, the % of radioactivity (%ATI) was calculated, as previously reported (Bernardo-Filho, 1994). A statistical analysis (Mann Whitneyt test, n=5) was utilized to compare the experimental data.

3 Results

Table 1 has shown the fixation of the radioactivity on blood elements isolated from samples of whole blood treated with *E. purpurea* extract. The analysis of the results indicates that there is a decrease ($P<0.05$) on the labeling of red blood cells. Samples of heparinized blood from Wistar Rats were incubated during 1 hour with the extract of *E. purpurea*, after that these samples were incubated for 1 hour with stannous chloride (1.2 μg/mL) and 99mTc, as sodium pertechnetate were added. These samples were centrifuged and plasma (P) and blood cells (BC) were separated. Samples (20 μl) of BC were precipitated with trichloroacetic acid (TCA) 5% and soluble (SF) and insoluble fractions (IF) were separated. The radioactivity in P, BC, SF-BC , IF-BC, SF-P and IF-P was determined in a well counter and the % of radioactivity (% ATI) was calculated. A statistical analysis (Tukey-Kramer Multiple Comparisons Test,

n=5) was used to compare the results. The values are averages ± SDs.

Table 1 Effect of *E. purpurea* on the labeling of red blood cells (BC), insoluble fraction of the red blood cells (IF-C) and in the insoluble fraction of the plasma (IF-P) with 99mTc.

Echinacea purpurea	BC	IF-C	IF-P
Control	93.09 ± 3.63	75.88 ± 1.81	69.33 ± 7.46
100%	91.81 ± 2.46	78.80 ± 2.42	71.63 ± 5.89
50 %	85.94 ± 7.51	77.73 ± 2.85	73.03 ± 4.48
25%	55.17 ± 7.85	77.15 ± 8.56	74.09 ± 4.03
12.5%	43.23 ± 3.92	61.97 ± 2.17	77.36 ± 2.85
6.25%	35.15 ± 2.36	74. 76 ± 1.59	72.58 ± 5.74

4 Discussion

Extracts of medicinal can also alter the labeling of blood elements with 99mTc. We agree with Hesslewood & Leung (1994), that many reports on drug interactions with radiopharmaceuticals are anecdotal and in some instances a direct cause and effect relationship has not been unequivocally established. This fact could be diminished with the development of *in vitro* tests to evaluate the drug/radiopharmaceuticals interactions and the consequence for the bioavailability of the radiopharmaceuticals and the labeling of blood constituents.

There are concerns that some natural medicines may contain potentially toxic ingredients and contaminants such heavy metals (Kam, 2002). Some substances may alter the labeling of blood constituents with 99mTc (Oliveira, 2003). In this study it was verified that in the samples of *Echinacea purpurea* extract on the radiolabeling of blood elements. Diré *et al*.(2001) have related that chayotte extract is capable of altering the biodistribution of sodium pertechnetate. Lima *et al*.(2001) described that an extract of cauliflower (*Brassica oleracea*) was not capable of altering the biodistribution of the referred radiopharmaceutical. Some authors have related that natural extracts may alter the labeling of blood elements with 99mTc (Braga, 2000). In the labeling process of blood constituents with 99mTc is needed a reducing agent, and probably the stannous ion would be oxidized. In *in vitro* studies was verified that the extracts of *Thuya ocidentallis* (Oliveira, 1997), *Nicotiana tabacum* (Vidal, 1998), *Maytenus ilicifolia* (Oliveira, 2000), *Syzygium jambolanum* (Santos, 2002), *Stryphnodendron adstringens (Mart.) Coville* (Costa, 2002) and *Ginkgo biloba* (Moreno, 2002*),* possibly, would have oxidants compounds, and the labeling of blood elements decrease in the presence of these extracts. In a research was verified that *Paullinia cupana* extract was capable of altering the radiolabeling of blood (Oliveira, 2002). In other *in vitro* study with *Fucus vesiculosus* extract was noticed that the referred extract has induced alterations on the labeling of blood elements with 99mTc (Oliveira, 2003). In an *in vivo* studies in this study it has demonstrated that the chayotte extracts were capable of altering the radiolabeling of blood elements. Similar results were observed with an extract of *Solanun melongena* (eggplant), which was capable of altering radiolabeling (Capriles, 2002). Moreno *et al*. (2002), eyed that in a *in vitro* study the extract of *Ginkgo biloba* altered the radiolabeling of blood elements. It was reported by Santos-Filho (2002), that the extracts of *Mentha crispa L*. (mint) were capable of altering the radiolabeling process. Braga *et al*. (2000), in an *in vitro* study demonstrated that *Peumus boldus* did not alter the labeling of blood elements with 99mTc similar results were observed by Santos-Filho *et al*. (2002) with the Kava Kava (*Piper methysticum*) extract in a *in vitro* study. Lima *et al*. (2002) in an *in vivo* study have shown that an extract of cauliflower (leaf) was not capable of altering the labeling of blood elements with technetium-99m. Diré *et al*. (2002), in an *in vitro* study eyed that the chayotte extracts were not capable of altering the radiolabeling of blood constituents. In the procedure of labeling RBC with 99mTc, the stannous and pertechnetate ions pass through the plasma membrane (Gutfilen, 1992). Then, as reported to the tobacco (Vidal, 1998) *Maytenus ilicifolia* (Oliveira, 2000), *Sechium edule* (Diré, 2001), *Mentha crispa L*. (Santos-Filho, 2002), *Paullinia cupana* (Oliveira, 2002), *Gingko biloba* (Moreno, 2002) and *Fucus vesiculosus* (Oliveira,

2003) extracts, histological alterations of red blood cells could be responsible for the modifications on the labeling of RBC with 99mTc. In this study, we observed that the extract of *E. purpurea* has been capable of altering the labeling of red blood cells to the concentrations of 25%; 12.5% and 6.25%, this results may be due to the fact that in these concentrations, the active principles may be capable of interfering strongly in the homeostasis of cell membrane. Like described by Oliveira *et al*., 2003 to the study of *F. vesiculosus*, the extract of *E. purpurea* could be acting in the oxireduction system or in the transport of ions through the membrane decreasing the radiolabeling process in the cells. Furthermore, we can speculate that if the chemical compounds present in these extracts could complex with these ions as a chelating agent, this fact could explain the decrease in the fixation of radioactivity on the blood elements. Diré *et al*.(2001), in a qualitative analysis *in vivo*, have eyed that a chayotte extract (macerated) has induced alteration on the shape of red blood cells together with alteration on the radiolabeling process. In this *in vitro* study although the morphology of the cells has not been analyzed similar to the studies which have focused the stabilizing of red blood cell membrane as well as the inducing of the generation of reactive oxygen species (ROS) as already reported to other natural product such as the *Maytenus icilifolia* (Oliveira, 2000) and *Fucus vesiculosus* (Oliveira, 2003) extracts we may suggest that a similar pattern could be observed to the effects of *E. purpurea* extract.

5 Conclusion

We may suggest that the *Echinacea purpurea* extract could be capable of generating of the reactive oxygen species with oxidant properties that could probably be responsible for the decreasing of the efficiency of radiolabeling of the blood cells.

Correspondence

Maria Luisa Gomes, Doctorat student
Universidade do Estado do Rio de Janeiro
Instituto de Biologia Roberto Alcantara Gomes
Departamento de Biofísica e Biometria
Laboratório de Radiofarmácia Experimental
Av. 28 de setembro, 87, Rio de Janeiro, RJ, Brasil, 20551-030.
Fax number: 55-21-2543532
E-mail: bernardo@uerj.br or malu-gomes@ig.com.br

References

[1] Barret B. Medicinal properties of Echinacea: a critical review. Phytomedicine, 2003,10:66-86.

[2] Bernardo-Filho M, Gutfilen B, Maciel OS. Technetium-99m binding on plasma proteins and red blood cells: role of various precipitating agents. Biomed Letters, 1994, 50:17-24.

[3] Braga ACS, Oliveira MBN, Feliciano GD, Reiniger IW, Oliveira JF, Silva CR, Bernardo- Filho M. The effect of drugs on the labeling of blood elements with technetium-99m. Curr Pharm Design , 2000 , 6:1179-91.

[4] Capriles PVSZ, Dias APM, Costa TEMM, Oliveira MBN, Faria MVC, Moura EG, Abreu BAL, Bernardo-Filho M. Effect of eggplant (*Solanum melongena*) extract on the *in vitro* labeling of blood elements with technetium-99m and on the biodistribution of sodium pertechnetate in rats. Cell Mol Biol , 2002, 48:771-6.

[5] Costa TEMM, Dias APM, Capriles PVSZ, Oliveira MBN, Amorim ELC, Lima CSA, Bernardo-Filho M. Effect of barbatimão [*Stryphnodendron adstringens* (*Mart.*) *Coville*] infusion on the labeling of blood elements with technetium-99m. Rer Bras Farmacogn , 2002 , 12:7-9.

[6] Diré G, Lima E, Mattos D, Oliveira MB, Pereira MJ, Moreno S, Freitas R, Gomes ML, Bernardo-Filho M. Effect of chayotte (*Sechium edule*) extract on the biodistribution of technetium-99m and on the morphometry of red blood cells. J labelled Cpd Radiopharm, 2001, 44: 648-50.

[7] Diré GF, Lima EAC, Pereira MJS, Oliveira MBN, Moreno RF, Mattos DMM, Jales RL, Bernardo-Filho M. Effect of a chayotte (*Sechium edule*) extract on the labeling of red blood cells and plasma proteins with technetium-99m: *in vitro* and *in vivo* studies. Cell Mol Biol , 2002 , 48:751-5.

[8] Early PJ, Sodee DB. Principles and Practice of Nuclear Medicine. 2 ed. New York, USA, 1995.

[9] Gutfilen B, Boasquevisque EM, Bernardo-Filho M. Calcium channel blockers: interference on red blood cells and plasma proteins labeling with Tc-99m. Rev Esp Med Nucl , 1992, 11:195-9.

[10] Hesslewood S, Leung E. Drug interactions with radiopharmaceuticals. Eur J Nucl Med , 1994 , 21: 348-56.

[11] Jensen LP, Lai AR. Chayote (*Sechium edule*) causing hypokalemia in pregnancy. Am J Obstet Gynecol , 1986 , 5:1048-9.

[12] Kam PCA, Liew S.. Traditional Chinese herbal medicine and anaesthesia. Anaesthesia , 2002 , 57:1083-9.

[13] Lima EAC, Diré G, Mattos DMM, Oliveira MN, Mattos JCP, Dantas FJS, Caldeira-de-Araújo A, Bernardo-Filho M. Effect of the leaf extract from cauliflower (*Brassica oleracea L.* var. *Botrytis*) on the biodistribution of. the radiopharmaceutical sodium pertechnetate in mice and on the electrophoretic

mobility of plasmid pUC 9.1 DNA. J Labelled Cpd Radiopharm , 2001 , 44:642-4.

[14] Lima EAC, Diré G, Mattos DMM, Freitas RS, Gomes ML, Oliveira MBN, Faria MVC, Jales RL, Bernardo-Filho M. Effect of an extract of cauliflower (leaf) on the labeling of blood elements with technetium-99m and on the survival of *Escherichia coli* AB1157 submitted to the treatment with stannous chloride. Food Chem Toxicol , 2002 , 40:919-23.

[15] Moura CM. Metodologia enzimática para a detecção de pesticidas organofosforados e carbamatos em água e frutas. Dissertação (Mestrado em Biologia), Universidade do Estado do Rio de Janeiro, Instituto de Biologia Roberto Alcantara Gomes, 1998.

[16] Moreno SRF, Diré GF, Freitas RS, Farah MB, Laurentino-Filho GL, Rocha EK, Jales RLC, Bernardo-Filho M. Effect of *Ginkgo biloba* on the labeling of blood elements with technetium-99m: *in vitro* study. Rer Bras Farmacogn , 2002 , 12:62-3.

[17] Moreno SRF, Freitas R, Diré G, Farah M, Lima E, Lima-Filho GL, Pereira M, Mandarim-Lacerda C, Rocha EK, Bernardo-Filho M. Evalution of the effect of a *Ginkgo biloba* extract on the biodistribution of sodium pertechnetate in rats and on the morphology of red blood cells. Technetium, Rhenium and Other Metals in Chemistry and Nuclear Medicine. SGEditoriali, Padova , 2002 , 6:531-3.

[18] Oliveira JF, Braga ACS, Ávila ASR, Gutfilen B, Bernardo-Filho M. Effect of *Thuya occidentalis* on the labeling of red blood cells and plasma proteins with technetium-99m. Yale. J Biol Med , 1997 , 69:489-94.

[19] Oliveira JF, Braga ACS, Ávila ASR, Araújo AC, Cardoso VN, Bezerra RJAC, Bernardo-Filho M. Assessment of the effect of *Maytenus ilicifolia* (espinheira santa) extract on the labeling of red blood cells and plasma proteins with technetium-99m. J Ethnopharmacol , 2000 , 72:179-84.

[20] Oliveira JF, Ávila AS, Braga ACS, Oliveira MBN, Boasquevisque EM, Jales RL, Cardoso VN, Bernardo-Filho M. Effect of extract of medicinal plants on the labeling of blood elements with Technetium-99m and on the morphology of red blood cells: a study with *Paullinia cupana*. Fitoterapia, 2002 , 73: 305-12.

[21] Oliveira JF, Oliveira MB, Ávila AS, Braga A CS, Catanho MTJA, Jales RLC, CardosoVN, Bernardo-Filho M. Assessment of the effect of *Fucus vesiculosos* extract on the labeling of blood constituents with technetium-99m and the histological modifications on the shape of the red blood cells. Food Chem Toxicol , 2003 , 41: 15-20.

[22] Reiniger IW, Oliveira JF, Caldeira-de-Araújo A, Bernardo-Filho M. Effect of *Peumus boldus* on the labeling of red blood cells and plasma proteins with technetium-99m. Appl Radiat Isto , 1999, 51: 145-9.

[23] Saha GB. Fundamentals of Nuclear Pharmacy. 4th ed. New York: Springer-Verlag, 1998.

[24] Sampson CB. Complications and difficulties in radiolabelling blood cells: a review. Nucl Med Commun , 1996 , 17:648-58.

[25] Santos AEO dos, Moreira C dos S, Oliveira MBN, Diré G, Jales RL, Bernardo-Filho M. Effect of a *Syzygium jambolanum* (jamelão) extract on the labeling of blood elements with sodium pertechnetate ($Na^{99m}TcO_4$). Rev Bras Pl Med , 2002 , 5: 63-7.

[26] Santos JS, Paula EF, Correa TG, Freitas LC, Fonseca LM, Gutfilen B, Bernardo-Filho M. Effect of cyclophosphamide on the binding of $^{99m}TcO^-_4$ and ^{99m}Tc-MDP to blood cells and plasma proteins. *Braz* J Med Biol Res , 1995 , 28: 131-5.

[27] Santos-Filho SD, Ribeiro CK, Diré GF, Lima E, Pereira M, Bernardo-Filho M. Morphological alterations on red blood cells labeled with technetium-99m: the effect of *Mentha crispa L.* (Hortelã) and *Piper methysticum* (Kava Kava) extracts. Technetium, Rhenium and Other Metals in Chemistry and Nuclear Medicine. SGEditoriali, Padova , 2002 , 6:503-5.

[28] Silva CR, Oliveira MBN, Melo SF, Damtas FJS, Mattos JCP, Bezerra RJAC, Caldeira-de-Araújo A, Duatti A, Bernardo-Filho M. Biological effects of stannous chloride, a substance that can produce stimulation or depression of the central nervous system. Brain Res Bull , 2002 , 59: 213-6.

[29] Srivastava SC, Straub RF. Blood cell labeling with tc-99m: progress and perspectives. Semin Nucl Med , 1990, 1:41-51.

[30] Vidal MV, Gutfilen B, Barbosa-da-Fonseca LM, Bernardo-Filho M. Influence of tobacco on the labelling of red blood cells and plasma proteins with technetium-99m. J Exp Clin Cancer Res , 1998 , 1: 1-6.

An *In Vivo* Evaluation of an Aqueous Extract of *Uncaria Tomentosa* on the Morphology on the Labeling of Blood Constituents with ^{99m} Technetium

Gláucio F. Diré [1], Hayden P. Honeycutt [2], Maria L. Gomes [1], Elaine A. C. Lima [1], Deise M. M. Mattos [1], Mario Bernardo-Filho [1, 3]

(1. Universidade do Estado do Rio de Janeiro, Instituto de Biologia Alberto Alcantara Gomes, Departamento de Biofisica e Biometria, Av. 28 de setembro n 87, 20551-030, Rio de Janeiro, Brasil;
2. University of North Carolina, School of Pharmacy, Chapel Hill 27599-7360, North Carolina, USA;
3. Instituto Nacional do Câncer, Coordenadoria de Pesquisa, Praça Cruz Vermelha, 23, Rio de Janeiro, RJ, Brasil, 20230-130. E-mail: Bernardo@uerj.br)

Abstract: *Uncaria tomentosa* (Cat's Claw, Unha de Gato) is a commonly used medicinal plant, which has demonstrated to have antioxidant and antimutagenic properties. Blood cells (BC) labeling with ^{99m}Tc(technetium-99m) has progressed around the world. The influence of drugs on the labeling of blood elements with ^{99m}Tc has been reported. The purpose of this study was to examine the effect of Unha de Gato extract on the radiolabeling of blood elements with ^{99m}Tc and on the morphology of red blood cell (RBC). Extract (32 mg/mL) was prepared with NaCl (0.9%). The extract was administered to the animals via gavage (for seven days). Blood was withdrawn and it was incubated with stannous chloride for one hour followed by the addition of ^{99m}Tc. Plasma (P) and BC were separated. P and cell (C) were precipitated with 5% trichloroacetic acid (TCA) and soluble fraction (SF) and insoluble fraction (IF) were obtained. The percentage of radioactivity (%ATI) was determined. For the morphology the smears were evaluated and RBCs were analyzed. We can conclude that *Uncaria* extract was not capable to alter the radiolabeling of blood elements with ^{99m}Tc and the morphology of red blood cells. We suggest that the studied natural product, may be heavily metabolized by the liver, resulting in inactive metabolites that do not alter the labeling procedure and the morphology of RBCs. [Nature and Science, 2004,2(1):6-10].

Key words: Unha de Gato; red blood cells; plasma proteins; technetium-99m

1 Introduction

Many plant species are used medicinally. In Brazil there are many vegetables that are traditionally used in folk medicine. Uncaria tomentosa (Unha de Gato) from Rubiaceae family is a plant from the Peruvian Amazon. Cat's Claw is a commonly used medicinal plant for a variety of indications including, rheumatoid and osteoarthritis, sinusitis, rhinitis, tonsillitis, and cutaneous abscesses. It has previously been demonstrated to have immunostimulant, antioxidant, and more recently antimutagenic properties. It has been demonstrated that Uncaria has a potential antiviral and immunomodulating activity (Williams, 2001). The biodistribution of the radiopharmaceuticals can be altered by natural and synthetic drugs as well as the radiolabeling of blood elements with technetium-99m (99mTc) (Diré, 2001; Mattos, 1997, 2000, 2002; Vidal, 1998). When a radionuclide have its capability to bind to blood elements altered by drugs therapy, the process of labeled red blood cells may be repeated, resulting in an additional radiation dose to the patient (Early, 1995; Hesselewwod, 1994).

99m Tc has been the most utilized radionuclide in nuclear medicine procedures and it has also been used in basic research (Early, 1995; Gutfilen, 1996; Mattos, 2001; Saha, 1998). The wide utilized in nuclear medicine is due to its optimal physical characteristics (half-life of 6 h, gamma rays energy of 140 keV and minimal dose to the patients), convenient availability from 99Mo/99mTc generator and negligible environmental impact. Nearly almost all scanning devices currently in use are optimized for detecting the eletromagnetic emission from this radionuclide (Early, 1995; Hesselewwod, 1994).

There are many applications of 99mTc-labeled red

blood cells (RBC). The most important is in cardiovascular nuclear medicine, where one tries to image the heart to determine its functional status as a pump, to calculate the left ventricular function by measuring the ejection fractions, and to evaluate wall motion abnormalities. Some other applications are in the detection of gastrointestinal bleeding, and in the determination of the RBC mass in patients (Early, 1995; Hesselewwod, 1994). The labeled process with 99mTc depends on a reducing agent and stannous ion (Sn2+), mainly as stannous chloride, is usually used for this purpose (Early, 1995; Gutfilen, 1993, 1996; Hesselewwod, 1994; Saha, 1998; Sampson, 1996). When whole blood is used in the labeling of RBC with 99mTc, radioactivity is found on blood cells, however it is also bound on plasma proteins. This labeling process depends on optimal stannous chloride concentration and stannous and pertechnetate ions across the RBC membrane, probably spending energy and the radionuclide is mainly bound to hemoglobin molecule (Gutfilen, 1996; Hesselewwod, 1994; Hladik, 1987). Several of the cellular labeling steps have been well characterized. The band-3 anion transport system and calcium channels may be the ways that 99mTc and Sn+2, respectively, reach the interior of the RBC (Gutfilen, 1996; Srivastava, 1984). If one damages the RBC, one can do selective spleen imaging since damaged cells are rapidly sequestrated by the spleen. RBC has been labeled with 99mTc for in vitro in vivo or in vivo/ in vitro techniques (Srivastava, 1984).

Plasma proteins (PP) have also been labeled with the referred radionuclide. 99mTc -labeled PP has been used to locate placenta, to evaluate the cardiac function and pulmonary perfusion, to determine blood volume and to study the gastrointestinal protein loss (Early, 1995; Hesselewwod, 1994).

The labeling of red blood cells with 99mTc has been influenced by patient medications, by the labeling conditions (Early, 1995; Hesselewwod, 1994; Santos, 1995) or by the presence of extracts of plants, as Paullinia cupana (Mattos, 2002), Maytenus ilicifolia (Mattos, 2000), Thuya occidentalis (Mattos, 1997), Nicotiana tabacum (Vidal, 1998), and. Nevertheless, there is not a well established in vitro/in vivo model to study the interaction of therapeutic drugs with radiopharmaceuticals (Early, 1995; Sampson, 1996; Santos, 1995). Then, we have evaluated the influence of an Uncaria extract (i) on the labeling of blood elements with 99mTc and (ii) on the morphology of RBC.

2 Material and Methods

2.1 Plant material

A commercial dried powder of Unha de Gato was obtained from the Laboratory Herbarium, Laboratório Botânico, Brazil, Lot 923661 (June, 2001 and validity June 2004). To prepare the solution which was considered like 100% it was diluted 320 mg of Uncaria into 10 mL of saline solution (NaCl 0.9%) obtained a solution 100% (32 mg/mL).

2.2 Animals

Male Wistar rats (200-250 g) from Universidade do Estado do Rio de Janeiro were used. The animals received a standard pellet rat diet and water, they were maintained under constant environmental conditions (22±5°C, 12 h of light/dark cycle).

In six male Wistar rats were administered 1 mL of Unha de Gato solution via oral gavage for seven days. Similarly, six other male rats were treated with normal saline to serve as control.

2.3 Study protocol

Samples of heparinized (0.5 mL) blood were withdrawn from animals and incubated with 0.5 mL of stannous chloride (1.2 µg/mL), as SnCl2.2H2O for 1 h at room temperature. After this period of time, 99mTc (0.1 mL), as sodium pertechnetate, was added and the incubation continued for another 10 min. These samples were centrifuged and plasma (P) and blood cells (BC) were separated. Samples (20 µl) of P and BC were precipitated with 1 mL of trichloroacetic acid (TCA) 5% and soluble fraction (SF) and insoluble fraction (IF) were separated. The radioactivity in P, BC, IF-P, SF-P, IF-BC and SF-BC were determined in a well counter. After that, the % of radioactivity (%ATI) was calculated. A statistical analysis (Mann Whitney and Kruskal Wallis tests) was utilized to compare the experimental data.

For the morphology study, the blood was collected from the same rats treated with Unha de Gato and saline solution. Blood smears were prepared, dried, fixed and staining. Five slides per rat were analyzed for a total of 60 slides. Five frames were evaluated per slide andthemorphology of the red blood cells observed in each frame was quantitatively analyzed under optical microscope by Image Pro-Plus software.

3 Results

Samples of whole blood from the animals (control

and treated with uncaria extract) were incubated with SnCl2 for 1h and after with 99mTcO4Na. Blood smears were prepared, dried, fixed and staining. After that, the morphology of RBC was evaluated under optical microscope (x1000) (Figure 1, 2).

Table 1 has shown the effect of uncaria (in vivo) on the labeling of red blood cells (BC), insoluble fraction of the red blood cells (IF-C) and in the insoluble fraction of the plasma (IF-P) with 99mTc. The analysis of the results indicates that the referred extract is not capable to reduce the labeling efficiency of blood elements with 99mTc.

Table 2 has shown the morphology of red cells of the blood withdrawn from animals that have received the extract (7 days), by gavage via. The analysis of the results indicates that there is no alteration in the morphometric analysis ($p>0.05$) when the control group was compared with the treated one.

4 Discussion

Many authors have described a great number of drugs which can be due to the causes of some diseases of red cells (Bernardo, 1994; Braga, 2000; Sampson, 1996). There are evidences that drugs can affect either radiolabeling or biodistribution of blood cells in the context of the nuclear medicine. In the literature some researches have turned their attention to in vitro testing of the drug with labeled cells (Bernardo, 1994; Braga, 2000; Hladik, 1987; Sampson, 1996).

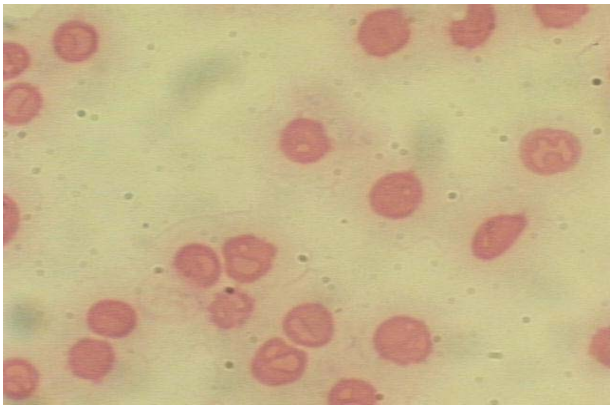

Figure 1 – control

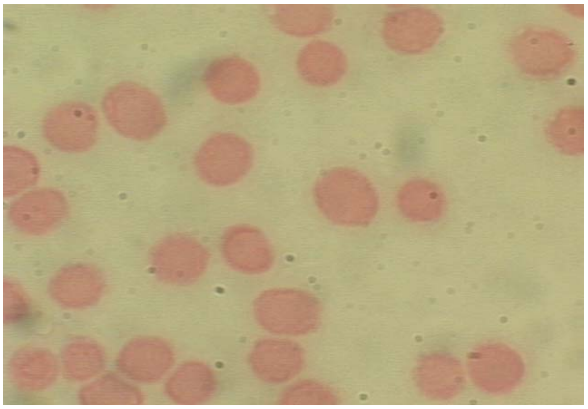

Figure 2 - treated

Figures 1 and 2 Photomicrography of blood smears prepared with samples of whole blood used to label RBC with ^{99m} Tc (control and treated)

Table 1 Effect of uncaria (*in vivo*) on the labeling of red blood cells (BC), insoluble fraction of the red blood cells (IF-C) and in the insoluble fraction of the plasma (IF-P) with ^{99m}Tc.

Sechium edule	BC	IF-C	IF-P
Control	91.62 ± 3.90	79.50 ± 1.84	71.43 ± 0.37
100 %	97.01 ± 0.70	83.30 ± 0.90	72.70 ± 0.43

Samples of heparinized blood from animals treated with the referred extract were incubated for 1 hour with stannous chloride (1.2 µg/mL) and ^{99m}Tc, as sodium pertechnetate. These samples were centrifuged and plasma (P) and blood cells (BC) were separated. Samples (20 µl) of BC were precipitated with trichloroacetic acid (TCA) 5% and soluble (SF) and insoluble fractions (IF) were separated. The radioactivity in P, BC, SF-BC , IF-BC, SF-P and IF-P was determined in a well counter and the % of radioactivity (% ATI) was calculated. A statistical analysis (Kruskal Wallis test, n= 6) was used to compare the results. The values are averages ± SDs.

Table 2 - Effect of uncaria (*in vivo*) on the morphology of red blood cells (BC)

Groups	Mean of the perimeter/area
Control	0.65 ± 0.04
Treated (100 %)	0.63 ± 0.02

Histological evaluations were performed with blood samples treated with *Uncaria* for 60 min at room temperature. Blood smears were prepared, dried, fixed and staining. After that, the morphology of the red blood cells was observed under optical microscope.

The use of natural products, as medicinal plants, is very frequent in folk medicine around the world and *Uncaria* is utilized as a therapeutic plant due to this antiinflammatory properties such as rheumatoid and osteoarthritis, sinusitis, rhinitis, amigdalite, and cutaneous abscesses (Williams, 2001).

It has been described by our research group the effect of some natural products as *Thuya occidentalis* (Mattos, 1997), *Nicotiana tabacum*, (Vidal, 1998), *Maytenus ilicifolia* (Mattos, 2000) and *Paullinia cupana* (Mattos, 2002) on the radiolabeling of blood elements with ^{99m}Tc. These extracts are capable to reduce this labeling procedure in *in vitro* studies.

In the present study, uncaria extract was not capable to alter the radiolabeling of blood constituents with ^{99m}Tc like it was observed with an extract of cauliflower (leaf) (Lima, 2002). The results obtained with the quality and quantity comparison of the shape of the RBC (control and treated groups) under optical microscopy could justify the fact that uncaria extract was not capable to alter the radiolabeling procedure. In other study, Diré *et al*, 2001 has reported that chayote extract was able to alter de morphology of red cells. Thompson *et al*., 1981 studied the labeling of intact human erythrocytes with ^{99m}Tc. The analysis of the membranes of labeled erythrocytes showed that the label bear is not due to the binding of technetium to residual hemoglobin but its binding to constituent membrane proteins demonstrating the importance of the integrity of the morphology of the cells due to radiolabeling process. We can suggest that like *Peumus boldus* (Reiniger, 1999), the effect of uncaria could be explained by its anti-oxidant properties that can be due to the fact that uncaria may be heavily metabolized by the liver, resulting in inactive metabolites that do not alter the labeling of blood elements with ^{99m}Tc.

Many reports about medicine plants are rarely written up in the traditional medicine literature. In order to make an accurate assessment of the impact of drugs and other factors on the biological systems additional data are required (Braga, 2000, Sampson, 1996).

5 Conclusion

We can conclude that *Uncaria* extract was not capable to alter the radiolabeling of blood elements with ^{99m}Tc and the morphology of red blood cells. We suggest that the studied natural product, may be heavily metabolized by the liver, resulting in inactive metabolites that do not alter the labeling procedure and the morphology of red blood cells.

References

[1] Bernardo Filho M, Gutfilen B, Maciel OS. Effect of different anticoagulants on the labeling of red blood cells and plasma proteins with Tc-99m. *Nucl Med Comm* , 1994 , 15:730.

[2] Braga ACS, Oliveira MBN, Feliciano GD, Reninger IW, Fonseca JF, Silva CR, Bernardo-Filho M. The effect of drugs on the labeling of blood elements with technetium-99m. *Curr Pharm Design* , 2000 , 6:1179.

[3] Diré G, Lima E, Mattos D, Oliveira MB, Pereira MJ, Moreno, Freitas R, Gomes ML, Bernardo-Filho M. *J Labeled Compds Radiopharm* , 2001, Suppl 1:44.

[4] Early PJ, Sodee DB. Principles and Practice of Nuclear Medicine. *Mosby-Year Book*, Inc., Toronto , 1995 , 877.

[5] Gutfilen B, Bernardo-Filho M. *M Rer Bras Pesq Desenvolv*, 1996 , 3:93.

[6] Gutfilen B, Pontes LFS, Alencar ISC, Bernardo-Filho M. *Biomed Letter* , 1993 , 48:305.

[7] Hesselewwod S, Leung E. Drug interactions with radiopharmaceuticals. *Eur J Nucl Med* , 1994 , 21:348.

[8] Hladik III WB, Saha GB, Study KT. Essentials of Nuclear Medicine Science, Williams and Wilkings: Baltimore-London, 1987.

[9] Lima EAC, Diré G, Mattos DMM, Freitas R, Gomes ML, Oliveira MB, Faria MVC, Jales RL, Bernardo-Filho M. Effect of an extract of cauliflower (leaf) on the labeling of blood elements with technetium-99m and on the survival of *Escherichia coli* AB1157 submitted to the treatment with stannous chloride. *Food Chem Toxicolv* , 2002;40:919-923.

[10] Mattos DMM, Gomes ML, Freitas RS, Moreno S, Lima-Filho GL, Paula EF, Jales RLC, Bernardo-Filho. Which are the most used radionuclides in the pet and in the spect techniques in the world. *J Labeled Cpd Radiopharm* , 2001 , Suppl 1:44.

[11] Oliveira JF, Ávila AS, Braga ACS, Oliveira MBN, Boasquevisque EM, Jales RL, Cardoso VN, Bernardo-Filho M. Effect of extract of medicinal plants on the labeling of blood elements with Technetium-99m and on the morphology of red blood cells: a study with *Paullinia cupana Fitoterapia* , 2002 , 73:305.

[12] Oliveira JF, Braga ACS, Ávila ASR, Araújo AC, Cardoso VN, Bezerra RJAC, Bernardo-Filho M. Assessment of the effect of *Maytenus ilicifolia* (espineira santa) extract on the labeling of red blood cells and plasma proteins with technetium-99m. *J Ethnopharmacol* , 2000 , 72:179.

[13] Oliveira JF, Braga ACS, Ávila ASR, Gutfilen B and Bernardo-Filho M. Effect of *Thuya occidentalis* on the labeling of red blood cells and plasma proteins with technetium-99m. *Yale J*

Biol Med , 1997 , 69:489.

[14] Reiniger IW, Oliveira JF, Caldeira-de-Araújo A, Bernardo-Filho M. *Appl Radiat Isto* , 1999 , 51:145.

[15] Saha GB. Fundamentals of Nuclear Pharmacy. *Springer-Verlag*, New York , 1998 , 331 .

[16] Sampson CB. *Nucl Med Commun* , 1996 , 17:648.

[17] Santos JS, Paula EF, Correa TG, Freitas LC, Fonseca LM, Gutfilen B, Bernardo-Filho M. *Braz J Med Biol Res* , 1995 , 41:1575.

[18] Srivastava SC, Straub RF, Richards PJ. *Labeled Compds Radiopharm* , 1984 , 21:1055.

[19] Vidal MV, Gutfilen B, Barbosa-da-Fonseca LM, Bernardo-Filho MM. *J Exp Clin Cancer Res* , 1998 , 17:41.

[20] Williams JE. Review of antiviral and immunomodulating properties of plants of the Peruvian rainforest with a particular emphasis on Una de Gato and Sangre de Grado. *Altern Med Rev* , 2001 , 6:567.

Nanofiltration for Mixed Ion Systems with Commercial and Pore-Filled Membranes

Wayne W Jiang[a*], Jesus Garcia-Aleman[b], James M Dickson[b], and Ronald F Childs[a]

(Departments of [a]Chemistry and [b]Chemical Engineering, McMaster University, Hamilton, ON L8S 4M1Canada,
Tel : +1(905) 525-9140; Fax: +1(905)522-2509; E-mail: wenyi@chemistry.mcmaster.ca)

Abstract: Nanofiltration for mixed ion systems with commercial and pore-filled membranes was studied. A modified model was proposed based on the extended Nernst-Planck equation, Donnan equilibrium, and Gouy-Chapman theory. The performance of the commercial membrane (DDS HC50) was described successfully using this model. The model was also used to predict the performance of a pore-filled membrane. The model predicted the performance of the commercial membrane but failed to describe all the observed behavior of the pore-filled membrane. [Nature and Science, 2004,2(1):11-16].

Key words: modelling; extended Nernst-Planck equation, nanofiltration, mixed ion system

1 Introduction

Nanofiltration (NF) is a pressure driven membrane separation process where a solute is separated from a solution under pressure through a membrane. Nanofiltration membranes are considered to be "leaky" reverse osmosis (RO) membranes and nanofiltration is under lower pressure than reverse osmosis. NF membranes have intermediate molecular weight cut-off between reverse osmosis and ultrafiltration (UF) membranes (Petersen 1993). Nanofiltration has become an important process for various applications, including pulp processing (Peterson 1993), water purification, demineralization of whey in the dairy industry (van der Horst 1995), to concentrate organics (Perry 1989), and water softening (Mika 1999), etc.

Many researchers have investigated nanofiltration for salt separations in order to properly design and predict performance using mathematical models. When mixed solutes are present, the interaction between ions becomes large and is significantly influenced by Donnan equilibrium (Josson 1980, Nielson 1994, Tsuru 1991, Rios 1996, Mika 2001, Jiang 2003). The extended Nernst-Planck equation has been extensively used to model charged membranes (Dresner 1972, Josson 1980, Buck 1984, Tsuru 1991, and Petersen 1993). The basis and limitations of the extended Nernst-Planck equation applied to ionic transport in charged membranes have been discussed.

It has not been concluded whether high performance membranes for nanofiltration have porous heterogeneous or homogeneous structures. Mathematic models have been proposed to understand nanofiltration, such as a bundle of capillaries model (Wang 1995), the Hybrid Model (Bowen 1996 and 1997), etc. For example, Bowen *et al.* (1997) determined that activities inside membrane pores caused by solute-solute and solute-membrane ion interactions were accounted for by the effective charge density. This model contained three structural parameters: the effective membrane thickness, the effective charge density, and the membrane pore radius. The hindrance factors were related linearly to the ratio of solute to pore radius using finite element calculation (Bowen 1996 and 1997, Dean 1987). Using single electrolyte data, they were able to correlate the dependence of the effective charge density on the bulk concentration through a Freundlich type isotherm.

Josson (1980) successfully predicted negative rejections in reverse osmosis cellulose acetate membranes using the extended Nernst-Planck equation combined with a frictional and exclusion model. He assumed that Donnan equilibrium was valid through all the membrane thickness (Helfferich 1962). Recently, Nielson and Josson (1994) tried to introduce an analytical solution to the same problem. They were able to predict negative rejection in limiting cases based on bulk solution concentration. Rios (1996) established a mathematic model for the separation of Nafion membranes by simplifying the Nernst-Planck equation

by limiting to sufficiently high volume fluxes. Van der Horst (1995) solved the Nernst Planck equation as a difference equation. The accounted for concentration polarization due to the nature of solutes (whey permeate). Model predictions were in good agreement with the experimental data, but the parameters had limited physical significance.

In this study, the model of Josson (1994) is modified and compared to two sets of data, i.e., one is obtained from a commercial membrane (DDS HC50) and the other from a pore-filled cation-exchange membrane (Jiang 1999).

2 Model Derivations

The concentration profile across the membrane is obtained by rearranging Eq. 7 and using Eq. 2,

$$\frac{dC_{i,p}(x)}{dx} = \frac{J_V}{D_{i,\infty}E}\left(a_i C_{i,p}(x) - b_i C_i^p(x)\right) - \frac{z_i F C_{i,p}}{RT}\frac{d\Psi(x)}{dx} \quad (8)$$

Thus, the potential gradient is obtained as a function of the volume flux and ion concentrations,

$$\frac{d\Psi(x)}{dx} = \frac{RT}{FE}\cdot\frac{\sum\left(\frac{z_i}{D_{i,\infty}}\right)(a_i C_{i,p}(x) - b_i C_{i,p}^p}{\sum z^2 C_{i,p}(x)} J_v \quad (9)$$

Eq. 9 is solved using the following boundary conditions, assuming (i) the concentration of species i in the feed is equal to that on the surface of membrane on the feed side ($x = 0$), Eq. 10, and (ii) the concentration of species i in the permeate is equal to that on the surface of membrane on the permeate side ($x = \lambda$),

$$C_{i,p}(0) = C_i^F \quad (10)$$

$$C_{i,p}(\lambda) = C_i^P \quad (11)$$

where λ is membrane thickness (m).

The concentrations at the interfaces between the membrane and feed/permeate solutions are calculated from Donnan equilibrium,

$$\frac{K_i}{K_{i,0}} = \left(\frac{C_{i,p}}{C_i}\right)\left(\frac{\gamma_{i,p}}{\gamma_i}\right) = \exp\left(-\frac{z_i F}{RT}\Delta\Psi_D\right) \quad (12)$$

where K_i, $K_{i,0}$, γ_i, and $\gamma_{i,p}$ are partition coefficient, zero partition coefficient, activity coefficient, and activity coefficient in membrane pores, respectively.

For (n) ions the model consists of (n - 1) coupled ODE that have to be solved numerically. The model has (3n + 2) parameters ($K_{i,0}$, b_i, a_i, X, λ/E) which account for membrane characteristics and solute-membrane interactions. The model was solved numerically using a variable order method for still/non-stiff ODE solver, and the parameters were estimated using a nonlinear least-squares routine (Levenberg-Marquardt).

For a dilute solution ($\gamma_i \approx \gamma_{i,p} \approx 1$), Eq. 8 can be modified to account for Donnan equilibrium, Eq. 12, throughout membrane cross section when pores are assumed to exist,

$$\frac{dC_{i,p}(x)}{dx} = \frac{J_v}{D_{i,\infty}E}\left(a_i C_{i,p}(x) - \frac{b_i C_i^p K_i^p}{K_i}\right) - \frac{z_i F C_{i,p}}{RT}\frac{d\Psi(x)}{d(x)} \quad (13)$$

and the electrical potential is given by

$$\frac{d\Psi(x)}{dx} = \frac{RT}{FR}\cdot\frac{\sum\left(\frac{z_i}{D_{i,\infty}}\right)\left(\frac{a_i C_{i,p}(x)}{K_i} - b_i C_i^p K_i^p\right)}{\sum z_i^2 K_i C_i(x)} J_v \quad (14)$$

3 Experimental

The cation exchange membranes investigated in this study were a commercial reverse osmosis membrane and a pore-filled membrane. The commercial cation-exchange membrane is DDS HC50. The HC50 is a commercial membrane that consists of polyamide layer on a polysulfone support.

The pore-filled cation-exchange membrane was fabricated as described elsewhere (Jiang 1999). This pore-filled membrane consists of a polyethylene microfiltration substrate (pore size of 0.19 μm, thickness of 45 μm, and porosity of 78%) fabricated by the 3M Company (St. Paul, Minnesota, USA) and the polyelectrolytes, i.e., poly(styrene-sulfonic acid) groups. The pore-filled membrane used in this study had the following characteristics: 80% of mass gain of polystyrene, 2.5% of divinylbenzene, 67% of water content, and an ion-exchange capacity of 2.2 meq/g.

The pressure-driven experiments were carried out in a reverse osmosis/nanofiltration apparatus at 25°C (Jiang 2003). The solutes used were sodium chloride, sodium sulfate, magnesium chloride, and magnesium sulfate (Aldrich, analytical grade). The water used in

this study was deionzed water and carbon filtered. The concentrations of salts were measured using a Dionex ion chromatography, (Sunnyvale, California, USA).

4 Results and Discussion

This paper studied the nanofiltration performance predicted by the model developed above. The model was simplified by allowing the effective charges density to be accounted for by the zero partition coefficients. The following two sections describe the understanding of the membrane performance of separating mixed salts using an HC50 membrane and a pore-filled ion-exchange membrane.

5 Performance of HC50 Membrane

The water flux and an NaCl solution flux of the HC50 commercial membrane were measured. Fig. 1 shows the relationship between flux and pressure. It is not surprised to see that the linear relationships between the flux and the applied pressure. This is consistent with the findings of other researchers.

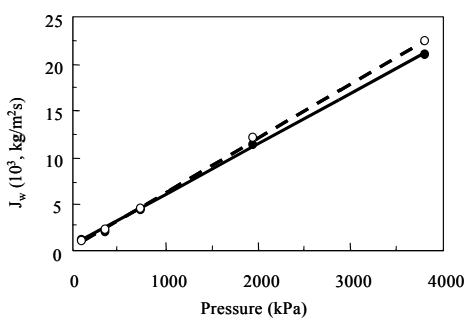

Fig.1 Flux versus applied pressure for water(dashed curve) and a 2 mol/m^3 of NaCl solution (solid curve)

The HC50 membrane was used in nanofiltration with a mixed salt solution system of $NaNO_3$ and Na_2SO_4. Fig. 2 shows the nanofiltration results for the commercial HC50 RO membrane. Fig. 2 is obtained by plotting the coion rejection versus the flux. The curves are the rejections predicted by the model proposed above. The data points are experimental data. Two different concentration ratios were used in the test, one marked as ▲ is 1:1 $NaNO_3$:Na_2SO_4 and the other as Δ is 1:10 $NaNO_3$:Na_2SO_4. As can be seen in Fig. 2, the model proposed above successfully predicted the performance of the commercial membranes, HC50.

The model predictions agree with the experimental nitrate rejection with great accuracy. The rejection greatly depends on the permeate flux. For example, the rejection of the more permeate ion (nitrate) decreases and of the less permeable ion (sulfate) increases as increasing the concentration of the less permeate ion (sulfate).

As can bee seen in Fig. 2, the model is able to predict a limiting rejection at infinite flux, and the minimum in nitrate rejection at low fluxes. The parameter estimated are given in Table 1. It can be inferred that Donnan exclusion (Kio's) dominates ion selectivity by the membrane. It is observed that the zero partition coefficient for the bivalent coion is several order of magnitude smaller that that for the monovalent coion and any counterion, which agrees with previous findings (Josson 1980). Steric effects are also shown to be important. At low flux, they are overpowered by Donnan exclusion mechanism. At higher flux, they have a greater contribution to solute transport. The values of the hindered diffusion and convection are relatively high compared to those obtained from the formulas of the ratio of solute to pore radius. But there is an agreement in that there is a greater correction in the dissuasive term than the convective term.

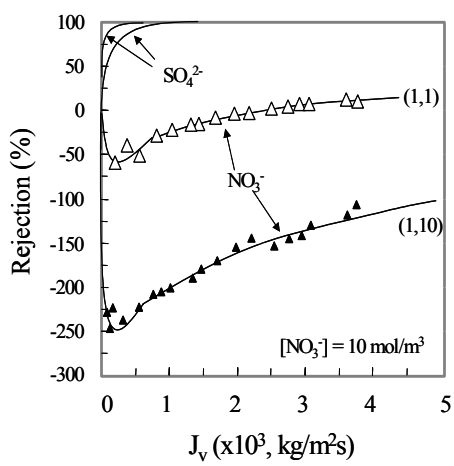

Fig. 2 Ion rejection versus permeate flux. The points (marked as ▲ and Δ) are experimental data and the curves are the model prediction. The nitrate concentration was kept constant (10 mol/m^3)

Table 1 Parameter estimates and 95% confidence intervals for membrane HC50 ($NaNO_3$ and Na_2SO_4)

Parameter	Numerical value	95% Confidence interval
K NO_3 0	0.52131	0.04364
K SO_4 0	0.00735	0.00052

K Na 0	0.30901	0.02123
b NO_3 0	2.41325	0.16892
b SO_4 0	73.5122	11.0268
b Na 0	5.21325	0.26066
a NO_3 0	0.91235	0.09123
a SO_4 0	0.84233	0.04211
a Na 0	0.89123	0.10694
λ/E(le4m)	0.27481	0.00311
Sum of square	0.33312	

The values obtained for the hindered diffusion and convection coefficients (Table 1) were used to back calculate a pore radius as described by Bowen *et al*.(1996 and 1997). The results is a pore radius of approximately 0.40 nm. With this we were able to compare the calculated value of the membrane effective thickness/water content with other authors. Bowen (1996) obtained an effective membrane thickness of 165 μm. They used a pore radius of 1 nm (mild steric effects) and set the porosity to unity. Taking into account that the characterization of the same membrane with a smaller pore radius would imply higher steric effects, and consequently the effective membrane thickness should be reasonably smaller (< 25 μm), in order to obtain the same performance.

6 Performance of Pore-filled Membrane

Fig. 3 shows the relationship between flux and pressure. A non-linear relationship was observed. This is consistent with the findings of other pore-filled membranes (Mika 1995, 1997, and 1999). However, this is not consistent with the data observed above for the commercial membrane. Another observation is that the pure water flux was lower than the solution flux. This is opposite to the results obtained for the commercial membrane. This is likely due to the change in conformation of polyelectrolytes in the pore-filled membrane with changing the pressure or ion strength. If this was true, the model should be modified accordingly.

The pore-filled membranes have a particular characteristics, especially the addition of an electrolyte leads to an increase in solution flux. This performance is inconsistent with that of commercial membranes where a higher feed concentration leads to a lower flux.

Polyelectrolytes play an important role in these processes. The higher flux is due to the interactions between the electrolyte solution and polyelectrolytes gels fixed in membrane pores. When pure water is used, the interactions between charged polyelectrolyte segments repel each other and the polyelectrolyte chains are forced to extend into the pores of the membranes. As the electrolyte concentration increases, the fixed charges are neutralized by the counterions, i.e., sodium ion, known as charge screening. Higher concentration of electrolyte leads to a greater internal pressure generated by the elastic springs in membrane pores. As a result, the balance results in a constant flux when the feed concentration is increased (Jiang 2003). If the concentration increases too high, the elastic springs may break. This may a possible explanation of the enhanced flux at high feed concentration.

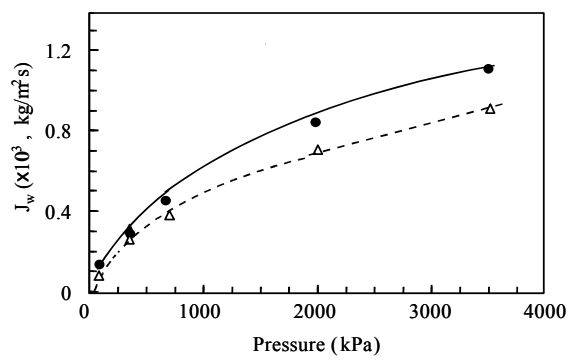

Fig. 3 Flux versus applied pressure for water (dashed curve) and a 2 mol/m^3 of NaCl solution (solid curve)

Fig. 4 shows the rejection as a function of permeate flux with two concentration ratios, i.e., [Na^+/Mg^{2+}] = 1:1 and 1:2. The points are the data of the experimental results and the curves are the model prediction. In both cases of two concentration ratios, the model was able to predict most of the data points for magnesium but could not predict the performance of sodium. It can be concluded that the model proposed here failed to predict consistently the performance of the pore-filled membranes, although the parameter estimates give a qualitative basis to analyze the behavior of this membrane. The parameter estimates used in the calculation are summarized in Table 2.

Donnan equilibrium plays an important roll in the separation of the pore-filled membrane. The parameter estimates show the same trend as the commercial membrane. Coions have smaller ratios of activities, and counterions have larger. Nevertheless, the values are much smaller in the pore-filled membrane which means that a greater charge in the membrane groups exists, thus a greater exclusion effect. For example, the zero

partition coefficient for sodium is three lower for the pore-filled than the commercial membrane.

(A) $[Na^+]$ = 1 mol/m^3 and $[Mg^{2+}]$ = 1 mol/m^3

(B) $[Na^+]$ = 1 mol/m^3 and $[Mg^{2+}]$ = 2 mol/m^3.

The model proposed in this work, as well as the models mentioned in Introduction under several assumptions. First, the solution flux should decrease with increasing feed concentration (osmotic pressure) since it is a function of the intrinsic permeability of the membrane (constant) and the effective pressure. The model cannot possibly predict higher values of J_v with

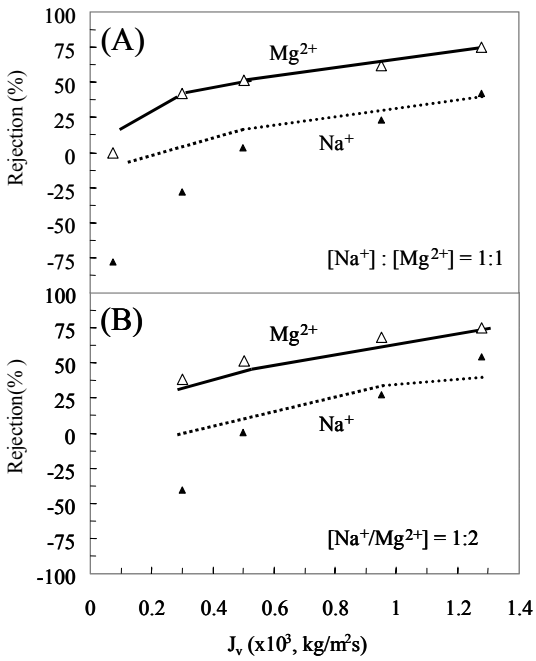

Fig. 4 Ion rejection as a function of permeate flux. The dotted and solid curves are model predictions for magnesium and sodium, respectively, and points are experimental data

Table 2 Parameter estimates and 95% confidence intervals for pore-filled membrane ($NaCl:MgCl_2$)

Parameter	Numerical value	95% Confidence interval
K Na 0	0.10020	0.103
K Mg 0	0.45162	0.377
K Cl 0	0.10218	0.974
b Na 0	7.98953	10.32
b Mg 0	10.3928	19.48
b Cl 0	1.00005	1.826
a Na 0	0.57266	0.688
a Mg 0	0.61570	0.688
a Cl 0	0.57767	1.127
λ/E(le4m)	12.8645	12.56
Sum of square	0.98541	

increasing bulk concentration as no charge screening effect is included.

Second, the structural properties of the membrane parameters are considered to be constant, ie., thickness, water content, pore size, gel structure, etc. However, it was found that the parameters of pore-filled membranes may change as changing conditions such as pressure, ion strength, pH, etc., due to the nature of polylectrolytes (Mika 1995, 1997, 1999 and Jiang 2003).

Third, the steric hindrance coefficients do not depend on pressure or solute concentration. Using the explanation for charge screening and a correlation from Table 1, the friction parameters should decrease as the pore radius increases, i.e., as ion concentration increase in the pore-filled membrane. The crosslinking of the polyelectrolyte protects the pore-filling from total collapse due to charge screening and then the flux stays constant at the higher concentrations. Nevertheless, it is evident that model fits the data properly at high fluxes.

7 Conclusion

The performance of a commercial membrane was described successfully using a modified model based on the extended Nernst-Planck equation and Donnan exclusion. The model showed agreement with results obtained by other authors. The model also was used to predict the performance of a pore-filled membranes. In this case there was insufficient data to fit the model well and the model could not describe all the observed behavior.

However, new directions to extend the membrane modeling to such phenomena are suggested. There has to be developed an effective mean to account charge screening since this interaction not only dynamically affects the pore radius and hence steric but also has an effect on the effective charge density distribution and ion partition into the membrane.

The authors acknowledge the financial support from the Natural Sciences and Engineering Research Council of Canada and the Science and Technology National Council of Mexico. Data of this work were presented at the International Conference on Membranes and Membrane Processes, Toronto, Ontario, Canada (May 1999).

Symbols

a : hindered convection parameter
b_i : hindered diffusion parameter
C_i : ion concentration in solution, mol/m^3
$C_{i,p}(x)$: ion concentration in pore at point x, mol/m^3
C_X : membrane volumetric charge density, mol/m^3
D_i : ionic diffusivity inside the pore, m^2/s
$D_{i,4}$: ionic diffusivity at infinite dilution, m^2/s
E : electric potential, V
F : Faraday's constant, 9,6487.0 C/mol
I : electrical current, C/s
J_i : ion flux based on membrane area, mol/m^2 s
J_v : volumetric solution flux, m^3/m^2 s
K_i : partition coefficient, dimensionless
$K_{i,0}$: zero partition coefficient, dimensionless
m : molality, mol/kg
n : total number of ions, dimensionless
R : universal gas constant, 8.314 J/mol K
T : absolute temperature, K
x : axial coordinate, m
z_i : ion valence, dimensionless
, : membrane porosity dimensionless
8 : effective thickness of the membrane, m
Θ : membrane electrical potential, V
T : sign of the charge density of membrane

Corresponding to (Current address):

Wayne Jiang
National Food Safety and Toxicology Center
Michigan State University
East Lansing, Michigan 48824-1302, USA
Telephone: 517-432-3100
Fax: 517-432-2310
E-mail: jiangw@cvm.msu.edu

References

[1] Bowen WR, Mohammad, AW Hilal N. Characterisation of nanofiltration membranes for predictive purposes – Use of salt, uncharged solutes and atomic force microscopy. J Membrane Sci , 1997,126:91-105.

[2] Bowen WR, Mukhtar H. Characterisation and prediction of separation performance of nanofiltration membranes. J Membrane Sci , 1996,112: 263-74.

[3] Buck RP. Kinetics of bulk and interfacial ionic motion: Microscopic bases and limits for the Nernst-Planck equation applied to membrane systems. J Membrane Sci , 1984 ,17:51-62.

[4] Cussler EL. Diffusion: Mass Transfer in Fluid System, Cambridge University Press, Cambridge, UK , 1985.

[5] Deen WM. Hindered transport of large molecules in liquid-filled pores. AIChE J , 1987;33(9):1409-25.

[6] Dresner L. Stability of the extended Nernst-Plank equations in the description of hyperfiltration through ion-exchange membranes. J Physical Chem , 1982;76(6):16.

[7] Helfferich H. Ion Exchange, McGraw-Hill, New York, New York , 1962.

[8] Jiang W. Preparation and characterization of pore-filled cation-exchange membranes, Ph.D. Thesis, McMaster University, Hamilton, Ontario , 1999.

[9] Jiang W, Childs RF, Mika AM, Dickson JM, Pore-filled cation-exchange membranes containing poly(styrene-sulfonic acid) gels. Desalination , 2003 , 159:253-66.

[10] Jiang W, Childs RF, Mika AM, Dickson JM. Pore-filled membranes capable of selective negative rejections. Science and Nature., 2003 , 1(1) 21-6.

[11] Josson G. Coupling of ion fluxes by boundary-, diffusion- and streaming- potentials under reverse osmosis conditions, Proceedings of the 7th. International Symposium on Fresh Water from the Sea , 1980 , 2: 153.

[12] Mika AM, Childs RF, Dickson JM, McCarry BE, Gagnon DR. A new class of polyelectrolyte-filled microfiltration membranes with environmentally controlled porosity. J Membrane Sci , 1995 , 108:37-56.

[13] Mika AM, Childs RF, West M, Lott JNA, Poly(4-vinylpyridine)-filled microfiltration membranes: Physicochemical properties and morphology. J Membrane Sci , 1997;136:221-32.

[14] Mika AM, Childs RF, Dickson JM. Ultra-low pressure water softening: a new approach to membrane construction. Desalination, 1999;121:149-58.

[15] Mika AM, Pandey AK, Childs RF. Ultra-low-pressure water softening with pore-filled membranes. Desalination 2001;140:265-75.

[16] Mika AM, Childs RF, Dickson JM. Salt separation and hydrodynamic permeability of porous membrane filled with pH-sensitive gel. J Membrane Sci 2002;206:19-30.

[17] Nielsen DW, Josson G. Bulk-phase criteria for negative ion rejection in nanofiltration of multicomponent salt solutions. Sep. Sci. and Tech 1994;29(9):1165-82.

[18] Perry M, Linder C. Intermediate reverse osmosis ultrafiltration membranes for concentration and desalting of low molecular weight organic solutions. Desalination 1989;71:223-45.

[19] Petersen RJ. Composite reverse osmosis and nanofiltration membranes. J Membrane Sci 1993;83:81-95 (1993).

[20] Rios GM, Joulie R, Sarrade SJ, Carles M. Investigation of ion separation by microporous nanofiltration membranes. AIChE J 1996; 42(9):2521-2528.

[21] Sourirajan S. Reverse Osmosis, Academic Press, New York. 1970.

[22] Tsuru T, Nakao S, Kimura S. Calculation of ion rejection by extended Nernst-Plank equation with charged reverse osmosis membranes for single and mixed electrolyte solutions. J Chem Eng Japan 1991;24(4):511-7.

[23] Tsuru T, Urairi M, Nakao S, Kimura S. Reverse osmosis of single and mixed electrolytes with charged membranes:

Experiment and analysis, J. Chem. Eng. Japan 1991;24(4):518-524.

[24] Van der Horst HC, Timmer JMK, Leeders RJ. Use of Nanofiltration for concentration and demineralization in the dairy industry: Model for mass transport. J Membrane Sci 1995;104:205-217.

[25] Wang X, Tsuru T, Nakao S, and Kimura S. Electrolyte transport through nanofiltration membranes by the space-charged model and the comparison with Teorell-Myer-Sievers model. J Membrane Sci 1995;103:117-33.

[26] Wang X, Tsuru T, Togoh M, Nakao S, Kimura S. Evaluation of pore structure and electrical properties of nanofiltration membranes. J Chem Eng Japan 1995;28(2):168-92.

Theoretical Analysis of Potential Runoff Energy from a Grid DEM

Chuan Liang [1, 2], Zhongbo Yu [2]

（1. Department of Hydraulic Engineering, Sichuan University, Chengdu, Sichuan 610065, China, Lchester@scu.edu.cn;
2. Department of Geoscience, University of Nevada, Las Vegas, Nevada 454010, USA, Zhongbo@hydro.nevada.edu ）

Abstract: A simple potential runoff index (PRI) concept and its utility for distributed hydrological model is developed to compare a relative degree of potential runoff energy between different watersheds. In general, the actual response of hydrologic processes, while the time of precipitation processes from beginning to end, has closely correlations with the terrain relief on these watersheds, which usually can be expressed through a hypsometric curve. A traditional hypsometric curve was established by a linear regression analysis based on some relief data such as basin area, landform, topographical relief, drainage pattern and so on, but it absent a physically-based distributed hydrological model system and yet cannot be reflected the basin heterogeneities of topography, land cover and soil types so that only be used for local catchment area. Therefore, a new hypsometric curve based on digital elevation model (DEM) is produced in this study. In according with the new hypsometric curve a theoretical lag time of flow (TLTF) was computed, and then the PRI is defined an index which multiply TLTF by the relative catchment area, which the calculation of PRI from a grid DEM is finished automatically through GIS system using ARC/INFO functions. Furthermore, the PRI is used to estimate the potential runoff energy of several sub-basins within the Susquehanna River Basin in Pennsylvania, and the spatially distributive results of PRI are in good agreement with the historical runoff investigations. In addition, the PRI would be used to estimate a synthetic roughness (SR) of watershed, and further to analyze some correlations between SR and flood event, between runoff magnitude and soil moisture, as well as between runoff magnitude and land use or cropping pattern in agriculture, etc. [Nature and Science, 2004,2(1):17-23].

Key words: hypsometric curve; potential runoff index (PRI); distributed hydrological model; a grid DEM

1 Introduction

As well-know the topography of a basin has fundamental effects on its hydrologic response characteristics, the actual response of hydrologic processes has a closely correlation with the terrain relief in anywhere river basin, but both catchment area and landform are two crucial impact parameters (Black, 1996). The both important parameters were skillfully composed by a kind of hypsometric curve (Strahler, 1952) at the same time, which included a lot of topographical features in catchment area of the river basin and provides a visual representation of the watershed's profile too (Jenson, 1988; Verdin, 1999). Once the hypsometric curve is as a kind of cumulative frequency distribution these geomorphologic differences in the watershed can be computed by mathematical statistical analysis of hydrology (Harlin, 1978), for example, a coefficient of skewness will exits a significance correlation with a time of hydrograph peak (Harlin, 1984).

Such a correlation parameters, however, were produced with empirical data during the past decades, and still were incapable of reflecting the reality of water flow in catchment networks until now. Moreover, a traditional hypsometric curve has been created by regression equation based on some relief data such as basin area, landform, topographical relief, drainage pattern and so on, which the hypsometric curve only be used for local catchment area and is improper to apply to distributed hydrological models directly. Consequently, a new hypsometric curve based on digital elevation model in distributed hydrologic model system is developed.

The extraction of potential runoff energy from a grid DEM is one of the essential components of most physically based distributed hydrological models. On the one hand, the spatial distribution of topographic index may be derived from the DEM of the basin

(Jenson, 1993; Quinn, 1995; Yu, 2001a). On the other hand, because land surface of study area is not a homogeneous, a basic strategy to solve this problem is to subdivide the watershed into some different relatively homogeneous parts (Ao, 1999). The main aim of this study focused on the development of a new hypsometric curve using distributed hydrological model system and the assessment of potential runoff energy in the catchment area through the PRI. Meanwhile, in order to make it suitable to handle the spatial heterogeneities of factors such as vegetation, soil properties, etc., a block-wise method use of the new hypsometric curve was proposed for runoff generation in this study.

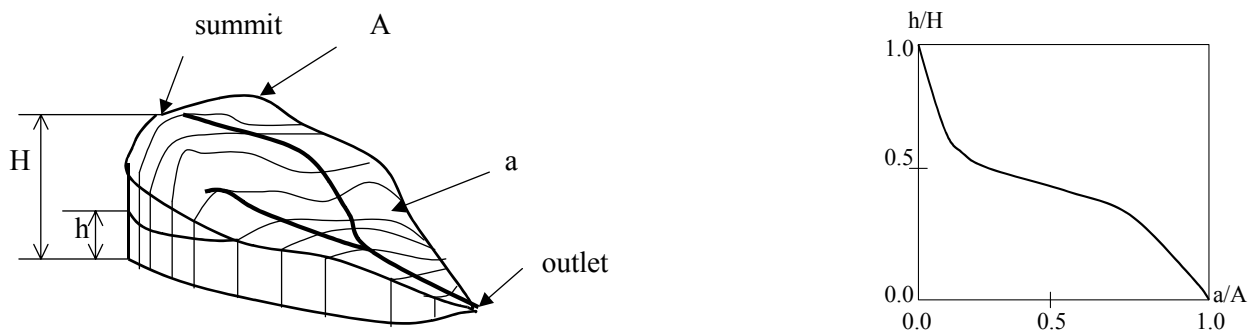

Figure 1 A Catchment area and its general longitudinal section profile

2 Methods

2. 1 Hypsometric curve

Due to hydrological properties of a basin are relative to the geological and topographical features of the ground surface, a new hypsometric curve based on digital elevation model usually describes a correlation both elevation and catchment area in river basin, which can be expressed by a general longitudinal section profile in the watershed as shown in Figure 1. For regional analytical geomorphic research, the axis is plotted as rations of each zone to the total relief or area. Thus, the hypsometric curve is defined by multinomial equation as following

$$y = c_0 + c_1 x + c_2 x^2 + \cdots + c_n x^n \qquad (1)$$

where y is the relative height, $y = h / H$; x is the relative area, $x = a / A$; c_i is multinomial constant coefficient, $0 \le i \le n$, in general, n=3~5 (Harlin, 1978).

2. 2 Theoretical lag time of flow

We assume, when a unit quantity water droplet flows along the longitudinal section profile from top to bottom in the whole hydrological processes, that the time of flowing-through period is called theoretical lag time of flow (TLTF), i.e. so-called lag time of watershed. If any one point $x = x_0$, on the curve of the longitudinal section profile (Figure 2), it can be written into one order integral form (Lou, 1998)

$$\tan\theta = y' = c_1 + 2c_2 x + \cdots + nc_n x^{n-1} \qquad (2)$$

While a unit quantity water droplet m flows down along the longitudinal section profile (impervious), the water droplet has an equilibrant equation at $x=x_0$, namely,

$$mg\sin\theta - \mu mg\cos\theta = ma \qquad (3)$$

Where g is gravity accelerated coefficient, g=9.8 m/s^2; a is a tangential acceleration at $x=x_0$; μ is a

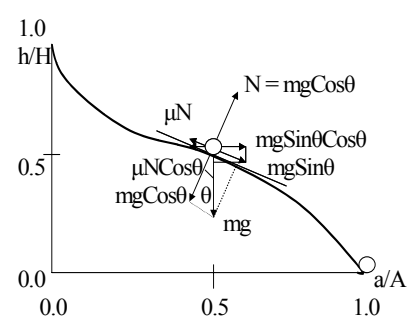

Figure 2 The new hypsometric curve

friction factor, that is as a considerable index reflecting synthetic roughness (SR) of catchment area either.

Furthermore, a horizontal component of the tangential acceleration will be expressed as

$$a_x = a\cos\theta = (g\sin\theta - \mu g\cos\theta)\cos\theta$$
$$= g(\frac{\tan\theta}{1+\tan^2\theta} - \mu\frac{1}{1+\tan^2\theta}) \quad (4)$$

At the moment *t*, if the water droplet has a rate $v_x(t)$ and moves a distance dx in a interval time, from t to *t+dt*, the changing rate is given by

$$dx = v_x dt \quad \text{and} \quad dv_x = a_x dt \quad (5)$$

$$\text{or } dt = \frac{dx}{v_x} \quad (6)$$

by using (5), equation (6) becomes

$$v_x dv_x = a_x dx \quad (7)$$

and integrating equation (7)

$$\frac{v_x^2}{2} = \int_0^x a_x dx \quad (8)$$

combining equation (6) with substituting (8), thus

$$t = \int_0^t dt = \int_0^1 \frac{dx}{v_x} = \int_0^1 \frac{dx}{\sqrt{2\int_0^x a_x dx}} \quad (9)$$

In here, t is called TLTF, which the TLTF is easy to be automatically computed using Newton's law and numerical integral method from a grid DEM in Unix Workstation System (Jenson, 1993; Yu, 2000b). Within equation (9), the gravity acceleration constant has been regularity divided by a difference from summit to outlet in the study watershed.

2. 3 Potential runoff index

If that a "regular lag time" (RLT) of the watershed to be defined by a time of practical observation time divided by relative catchment area, while the actual response of hydrologic processes from summit to outlet on the river basin, the difference between TLTF and RLT exist usually a positive linear correlation, shown in reference (Saghafian, 1995). Therefore, it is possible that a simple potential runoff index (PRI) with multiply TLTF by the catchment area can be as a special index using for compare relative degree of runoff potential energy between different watersheds (Lou, 1997). The PRI is defined as follows:

$$\text{PRI} = \text{TLTE} \times \text{a catchment area} \quad (10)$$

We will pay attention to that TLTF does not directly equal practical observation value (i.e. a lag time of hydrograph peak (LTHP)), but a difference between TLTF and LTHP still performs some important differences of the topographical features in different catchment area. Meanwhile, under the same condition of precipitation the short this TLTF is, the larger the potential runoff energy is, that is, the more the possibility of runoff or flood appears in the watershed.

3 A Grid DEM

For this study, the DEM was generalized to the grid. To extracted topographical features of the study area, an interactive command system called "GRID" in the ARC/INFO package performs such tasks, and the features data obtained from the ARC/INFO processing procedures are in the form of grids, which the elevation at each 3-arc second grid point was assumed to be the average elevation over a 3×3 arc-second rectangle (every grid cell is about 100 m by 100 m).

To improve accuracy for predicting hydrological responses in watershed area, a study basin will be divided into different relatively homogeneous blocks, which size of the blocks depends on the heterogeneity of topography and land cover as well as the basin scale. Each block size is comprised of numerous grid cells but this manageable block size is one in which the friction factor (i.e. SR) can be identified by different soil type or land cover. Based on the subdivision of the basin, the friction factor is calibrated for each block rather than the whole catchment, and synthetic roughness index is also calculated for each block. Through this improvement the heterogeneities of topography, land cover and soil type in a large basin can be approximated. Certainly, this subdividing method is not perfect, but it has the advantages of simplicity and flexibility in using GIS information (Gurmell, 2000).

4 Primary Application

4. 1 Researching basins (Yu, 1999, 2000a, 2001b)

The area of these applications is the Susquehanna River Basin (SRB), which is 80,300 km^2 watershed covering portions of New York, Pennsylvania, and Maryland of the United States. The SRB flows south into the Chesapeake Bay at Baltimore, Maryland (Lakhtakia, 1998). The applicability of the new

hypsometric curve and PRI are examined in four sub-basins within the SRB, in which there are different sizes and various terrain characteristics and show in Table 1 and Figure 3.

Table 1 General description of the four sub-basins in SRB

	Drainage Area (km^2)	H(m)	Streamflow (m^3/sec)	M
WE-38	7.5	267	0.69	0.088
Mt	422	396	1.52	0.085
UWB	7,952	495	2100	0.035
UNB	10,016	495	2810	0.033

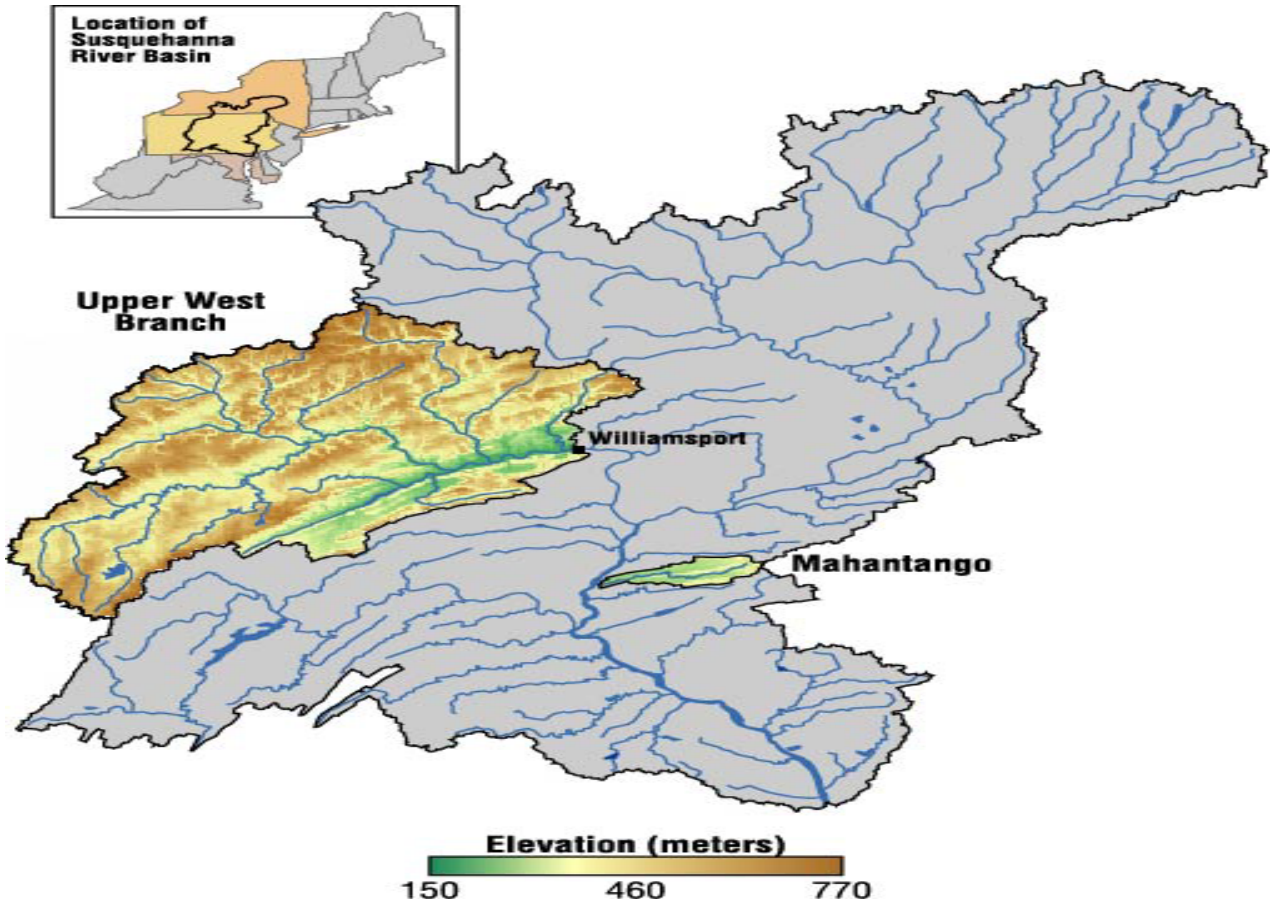

Figure 3 Location map of four sub-basins in susquehanna river basin

The Upper West Branch (UWB) watershed is a sub-basin of the SRB and located in north-central Pennsylvania with an area of 14,710 km^2. The watershed lies within the Appalachian Plateau Physiographic Province and is mainly covered by forest. The stream generally flows east and merges with the Susquehanna River at Williamsport, Pennsylvania. Another sub-basin of the SRB is the upper north branch (UNB) with an area of 27,518 km^2, which lies within the glaciated Appalachian Plateau Physiographic Province. The lower portion of the SRB is in the Appalachian Mountain section of the valley and ridge Physiographic Province. The topography in this region is controlled by a succession of narrow, step-sided ridges and valleys, trending northeast to southwest, and is prone to runoff. Detailed information on climate, soil, vegetation, topography, surface hydrologic parameters, and subsurface hydrology is provided in Yu et al (2000a). One of example is implemented in the WE-38 watershed. The WE-38 is a typical upland agricultural

sub-watershed with a catchment area of 7.29 km^2 in the East Mahantago Creek of the SRB. Elevation within the watershed ranges from 230 m at the watershed outlet to 490 m above sea level (msl) at the top of the watershed divided, and its dip is about 22°-30° from south to north.

4.2 Block-wises use of distributed hydrologic model

The previous generation of hypsometric curve cannot reflect the effects of catchment changes on hydrological responses, and it is incapable of analyzing general and specific hydrological processes, one of main reasons is that the friction factor of the basin has be regardless. Theoretically, since the catchment was divided into blocks by referencing different land cover and soil types in the large watershed a synthetic roughness index can be reflected, while the friction factors were identified for each block rather than the whole basin.

Through this improvement the method simplicity is maintained, the new hypsometric curve can be used to provide a tool to explore general hydrological phenomena or specific runoff processes and to assess the impacts of anthropogenic basin changes on hydrological responses. And then its use of parameters which has a physical interpretation and the representation of spatial variability in parameter values, namely, further to reflect the influences of watershed changes on hydrological responses and be utilized for analyzing hydrologic processes. In the Table 1, for further consider land cover changes and /or influences, the four sub-basins with different friction factor -- natural and spurious pits or sinks, have to be divided into different blocks while used different μ value (assuming μ=0.015-0.250, Beven, 1997).

5 Results and Discussions

The grid DEMs used for the UWB is the USGS 3-arc second data set. Due to efforts of the scale varied in space have influence to the distribution of hypsometric curve; we compare different space scale effects with grid cell sizes or grid spacing of 15m, 50m,100m and 200 m.

5. 1 Effects of grid spacing

From Table 2, it seems that overall hydrological responses with various grid spacing from 15 m to 100 m give the same values both of TLTE and PRI in SRB. This is because the scale of grid size cannot change the distribution of hypsometric curve (Kalma, 1995), yet the potential runoff energy on the catchment area has not relationship with the scale of grid size in different distributed hydrologic model.

All of calculation results of PRI and relative streamflow of the catchments are shown in Figure 4. The practical application results in Susquehanna River Basin indicated that the response of runoff has marked correlation with topographical relief and that PRI compare well with the data of historical runoff record, and the relative coefficient of squared value on the chart is calculated about 0.992.

5. 2 Validation of land cover

Figure 4 or Table 3 shows the calculate resu-lts of TLTE and PRI of μ=0 are larger than that of μ≠0, which reflect the storage effect of land cover in the watershed. Obviously, the land cover is a very important factor to decide runoff processes in the catchment area. In the traditional hypsometric curve, hydrologic heterogeneity-ies such as topography, land use and soil properties have been considered as homogeneous, therefore traditional

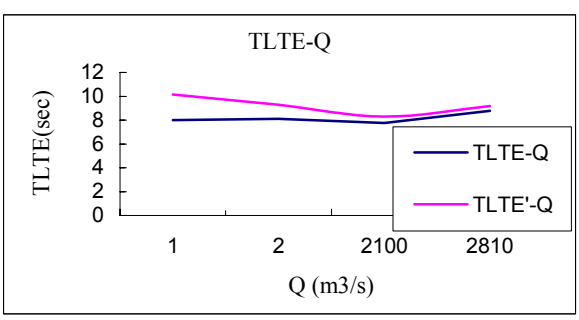

(a) Relationship of TLTE with different μ value (Scale: 100 m×100 m)

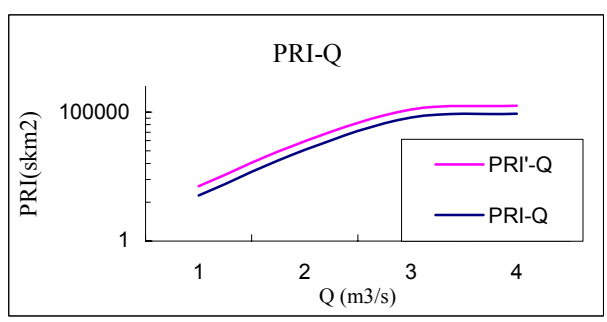

(b) Relationship of PRI with different μ value (Scale: 100 m×100 m)

Figure 4 The correlation between TLTE or PRI and streamflow of study areas

Table 2 TLTE and PRI of the Four Sub-basins in SRB

	TLTE				PRI			
Scale	15m	50m	100m	200m	15m	50m	100m	200m
WE-38	8.04	8.04	7.88	7.96	58.52	58.77	59.12	62.05
Mt	8.12	8.12	8.12	8.12	3424	3424	3424	3426
UWB	7.77	7.77	7.77	7.77	61773	61771	61771	61774
UNB	8.78	8.78	8.78	8.78	87942	87943	87915	87911

Table 3 Comparison of the values of TLTE and PRI

	M	TLTE	PRI	M	TLTE'	PRI'
WE-38	0.0	7.99	59	0.088	10.15	74
Mt	0.0	8.12	3425	0.085	9.29	3921
UWB	0.0	7.77	61772	0.035	8.01	63712
UNB	0.0	8.78	87928	0.033	9.18	91918

approaches are unable to provide insights into the understanding of the effects of hydrologic processes. On the contrary, a new distributed hypsometric curve emphasize spatially heterogeneity within individual grid cells and employ digital elevation model data to account for heterogeneity, so that a more realistic representation of spatial variations of various hydrologic processes is obtained.

5. 3 Treatment of special areas within grid DEM

Most pits are considered to be spurious, and large-scale pits are generally rare, it is, a fact that the percentage of pits in existing DEM is relatively low. We also compare the results both of original and filled terrain, the rations of removing or filling pit is usually small than 3% of the whole grid cells in SRB, so whether or not the pits and depressions have be filled do not yield deviation significantly either (Figure 4 (c)). In fact, whatever the creating methods or data sources of available a grid DEM, such as by interpolation from contour maps, i.e. by image correlation devices from aerial photographs including satellite imagines and regardless of its resolution. In natural landscapes, particularly in large scale, pits and flat surfaces are relatively rare (Garbercht, 1997) but in currently available various grid spacing, about 5% of grid points are pits (limited investigation).

The PRI, however, is also considered an index of hydrologic similarity and expressed as a distribution function. Because whether any watershed has a higher PRI will depend on some elements such as climatic condition, precipitation intensity and duration etc, so that the PRI can be used to compare the relative degree between different watersheds where happening runoff.

By the way, some relative index influencing runoff such as precipitation, infiltration and soil moisture didn't be considered in this study, but PRI still can be used to express a different potential runoff energy between different watersheds under above mentioned conditions.

6 Summary

From the foregoing discussions, we can see that topography and land cover predominantly affected the hydrological response process and pattern in a basin. The new hypsometric curve from a grid of digital elevation model had been given a simpler and efficient method to describe topographical features in the river basin, which is easy to be used for distribute hydrological modeling. Based on the new hypsometric curve the potential runoff index (PRI) is produced in this study. Under the influences of different terrain relief and relative drainage area, a PRI reflects the response of precipitation in researching watershed, and shows that the hydrologic possess and the potential runoff energy to compare with other watershed. Accordingly, through the conclusions derived from the above applications, it can be concluded that the PRI has broad applicability and can be used for different purposes; it can be applied to different catchments of

various sizes and to simulate the hydrological response processes in a basin; it is able to applied to un-gauged basins for hydrological simulations; and it can be used as a basic tool for finding out the relationship between model parameter values and GIS information, as well as for analyzing the effects of human influences on runoff characteristics through runoff simulations.

Acknowledgment

This study was partly funded by NASA and EPA. All computations were performed on the Unix workstation of Hydro-Computing Laboratory in the Department of Geosciences at UNLV.

References

[1] Ao TQ, Ishidaira H, Takechi K. Study of distributed runoff simulation model based on block type TOPMODEL and Muskingum-Cunge method. Annual Journal of Hydraulic Engineering (JSCE) , 1999 , 43:7-12.

[2] Beven KJ. TOPMODEL: A critique, hydrological processes. Special issue: TOPMODEL , 1997 , 11(9):1069-85.

[3] Black PE. Watershed Hydrology, Syracuse, New York , 1996.

[4] Garbrecht J, Martz LW. The assignment of drainage direction over flat surfaces in raster digital elevation models. J of Hydrology , 1997 , 193(1-4):204-13.

[5] Gurmell AM, Montgomery DR. Hydrological applications of GIS, Chichester, Wiley, New York , 2000.

[6] Harlin K. Statistical moments of the hypsometric curve and its density function, mathematical geology , 1978 , 10:59-72.

[7] Harlin K. Watershed morphometry and time to hydrograph peak. Journal of Hydrology , 1984 , 67:141-54.

[8] Jenson SK, Domingue JO. Extracting topographic structure from digital elevation data for geographic information system analysis, photogrammetric engineering and remote sensing , 1988 , 54(11):1593-600.

[9] Jenson SK. Application of Hhydrologic information Aautomatically Eextracted from Ddigital Eelevation Mmodel, Tterrain Aanalysis and Ddistributed Mmodelling in Hhydrology. John Wiley and Sons, 1993 , 35-48.

[10] Kalma JD, Sivapalan M. Scale issues in hydrological modelling, Chichester, New York, Wliey., 1995.

[11] Lakhtakia MN, Yarnal B, Johnson DL, White RA, Miller DA, Yu Z. A simulation of river-basin response to mesoscale meteorological forcing: the Susquehanna River Basin Experiment (SRBEX). Journal of American Water Resources Association , 1998 , 34(4):921-37.

[12] Lou W. Time to hydrograph peak and hypsometric curve. Geological society of america abstracts with programs,1997 , 29(7):330-4

[13] Lou W. Hypsometric analysis with a geographic information System, computers and geosciences. 1998 , 24(8):815-21.

[14] Quinn PF, Beven KJ, Lamb R. The ln(α/tanβ) index: How to calculate it and how to use it in the TOPMODEL framework. Hydrological Processes , 1995 , 9:161-82.

[15] Strahler AN. Hypsometric (Area-Altitude) analysis of erosion topography. Bulletin of Geological Society of America , 1952 , 63:1117-41.

[16] Verdin KL, Verdin JP. A topological system for delineation and codification of the earth's river basins. Journal of Hydrology , 1999 , 218:1-12.

[17] Yu Z, Lakhtakia MNB, Yarnal DL, Johnson RA.Simulating the river-basin response to atmospheric forcing by linking a mesoscale meteorological model and a hydrologic model system. Journal of Hydrology , 1999 , 218:72-91.

[18] Yu Z, Gburek WJ, Schwartz FW. Evaluating the spatial distribution of water balance in a small watershed, Pennsylvania. Hydrologic Processes , 2000a , 14(5):941-56.

[19] Yu Z, Schwartz FW. Assessing the response of sub-grid hydrologic processes to atmospheric forcing with a hydrologic model system. Global Planet, Change , 2000b , 25:1-17.

[20] Yu Z, Carlson TN, Barron EJ, Schwartz FW. On evaluating the spatial-temporal variation of soil moisture in the Susquehanna River Basin. Water Resources Research , 2001a , 37(5):1313-26.

[21] Yu Z, White RA, Guo YJ, et al. Stormflow simulation using a geographical information system with a distributed approach. Journal of the American Water Resources Association, 2001b;37(4):1-15.

Ideal Interval Method Based Model for Water Quality Evaluation

Juliang Jin [1], Shujuan Wang [1], Yiming Wei [2]

(1.College of Civil Engineering, Hefei University of Technology, Hefei, Anhui 230009, PRC, jinjl66@xinhuanet.com;
2. Institute of Policy and Management, Chinese Academy of Sciences, Beijing 100080, China)

Abstract: The key of water quality evaluation is to establish the nonlinear relation between water quality indexes and water quality grades. Nowadays only evaluation criterion of water quality, which is expressed by interval concept, reflects this relation information during practical evaluation process. For this reason, a new model for water quality evaluation is presented based on improved ideal interval method with using accelerating genetic algorithm (IIM-WQE). Research results show that IIM-WQE is directly driven by the example series produced from evaluation criterion of water quality, and water quality relative grades computed by using all membership degrees information are regarded as evaluation results of water quality, which can avoid distorting when using the principle of maximum membership degree and can heighten precision of water quality evaluation. IIM-WQE is visual, handy and universal, which can widely be applied to different system evaluations if only evaluation criterion or samples of evaluation indexes and evaluation result values are known. [Nature and Science 2004,2(1):24-28].

Key words: water environment systems engineering; evaluation of water quality; ideal interval method; genetic algorithm; relative membership degree

1 Introduction

Water Quality Evaluation (WQE) is to comprehensively evaluate water quality grades according to evaluation criterion of water quality and water quality indexes. It is very important to heighten the scientific level of water planning management and prevention and control of water pollution, to promote sustainable development of regional society, economy, resource and environment (Chen, 1998; Jin, 2002). Due to the incompatibility of evaluation results among individual water quality index of real water, it will lack practice for judgment of evaluate water quality grades by using evaluation criterion table of water quality directly, for this reason, many evaluation methods have been presented now. Each method has its applicability (Chen, 1998; Jin, 2000; 2001a; 2002a; 2002b; Hu, 1998). All the essences of these methods are try to describe the complex nonlinear relation between evaluation indexes and water quality grades, while nowadays only evaluation criterion of water quality which is expressed by interval concept (Chen, 1998; Hu, 1998) reflects this relation information during practical evaluation process. For this reason, in this paper a scheme of ideal interval method applied to evaluation of water quality, named IIM-WQE for short, is presented based on Yang (2003) and accelerating genetic algorithm (AGA) (Jin, 2001b; 2002a). The evaluation results of IIM-WQE continuous are real number values, so its evaluation precise is high. In the end an application case of IIM-WQE was done.

2 Establishment of IIM-WQE

Suppose evaluation criterion of water quality is $\{([a^*(i,j), b^*(i,j)], i)|i=1\sim ni, j=1\sim nj\}$. Where $a^*(i,j)$ and $b^*(i,j)$ are lower limit and upper limit of variation interval, which is named ideal interval (Yang, 2003) of ith water quality grade jth evaluation index respectively; i is criterion grade value of ith water quality grade; ni and nj are the number of grades and evaluation indexes of water quality evaluation criterion respectively. IIM-WQE establishment procedure includes four steps as follows:

Step1: to create sample series of water quality evaluation criterion randomly and standardize them. Produce uniformly and randomly nu index sample values $x^*(k,j)$ in the variation interval of each index , corresponding criterion grade values are $y(k)=i$; in order to fully reflect the importance of border values of each index in evaluation criterion, select each border value of indexes once, and corresponding criterion grade value is the average of the two criterion grades values related to this border value. Thus sample series of water quality evaluation criterion $\{x^*(k,j), y(k)\}|k=1\sim nk, j=1\sim nj\}$ are

obtained, where *nk* is the number of the samples. In order to eliminate dimensional effect, and to make IIM-WQE have universality, the indexes are treated as follows:

$$x(k,j) = x^*(k,j)/x_{\max}(j) \quad (k=1\sim nk,\ j=1,nj) \tag{1}$$

$$a(i,j) = a^*(i,j)/x_{\max}(j) \quad (i=1\sim ni,\ j=1,nj) \tag{2}$$

$$b(i,j) = b^*(i,j)/x_{\max}(j) \quad (i=1\sim ni,\ j=1,nj) \tag{3}$$

where $x_{\max}(j)$ is the maximum of the *j*th evaluation index in water quality evaluation criterion, that is $x_{\max}(j) = \max_i\{b(i,j)\}$.

Step 2: to compute the distance $D(k,i)$between criterion sample $x(k,j)$ and ideal interval of criterion grade $[a(i,j),\ b(i,j)]$:

$$D(k,i) = \sum_{j=1}^{nj} w(j)d(k,i,j) \tag{4}$$

$$d(k,i,j) = \begin{cases} a(i,j) - x(k,j), x(k,j) < a(i,j) \\ 0, x(k,j) \in [a(i,j), b(i,j)] \\ x(k,j) - b(i,j), x(k,j) > b(i,j) \end{cases} \tag{5}$$

where $w(j)$ is the weight of the *j*th index, it can be determined by consulting expert with subjective weight method based on the analytic hierarchy process, by objective weight method based on projection pursuit according to the sample series of water quality criterion (Jin, 2001a; 2002a), or by combining the subjective weight and objective weight; where $k=1\sim nk$, $i=1\sim ni$, $j=1\sim nj$.

Step 3: to compute relative membership degree values $r(k,i)$ of the sample $\{x(k,j)\}$ relative to criterion grade ideal interval:

$$r(k,i) = e^{-cD(k,i)} / \sum_{i=1}^{ni} e^{-cD(k,i)} \tag{6}$$

where *c* is a model parameter, it is a constant more than 1 generally. The more *c* is, the more easily criterion sample $x(k,j)$ tend to criterion grade which has small relative membership degree $D(k,i)$. In order to avoid a distorting judgment by using maximum membership degree rule, to utilize all the relative membership degree information, and to make the judgment more accord with apply the fact, water quality relative grade (Chen, 2002) can be adopted as computed value of water quality criterion grade which corresponds to the criterion sample $x(k,j)$:

$$h(k) = \sum_{i=1}^{ni} r(k,i)i \tag{7}$$

And then *c* can be optimized by solving equations (8)

$$\min \quad f(c) = \sum_{k=1}^{nk} |h(k) - y(k)| \tag{8}$$

AGA is a universal global optimization method, which simulates best selected and bad abandoned principle and chromosome population information exchange mechanism in the creation evaluation process. It is more handy and effective to solve optimization problem like equations (8). The detail algorithm of AGA can be seen in Jin (2002a) or Jin (2001b).

Step 4: to comprehensively evaluate water quality grade. Suppose each water quality evaluation index of researched water sample is $\{z^*(k,j)|k=1\sim nz,\ j=1\sim nj\}$, where nz is the number of water samples needed evaluation. Replace $x^*(k,j)$ with $z^*(k,j)$, put it into equations (1), and then water quality grade $h(k)$ ($k=1\sim nz$) can be computed corresponding to evaluation example according to equations from (2) to (8).

3 Case Study

Now as is a case, rich nutrient comprehensive evaluation of lake water environment quality illustrates the process of applying IIM-WQE. Evaluation criterion of lake water environment quality (Hu, 1998) is seen in Table 1, where the left end value of ideal interval of the first water quality grade of TP, TOD, TN indexes, and the right end value of that of transparency index are determined by the authors.

Table 1 Evaluation criterion of lake water environment quality (Hu, 1998)

evaluation index	water quality grade				
	even poor nutrition	poor nutrition	middle nutrition	rich nutrition	even rich nutrition
	1st grade	2nd grade	3rd grade	4th grade	5th grade
TP(μg/L)	[0, 1]	[1, 4]	[4, 23]	[23, 110]	[110, 660]
TOD(mg/L)	[0.00, 0.09]	[0.09, 0.36]	[0.36, 1.80]	[1.80, 7.10]	[7.10, 27.10]
Transparency(m)	[37, 74]	[12, 37]	[2.4, 12]	[0.55, 2.4]	[0.17, 0.55]
TN (mg/L)	[0.00, 0.02]	[0.02, 0.06]	[0.06, 0.31]	[0.31, 1.20]	[1.20, 4.60]

According to Table 1 and step 1 of IIM-WQE modeling, evaluation criterion sample series composed of 54 sample dots from No.1 to No.54 shown in Table 2 can be gained. Transform the 54 indexes sample values $\{x^*(k,j)|k=1\sim54,\ j=1\sim4\}$ to $\{x(k,j)|\ k=1\sim54,\ j=1\sim4\}$ according to equations (1), scale each interval in Table 1 by using equations (2) and equations (3), each index weight is 1/4, calculate evaluation criterion grade of water quality $h(k)$ (k=1~54) by using equations from (4) to (7), put them to equations (8) with $\{y(k)|k=1\sim54\}$, solve equations (8) by using AGA, and obtain the optimum evaluation value of c which is 99.888, and the corresponding minimum of objective function $f(c)$=2.771. Error analysis between evaluation criterion grades of water quality and grades of IIM-WQE are shown in Table 3 when c=99.888. Table 2 and Table 3 show that the nonlinear relation between water quality indexes and water quality grades described by IIM-WQE is satisfied. So IIM-WQE can be used to evaluate rich nutrition grades of the five lake water quality, its result is shown in Table 4, where the evaluation results of other methods are also listed. Table 5 shows the distances and membership degree values between lake water quality samples and ideal intervals of criterion grades.

Table 2 Comparison results between evaluation criterion samples of water quality and values of IIM-WQE

No.	water quality index				water quality grade		No.	water quality index				water quality grade	
	TP (μg/L)	TOD (mg/L)	transparency (m)	TN (mg/L)	criterion	IIM-WQE		TP (μg/L)	TOD (mg/L)	transparency (m)	TN (mg/L)	criterion	IIM-WQE
1	0.658	0.059	50.857	0.001	1.000	1.008	28	12.631	0.479	4.738	0.257	3.000	3.045
2	0.559	0.051	42.650	0.015	1.000	1.120	29	7.879	1.129	4.840	0.249	3.000	3.074
3	0.106	0.034	67.902	0.009	1.000	1.000	30	14.074	1.405	3.723	0.140	3.000	3.102
4	0.978	0.061	42.207	0.010	1.000	1.137	31	21.122	1.442	3.487	0.142	3.000	3.151
5	0.646	0.051	47.659	0.015	1.000	1.025	32	9.431	0.655	11.033	0.091	3.000	2.729
6	0.078	0.056	73.851	0.010	1.000	1.000	33	23.000	1.800	2.400	0.310	3.500	3.499
7	0.742	0.086	54.876	0.013	1.000	1.002	34	36.301	2.753	1.872	0.802	4.000	3.986
8	0.607	0.014	54.330	0.011	1.000	1.003	35	63.988	3.232	1.064	1.159	4.000	4.003
9	0.142	0.029	43.305	0.000	1.000	1.089	36	84.708	4.817	2.045	0.465	4.000	3.998
10	0.316	0.003	48.395	0.008	1.000	1.018	37	95.742	5.358	0.594	0.805	4.000	4.013
11	1.000	0.090	37.000	0.020	1.500	1.500	38	50.872	5.349	0.816	1.151	4.000	4.015
12	2.790	0.195	14.496	0.040	2.000	2.241	39	34.379	2.639	2.191	0.917	4.000	3.990
13	3.862	0.356	18.619	0.049	2.000	2.090	40	87.044	3.024	1.423	0.856	4.000	4.000
14	3.569	0.338	12.537	0.055	2.000	2.440	41	32.149	4.351	1.692	0.382	4.000	3.965
15	1.816	0.300	14.218	0.034	2.000	2.263	42	84.474	1.817	1.552	1.138	4.000	4.001
16	3.011	0.268	29.132	0.057	2.000	1.959	43	67.301	3.868	2.334	0.758	4.000	3.998
17	1.060	0.132	25.247	0.059	2.000	1.994	44	110.000	7.100	0.550	1.200	4.500	4.500
18	3.368	0.187	33.033	0.034	2.000	1.832	45	649.959	21.826	0.210	3.396	5.000	5.000
19	3.842	0.324	20.456	0.036	2.000	2.044	46	161.122	19.802	0.428	3.580	5.000	5.000
20	3.889	0.299	17.987	0.058	2.000	2.109	47	281.367	10.708	0.515	2.934	5.000	5.000
21	3.414	0.270	18.595	0.033	2.000	2.076	48	443.507	26.418	0.364	2.626	5.000	5.000
22	4.000	0.360	12.000	0.060	2.500	2.501	49	355.354	8.808	0.438	2.126	5.000	5.000
23	21.883	1.292	8.447	0.165	3.000	2.999	50	549.721	9.753	0.250	2.602	5.000	5.000
24	10.488	0.797	2.943	0.196	3.000	3.088	51	184.419	11.128	0.263	3.523	5.000	5.000
25	13.009	1.414	9.719	0.197	3.000	2.966	52	342.262	24.807	0.370	2.658	5.000	5.000
26	9.853	1.116	6.878	0.255	3.000	3.026	53	181.062	12.666	0.274	2.875	5.000	5.000
27	9.925	1.479	6.117	0.079	3.000	3.002	54	233.632	26.579	0.250	1.943	5.000	5.000

Table 3 Error analysis between evaluation criterion grades of water quality and grades of different models

Evaluation method	percent of absolute error falling the following range (%)						mean absolute error (grade)	mean relative error (%)
	[0, 0.1]	[0, 0.2]	[0, 0.3]	[0, 0.4]	[0, 0.5]	[0, 0.6]		
pp method[5]	48.00	68.00	92.00	92.00	96.00	100.00	0.15	7.74
interpolation method[6]	89.66	93.10	93.10	94.83	98.28	100.00	0.05	1.58
IIM-WQE	81.48	92.59	98.15	98.15	100.00	100.00	0.05	2.65

Table 4 Computed grades of five lakes water quality by using different model

Lake	water quality index				computed water quality grades of different models			
	TP (μg/L)	TOD (mg/L)	Transparency (m)	TN (mg/L)	NN[3]	Logistic curve[4]	interpolation[6]	IIM-WQE
Hangzhou Xi Lake	130	10.30	0.35	2.76	5	4.92	4.860	5.000
Wuhan Dong Lake	105	10.70	0.40	2.00	4	4.80	4.546	4.999
Qinghai Lake	20	1.40	4.50	0.22	3	3.09	3.028	3.150
Chao Lake	30	6.26	0.25	1.67	4	4.59	4.058	4.241
Dian Lake	20	10.13	0.50	0.23	4	3.67	3.638	3.998

Table 5 Distance and membership degree values between lake water quality samples and ideal intervals

lake	distance between lake water quality samples and ideal intervals of criterion grades					membership degree values between lake water qualities samples and ideal intervals of criterion grades				
	1st grade	2nd grade	3rd grade	4th grade	5th grade	1st grade	2nd grade	3rd grade	4th grade	5th grade
Hangzhou Xi Lake	0.416	0.326	0.259	0.123	0.000	0.000	0.000	0.000	0.000	1.000
Wuhan Dong Lake	0.369	0.278	0.212	0.077	0.002	0.000	0.000	0.000	0.001	0.999
Qinghai Lake	0.140	0.050	0.000	0.017	0.153	0.000	0.006	0.838	0.156	0.000
Chao Lake	0.282	0.191	0.125	0.027	0.038	0.000	0.000	0.000	0.759	0.241
Dian Lake	0.235	0.144	0.083	0.034	0.087	0.000	0.000	0.007	0.988	0.005

Table 3, Table 4 and Table 5 show that: 1) The evaluation results of IIM-WQE are the same as other methods basically. 2) According to the evaluation criterion of environment quality in Table 1, the results of IIM-WQE are reasonable. 3) The results of IIM-WQE that the water quality grades of these five lake from big to small are Hangzhou Xi Lake, Wuhan Dong Lake, Chao Lake, Dian Lake, and Qinghai Lake in turn, where the first two lakes can be judged as 5th grade (even rich nutrition), the later lake can be judged as 3rd grade (middle nutrition), the rest can be judged as 4th grade (rich nutrition).

4 Conclusion

In order to describe the nonlinear relation between water quality indexes and water quality grades, a new method for water quality evaluation based on improved ideal interval method and accelerating genetic algorithm (IIM-WQE) is presented. IIM-WQE belongs to non-function model evaluation methods, its evaluation process is directly driven by sample series produced from water quality evaluation criterion, which overcomes the difficulty how evaluation function relation between evaluation indexes and evaluation grades is reasonably structured. The results of IIM-WQE are of real values, high precision. IIM-WQE is visual, handy and universal, which can widely be applied to system evaluation of evaluation criterion or evaluation indexes and comprehensive evaluation values are known.

Acknowledge

Foundation Item: The Excellent Young Teachers Program in Higher Education Institute of MOE, P.R.C.

[Department of Education and Person (2002)350], Anhui Provincial Science and Technology Fund of Excellence Youth, Anhui Provincial Natural Science Foundation (No. 01045102), Chinese National Natural Science Fund Project (No. 40271024).

References

[1] Chen S. Fuzzy optimum recognition theory and application for complex water resource system[M]. Changchun: Jilin University Press, 2002.

[2] Chen S. Theory and Application for Engineering Fuzzy Sets[M]. Beijing: Chinese National Defence Industry Press, 1998.

[3] Hu M, Guo D. Fuzzy Neural Network Method for Evaluation of Lake Water Quality Rich Nutrition[J]. Chinese Environment Science Research, 1998,(4):40-2.

[4] Jin J, Din J, Water Resource Systems Engineering[M]. Chendu: Science and Technology Press of Sichuan, 2002a.

[5] Jin J, Wei Y, Din J. Projection Pursuit Model for Comprehension Evaluation of Water Quality[J]. Chinese Journal of Environment Science, 2001a,21(4):431-434.

[6] Jin J, Wei Y, Fu Q, *et al.* An Interpolation Model for Comprehensive Evaluation of Water Quality [J]. Chinese Journal of Water Hydraulic, 2002b,(12): 91-4, 100.

[7] Jin J, Yang X, Din J. Improvement of Standard Genetic Algorithm-Accelerating Genetic Algorithm[J]. Systems

Engineering—Theory & Practice, 2001b , 21(4):8-13.

[8] Jin J, Yang X, Jin B, et al. New Model for Comprehensive Evaluation of Water Environment Quality[J]. Chinese Environment Monitor ,2000, 16(4):42-7.

[9] Yang X, Yang Z, Li J, et al. Comprehensive Evaluation of Atmosphere, Environment Quality for Multi-objective Decision-IIM[J]. Chinese Environmental Engineering, 2003, 21(3):70-2.

Technique of Animal Clone

Hongbao Ma

(Michigan State University, East Lansing, MI 48823, USA, hongbao@msu.edu)

Abstract: Animal clone as an exciting but criticized topic technique in the life science is extracting the whole human community's attention. Even with ethnic and safety concern, nobody can prevent the development of the animal clone science. This article is describing the principle techniques for the animal clone as the reference for the scientists and anyone who is interested in this field. [Nature and Science, 2004,2(1):29-35].

Key words: animal; clone; cell; technique

1 Introduction

Clone is a hot topic but the definition of clone sometimes is confused. Here are the several reasonable explanations for the clone:

As a none:

(1) A cell, group of cells, or organism that is descended from and genetically identical to a single common ancestor, such as a bacterial colony whose members arose from a single original cell.

(2) An organism descended asexually from a single ancestor, such as a plant produced by layering or a polyp produced by budding.

(3) A DNA sequence, such as a gene, that is transferred from one organism to another and replicated by genetic engineering techniques.

(4) Individual organisms that arise asexually from the somatic, or body, cells of the parent rather than from the specialized sexual cells.

As a verb:

(1) To make multiple identical copies of (a DNA sequence).

(2) To create or propagate (an organism) from a clone cell.

(3) To reproduce or propagate asexually.

(4) To produce a copy of one thing.

According to the report of American Cable News Network (CNN) on 2 February 12, 2004, South Korean researchers reported they have created human embryos through cloning and extracted embryonic stem cells, the universal cells that scientists expect will result in breakthroughs in medical research. But, it is illegal to clone human cells in the United States and the offense is punished in Michigan of USA with $1 million fine and 10 years in jail. However, it is legal to study the animal clone.

Seventy years ago, cloning was a work used mainly in pant research and application. Now, the clone can be done in all the kinds of living things, including human being. Cloning creates a genetically identical copy of an animal or plant. Transgenic animal and clone for the study of gene regulation and expression has become commonplace in the modern biological science now (Pinkert, 1999). The sheep Dolly was the world's most famous clone animal, but it was not the first one. Many animals - including frogs, mice, sheep and cows had been cloned before Dolly. Plants have been often cloned since ancient people. Human identical twins are also clones. Dolly was the first mammal to be cloned from an adult cell, rather than an embryo. This was a major scientific achievement of Dolly, but also raised scientific and ethical concerns. Since Dolly was born in 1996, many other animals have been cloned from adult cells, such as mice, pigs, goats and cattle, etc. Cloning by interspecies nuclear transfer offers the possibility of keeping the genetic stock of those species on hand without maintaining populations in captivity (Lanza, 2002), but also possibly creates the risk of biological calamity.

Recent years, many various species and cells from which viable somatic cell were cloned offspring have been produced. Production of mammals by nuclear transfer has become a useful tool for propagating valuable animals and can be used as a method to produce genetically modified animals (Niemann, 2003). But, the use of the technology has been limited because of the low survival rate of fetuses during the last trimester of gestation and compromised postnatal health of the offspring. There are many factors for the inefficiencies not fully understood, which may be

related to many factors such as the oocyte-donor cell interaction, the stage of the donor cell cycle, inadequate placentation, inappropriate or incomplete nuclear reprogramming following nuclear transfer, and the type of donor cell used. Now, the high rate of fetal loss in the third trimester and the increased calf loss in the first month of life in clones compared with conventional pregnancies and calves are primary limitations for the widespread application of this technology (McEvoy, 2003).

The stage of the donor cell cycle is a major factor in the success of nuclear transfer in mammals. Quiescent donor cells arrested in the G0 or G1 stage of the cell cycle have been used to produce cattle, pigs, mice, and sheep. Methods of arresting cells in this phase of the cell cycle have been explored using reversible cycle inhibitors, however, serum starvation is often used as a donor cell treatment prior to nuclear transfer (Gibbons, 2002).

Gene therapy can be defined as the deliberate transfer of DNA for therapeutic purposes. Many serious diseases such as the tragic mental and physical handicaps caused by some genetic metabolic disorders may healed by gene transfer protocol. Gene transfer is one of the key factors in gene therapy (Matsui, 2003), and it is one of the key purposes of the clone.

This article will describe the technique of the animal clone.

2 Materials and Methods

2.1 Cell preparation and culture

A primary cell line is isolated from a mature animal (such as a sheep). After isolated, cells are washed in Dulbecco minimal essential medium (DMEM) supplemented with 10% fetal calf serum (FCS) and 1% (v/v) penicillin/streptomycin, and the cells are seeded into six-well culture plates following typical cell culture techniques. Following the first passage, cells are grown to confluence and frozen in DMEM-F12 supplemented with 20% FCS and 10% dimethyl sulfoxide. After thawing, cells are cultured in DMEM supplemented with 10% FCS and 1% (v/v) penicillin/streptomycin to approximately 80% confluence (passages 2–5). Approximately half of the cells are allocated to be treated with culture medium containing 15 μM roscovitine (for approximately 24 hours prior to nuclear transfer), and the remaining cells are cultured with medium supplemented with 0.5% FCS (for 72 hours prior to nuclear transfer). The roscovitine-treated cells are exposed to the inhibitor throughout the nuclear transfer process. Donor cells to be submitted for flow cytometry sorting are trypsinized, centrifuged, and resuspended in 1 mL of physiological buffered solution (PBS). Cells are first incubated with DNase-free RNase A for 30 min at 37°C, then with 1 mg/mL propidium iodide for 10 min at 25°C before being processed on the flow cytometer (Campbell, 1999).

2.2 Oocyte preparation and nuclear transfer

Recipient oocytes are washed and selected after they are removed from animal. Only oocytes that have a homogenous cytoplasm and at least three layers of cumulus cells are selected for *in vitro* maturation. *In vitro* maturation medium consisted of tissue culture medium (TCM 199) supplemented with 10% FCS, 50 μg/mL sodium pyruvate, 1% penicillin/streptomycin (v/v), 1 ng/mL recombinant insulin-like growth factor 1, 0.01 U/mL bovine luteinizing hormone (LH), and 0.01 U/mL bovine follicle-stimulating hormone (FSH). Selected oocytes are placed in 0.5 mL of maturation medium overlaid with mineral oil (0.4 mL) and incubated for 16–18 hours at 37°C in 5% CO_2 and air. After maturation, oocytes are vortexed to remove expanded cumulus cells and stained with Hoechst 33342 (2 μg/mL) for the observation of DNA (chromatin). To make sure the enucleation, ultraviolet light is used to check DNA located in the polar body and the metaphase plate. Donor cells are trypsinized, pelleted, and resuspended in DMEM supplemented with either 0.5% FCS (serum starved) or 10% FCS and 15 μM roscovitine prior to transfer into recipient oocytes. Donor cells (one per oocyte) are microsurgically placed into the perivitelline space evacuated during enucleation, ensuring intimate contact between the donor cell and the recipient oocyte (Houdebine, 2003).

2.3 Nuclear transfer unit fusion and activation

The donor cell and recipient cytoplasm of the nuclear transfer couplets are fused approximately 22–24 hours postmaturation by a single direct electrical pulse (40 V) delivered through needle-type electrodes. Fusion took place in Zimmermann cell fusion medium by placing an electrode on each side of the nuclear transfer couplet (approximately 0.15 mm apart) and arranging the couplet so that the 20 μsec pulse is delivered perpendicular to the shared membrane space

of the donor cell/cytoplasm. A sample of couplets is examined 1 hour after the pulse to determine fusion efficiency. Activation of the couplets is performed beginning 2 hours after fusion as described previously, using TCM 199 plus 1.0% FCS supplemented with cytochalasin B (5 µg/mL), cycloheximide (10 µg/mL), and calcium ionophore (5 mM) for 10 min followed by TCM 199 plus 10.0% FCS supplemented with only cytochalasin B (5 µg/mL) and cycloheximide (10 µg/mL) for 1 hour in 5.0% CO_2 and air. A 5-hours culture period in TCM 199 plus 10.0% FCS and cycloheximide (10 µg/mL) alone is conducted under low oxygen tension (5.0% CO_2, 5.0% O_2, 90.0% N_2). Following activation, reconstructed embryos are cultured in BARC medium under low oxygen (5.0%) for 7 or 8 days (Chesne, 2002; Faurie, 2003).

2.4 Embryo transfer

Embryos that reaches the blastocyst stage are transferred into recipient animals approximately 7 days after synchronized estrus. One or two embryos per recipient are nonsurgically introduced into the uterine horn ipsilateral to the ovary containing a palpable corpus luteum. Pregnancy evaluation is performed using transrectal ultrasound approximately 21 days following embryo transfer (Day 28 of gestation). Recipients diagnosed as pregnant are evaluated weekly until approximately 100 days of gestation and then monthly thereafter to study fetal development. During the last month of gestation, recipients are monitored several times each week through palpation to evaluate the health of fetus. Recipients that are ketotic in the third trimester are treated with standard protocols, including a higher protein ration and propylene glycol (De Sousa, 2002).

2.5 Calving

Calving is done with a standing surgical route on approximately day 272 of gestation. Parturition induction began approximately 36 hours before scheduled cesarean section with 5 mg/kg of dexamethasone (3 i.m. injections every 12 hours) supplemented with 25 mg of prostaglandin (i.m.) at the time of the second steroid injection. If meconium is present at the time of delivery, a more aggressive approach (either via coupage or active suction) is adopted, consisting of multiple attempts to remove fluid from the lungs. Animals are given nasal oxygen at 2–10 l/min depending upon blood gas values. Plasma (e.g., 2 l/calf, i.v.), antibiotics, and colostrum (10%–15% of body weight, either by suckling or stomach tube) are given in the first 4 hours of life. More aggressive treatments (e.g., surfactant, inhaled steroids, bronchialdilators) are administered on a per case basis. The umbilicus is surgically removed to for the infection prevention. Animals are bottle-fed and weaned at several weeks of age following standard animal husbandry practices (Kishi, 2000; Heyman, 2002).

2.6 Cell lines

The adult cell line can be derived from a surgical excisional biopsy. Thin tissue sections are cut into 1- to 3-mm pieces with a sharp surgical blade, and explants are transferred into 25-mm2 flasks containing Dulbecco's modified Eagle's medium (DMEM-F12) + 10% fetal bovine serum (v/v) + 1% penicillin/streptomycin (v/v) (10 000 U/mL penicillin G, 10 000 µg/mL streptomycin) and then cultured at 37°C in air containing 5% CO2. When confluence is achieved at 14 days, cells are trypsinized for 5 min, and total cell count is determined using a Coulter counter. The recovered cells are centrifuged, and the pellet is resuspended at a concentration of 1 million cells per mL. Aliquots are either frozen in DMEM-F12 containing 10% dimethyl sulfoxide (DMSO) before storage at -80°C, or 250000 cells are transferred into a new 25-mm2 flask. As confluence is approached, the cells are passaged by trypsinization and again counted. The mean population doubling time for the first three passages (24 days in culture) could be 44 hours. A Day 40 fetus cloned from the adult cell line is surgically removed from the recipient cow's uterus. The head and viscera are removed, and the remainder of the fetal tissue is sliced into 2- to 5-mm pieces. These explants are then cultured as above. The mean population doubling time for the first eight passages (44 days in culture) could be 27.4 hours (Arat, 2001; Zakhartchenko, 1999).

2.7 Nuclear transfer

Recipient oocytes could be slaughterhouse-derived from predominantly Brahman-cross cattle and matured for 17 hours in Medium 199 supplemented with 10% fetal calf serum, FSH (0.1 U/mL), LH (0.1 U/mL), estradiol (1 µg/mL), pyruvate (28 µg/mL), EGF (0.05 µg/mL), and 1% penicillin streptomycin. The cumulus-oocyte complexes are vortexed at 17 hours postmaturation (hpm) for 1–2 min, and then the oocytes are washed, placed in 0.05% Pronase E (w/v) for 3 minutes, and held in Medium 199 + 10% FCS (Zakhartchenko, 1999; Kuhholzer, 2001).

2.8 Enucleation

Oocytes are enucleated at 19 hpm. Before enucleation, oocytes are placed for 15 minutes in Hepes-buffered synthetic oviductal fluid (H-SOF) with 4 mg/mL BSA that contained 7.5 µg/mL cytochalasin B and 5 µg/mL Hoechst 33342. At this time, oocytes are selected for presence of a polar body and homogeneous cytoplasm. Suitable oocytes are enucleated in H-SOF with 7.5 µg/mL cytochalasin B using a beveled 25-µm outside-diameter glass pipette. Only oocytes in which the removal of both the polar body and metaphase nucleus is confirmed by observation under UV light are included in the experiment. Oocytes are then randomly allocated to be combined with either adult or fetal fibroblasts (Oback, 2003).

2.9 Donor cells

Serum starvation of donor cells is achieved by culture in DMEM/F12 + 0.05% FCS for 1–5 days before nuclear. Fibroblasts are prepared by trypsinization of early-passage adult (passage [P] 3–4; Days 13–24 in culture) and fetal (P 3–4; Days 11–21 in culture) cells at 60–80% confluence (Clark, 2003).

2.10 Combining donor and recipient cells

Fibroblasts of median diameter are combined with enucleated oocytes in 7.5 µg/mL cytochalasin B in H-SOF using a 30-µm outside-diameter glass pipette, then returned to Medium 199 + 10% FCS. The oocyte-fibroblast couplets are manually aligned and fused in a 3.2-mm fusion chamber that contained Zimmerman cell fusion medium using 2 × 20-µsec 1.6-kV/cm DC fusion pulses delivered by a BTX Electrocell Manipulator 200 (BTX, San Diego, CA). Oocyte activation is performed 3–5 hours after fusion at 27 hpm, by a 4-min incubation in 5 µM ionomycin followed by 4 min in 3% BSA in Tyrode's lactate-Hepes and 4 min in H-SOF. Fusion is assessed at this time by light microscopy before transfer into 100 µM butyrolactone-I in SOF for 4 hours followed by transfer to Charles Rosenkrans medium #1 with added amino acids (CR1aa) + 10% FCS with buffalo rat liver coculture for 7 days (Zhu, 2002).

2.11 Embryo development

Embryos are classified as blastocysts according to their morphology on Day 7 or Day 8 following NT. Two or three blastocysts are nonsurgically transferred when synchronized recipients are available. Pregnancy status is assessed by transrectal ultrasonography (Aloka 500, 5-MHz transducer; Aloka Co., Tokyo, Japan) at 30 days post-nuclear transfer and confirmed 10 days later, with pregnant recipients rechecked every 2 weeks (Hill, 2000).

2.12 Microsatellite analysis

The genomic DNA is compared between adult animal tissue, fibroblasts from the regenerated fetus, and blood from the newborn animal (Taverne, 2002).

Briefly, the protocol of animal clone by nuclear transfer could be summarized in Figure 1, and composition of various useful base Media are given in Table 1.

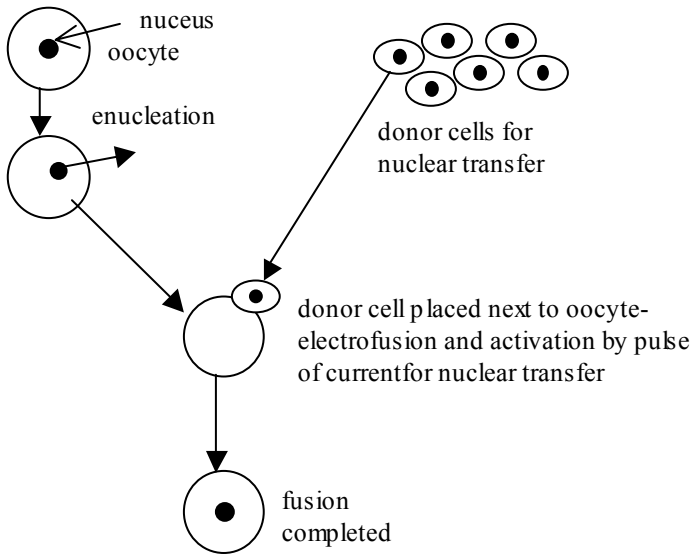

Figure 1. Animal Clone by Nuclear Transfer

Table 1. Composition of Various Base Media (mg/L)

No.	Components	IMDM	Mosier	Ham's F-12	RPMI 1640	Medium 199	DMEM
Inorganic Salts							
1	$CaCl_2$	165	99.1	33.2		200	200
2	$Ca(NO_3)_2$-$4H_2O$				100		
3	$CuSO_4$-$5H_2O$		0.00125	0.0025			
4	$Fe(NO_3)_3$-$9H_2O$					0.72	0.1
5	$FeSO_4$-$7H_2O$		0.415	0.83			
6	KCL	330	276.8	223.6	400	400	400
7	KNO_3	0.076	0.038				
8	$MgCl_2$		28.61	57.22			
9	$MgSO_4$	98	49		48.84	98	97.67
10	NaCl	4500	6049.5	7599	6000	6800	6400
11	$NaHCO_3$	3024	2100	1176	2000	2200	3700
12	Na_2HPO_4		71	142	800		
13	NaH_2PO_4-H_2O	125	62.5			140	125
14	$NaSeO_3$	0.017	0.0085				
15	$ZnSO_4$-$7H_2O$		0.43	0.96			
Amino Acids							
16	Ala	25	16.95	8.9		25	
17	Arg-HCl	84	118	211	200	70	84
18	Asn	25	49.5	15	50		
19	Asp	30	21.5	13	20	30	
20	Cys-HCl-H_2O		17.5	35		0.1	
21	Cystine-2HCl	91.2	45.6		65	26	63
22	Cytidine						
23	Glu	75	60.35	14.7	20	75	
24	Gln	584	365	146	300	100	584
25	Gly	30	18.75	7.5	10	50	30
26	His	42	31.5	21	15	22	42
27	Hydroxy-Pro				20	10	
28	Ile	105	54.5	4	50	40	105
29	Leu	105	59	13	50	60	105
30	Lys	146	91.25	36.5	40	70	146
31	Met	30	17.25	4.5	15	15	30
32	Phe	66	35.5	5	15	25	66
33	Pro	40	37.25	34.5	20	40	
34	Ser	42	26.25	10.5	30	25	42
35	Thr	95	53.5	12	20	30	95
36	Trp	16	9	2	5	10	16
37	Tyr	104	55.9	7.8			
38	Tyr-Na2-HCl				29	58	104
39	Val	94	52.85	11.7	20	25	94
Vitamin							
40	Para-Aminobenzoic				1		

	acid						
41	Biotin	0.013	0.01	0.007	0.2		
42	D-Calcium pantothenate	4	2.25	0.5	0.25		4
43	Choline chloride	4	9	14	3		4
44	Folic acid	4	2.15	1.3	1		4
45	i-Inositol	7.2	12.6	18	35		7.2
46	Niacinamide	4	2.02	0.04	1		4
47	Pyridoxal-HCl	4	2.03	0.06	1		
48	Pyridoxine-HCl						4
49	Riboflavin	0.4	0.22	0.04	0.2		0.4
50	Thiamine-HCl	4	2.15	0.3	1		4
51	Vitamin B_{12}	0.013	0.707	1.4	0.005		
Others							
52	Adenine sulphate					10	
53	Adenosine-5-triphosphate					1	
54	Adenosine-5-phosphate					.02	
55	Cholesterol					0.2	
56	2-Deoxy-D-ribose					0.5	
57	D-Glucose	4500	3151	1802	2000	1000	4500
58	Glutathione (reduced)				1	0.05	
59	Guanine-HCl					0.3	
60	HEPES	5958	1979				5958
61	Hypoxanthine-Na		2.385	4.77		0.4	
62	Linoleic acid		0.04	0.08			
63	Lipoic acid		0.155	0.21			
64	Phenol red	15 or none	8.1	2 or none	5 or none	20 or none	15 or none
65	Putrescine-2HCl		0.0805	0.161			
66	Ribose					0.5	
67	Sodium acetate					50	
68	Sodium pyruvate	110	110	110			
69	Thymidine		0.35	0.7		0.3	
70	Tween 80					20	
71	Uracil					0.3	
72	Xanthine-Na					0.34	

3 Discussion

The current century will bring tremendous changes to the science, technology, and the practice of medicine (Lushai, 2002). As a critical topic, animal clone attracts plenty attention by the whole human society. The success of animal clone by science and technology will be benefit for the civilization, and create the danger for the life in the earth either. Even opposed by all the governments and social groups in the world, the human clone will be coming finally, not longer than decades. Even with ethnic and safety concern, nobody can prevent the development of the animal clone science and technology. I personal think what we need to do is how to safety develop animal clone including human clone, rather than simply again it. This should be a scientific topic, rather a legal business, especially not a religious affair.

Correspondence to:
Hongbao Ma
B410 Clinical Center
Michigan State University
East Lansing, MI 48824, USA
Telephone: (517) 432-0623
Email: hongbao@msu.edu

References

[1] Arat S, Rzucidlo SJ, Gibbons J, Miyoshi K, Stice SL. Production of transgenic bovine embryos by transfer of transfected granulosa cells into enucleated oocytes. Mol Reprod Dev, 2001,60(1):20-6.

[2] Ausubel FM, Brent R, Kingston RE, Moore DD, Seidman JG, Smith JA, Struhl K. Short Protocols in Molecular Biology. Second Edition, Greene Publishing Associates, New York, 1992.

[3] Bechtel J Jr, Boring JR 3rd. Antibiotic-resistance transfer in Yersinia enterocolitica. Am J Clin Pathol, 1979,71:93-6.

[4] Campbell KH. Nuclear transfer in farm animal species. Semin Cell Dev Biol ,1999,10(3):245-52.

[5] Chesne P, Adenot PG, Viglietta C, Baratte M, Boulanger L,Renard JP. Cloned rabbits produced by nuclear transfer from adult somatic cells. Nat Biotechnol, 2002,20(4):366-9.

[6] Clark AJ, Ferrier P, Aslam S, Burl S, Denning C, Wylie D, Ross A, de Sousa P, Wilmut I, Cui W. Proliferative lifespan is conserved after nuclear transfer. Nat Cell Biol, 2003,5(6):535-8.

[7] De Sousa PA, Dobrinsky JR, Zhu J, Archibald AL, Ainslie A, Bosma W, Bowering J, Bracken J, Ferrier PM, Fletcher J, Gasparrini B, Harkness L, Johnston P, Ritchie M, Ritchie WA, Travers A, Albertini D, Dinnyes A, King TJ, Wilmut I. Somatic cell nuclear transfer in the pig: control of pronuclear formation and integration with improved methods for activation and maintenance of pregnancy. Biol Reprod,2002,66(3):642-50.

[8] Faurie C, Golzio M, Moller P, Teissie J, Rols MP. Cell and animal imaging of electrically mediated gene transfer. DNA Cell Biol, 2003,22(12):777-83.

[9] Gibbons J, Arat S, Rzucidlo J, Miyoshi K, Waltenburg R, Respess D, Venable A, Stice S. Enhanced survivability of cloned calves derived from roscovitine-treated adult somatic cells. Biol Reprod, 2002,66(4):895-900.

[10] Heyman Y, Zhou Q, Lebourhis D, Chavatte-Palmer P, Renard JP, Vignon X. Novel approaches and hurdles to somatic cloning in cattle. Cloning Stem Cells, 2002,4(1):47-55.

[11] Hill JR, Burghardt RC, Jones K, Long CR, Looney CR, Shin T, Spencer TE, Thompson JA, Winger QA, Westhusin ME. Evidence for placental abnormality as the major cause of mortality in first-trimester somatic cell cloned bovine fetuses. Biol Reprod ,2000,63(6):1787-94.

[12] Houdebine LM. Animal transgenesis and Cloning. John Wiley & Sons, Inc. Hoboken, NJ, USA, 2003,34-73.

[13] Kishi M, Itagaki Y, Takakura R, Imamura M, Sudo T, Yoshinari M, Tanimoto M, Yasue H, Kashima N. Nuclear transfer in cattle using colostrum-derived mammary gland epithelial cells and ear-derived fibroblast cells. Theriogenology ,2000,54(5):675-84.

[14] Kuhholzer B, Hawley RJ, Lai L, Kolber-Simonds D, Prather RS. Clonal lines of transgenic fibroblast cells derived from the same fetus result in different development when used for nuclear transfer in pigs. Biol Reprod ,2001,64(6):1695-8.

[15] LanzaRP, Dresser BL, Damiani P. Cloning Noah's ark, in Understanding Cloning. Scientific American, Inc. and Byron Preiss Visual Publications, Inc,2002,24-35.

[16] Lushai G, Loxdale HD. The biological improbability of a clone. Genet Res, 2002,79(1):1-9.

[17] Matsui T, Rosenzweig A. Targeting ischemic cardiac dysfunction through gene transfer. Curr Atheroscler Rep, 2003,5:191-5

.[18] McEvoy TG, Ashworth CJ, Rooke JA, Sinclair KD. Consequences of manipulating gametes and embryos of ruminant species. Reprod Suppl, 2003,61:167-82.

[19] Niemann H, Kues WA. Application of transgenesis in livestock for agriculture and biomedicine. Anim Reprod Sci, 2003,79(3-4):291-317.

[20] Oback B, Wiersema AT, Gaynor P, Laible G, Tucker FC, Oliver JE, Miller AL, Troskie HE, Wilson KL, Forsyth JT, Berg MC, Cockrem K, McMillan V, Tervit HR, Wells DN. Cloned cattle derived from a novel zona-free embryo reconstruction system. Cloning Stem Cells, 2003,5(1):3-12.

[21] Pinkert CA, Murray JD. Transgenic farm animals, in Transgenic Animal in Agriculture, Murray JD, Anderson GB, Oberbauer AM, McGloughlin MM (eds). CABI Publishing. New York, NY, USA,1999,1-18.

[22] Sambrook J, Fritsch EF, Maniatis T. Molecular Cloning, sec - ond edition, Cold Spring Harbor Laboratory Press, New York, 1989.

[23] Taverne MA, Breukelman SP, Perenyi Z, Dieleman SJ, Vosa PL, Jonker HH, de Ruigh L, Van Wagtendonk-de Leeuw JM, Beckers JF. The monitoring of bovine pregnancies derived from transfer of *in vitro* produced embryos. Reprod Nutr Dev, 2002,42(6):613-24.

[24] Temple GF, Dozy AM, Roy KL, Kan YW. Construction of a functional human suppressor tRNA gene: an approach to gene therapy for beta-thalassaemia. Nature, 1982,296:537-40.

[25] Zakhartchenko V, Alberio R, Stojkovic M, Prelle K, Schernthaner W, Stojkovic P, Wenigerkind H, Wanke R, Duchler M, Steinborn R, Mueller M, Brem G, Wolf E. Adult cloning in cattle: potential of nuclei from a permanent cell line and from primary cultures. Mol Reprod Dev, 1999,54(3):264-72.

[26] Zhu J, Telfer EE, Fletcher J, Springbett A, Dobrinsky JR, De Sousa PA, Wilmut I. Improvement of an electrical activation protocol for porcine oocytes. Biol Reprod, 2002,66(3):635-41.

Self-Exciting Threshold Auto-Regressive Model (SETAR) to Forecast the Well Irrigation Rice Water Requirement

Qiang Fu[1], Hong Fu[1], Yankun Sun[2]

(1.School of Water Conservancy & Civil Engineering, Northeast Agriculture University, Harbin, Heilongjiang 150030, China, fuqiang100@371.net;
2.School of Resources & Environment, Northeast Agriculture University, Harbin, Heilongjiang 150030, China)

Abstract: Some periodicity was noticed in records of water usage for rice irrigation, which was analyzed using the Self-Exciting Threshold Auto-Regressive (SETAR) model. Using auto-correlation analysis, values of rice evapotranspiration for different growth phases were found to depend on each other. Weather and other factors cause the rice evapotranspiration to change periodically. So the SETAR model was prepared for analysis of groundwater usage to irrigate rice in the Sanjiang Plain. Nine parameters were used to describe the periodicity of weather factors. By comparison with practical values, the precision is high. So, the model can be used to help layout and manage an irrigation area. At the same time, it can be applied to optimizing an irrigation system. [Nature and Science 2004,2(1):36-43].

Key words: SETAR model, well irrigation rice, water requirements

1 Introduction

There are many models to estimate rice crop water requirements based on either simple regressions linked to temperature or radiation and the physically based equations of Penman and Monteith. A sequential analysis method may also be used to identify an auto-regression model $AR(p)$ containing a trend and cyclic component of a water requirement sequence. This article establishes a sectional auto-regression model $AR(p)$ to describe the mean annual sequence of irrigation water requirements. The SETAR model was established by locating threshold values r and selecting suitable delay steps d and threshold ranges L.

2 Brief Introduction on SETAR Model

Tong (1978) first proposed the Self-Exciting Threshold Auto-Regressive Model (SETAR). Its basic idea is to introduce $l-1$ thresholds $r_j(j=1,2,3,\cdots,l-1)$ in the range of an observed sequence $\{x(t)\}$, divide time axis into l ranges, distribute observation sequence $\{x(t)\}$ into different threshold ranges according to the value of $\{x(t-d)\}$ by delay steps d and then adopt different AR model to describe the entire system for $x(t)$ in each range. The common form of Threshold Auto-Regressive Model (TAR) is：

$$x(t)=\varphi_j(0)+\sum_{i=1}^{nj}\varphi_j(i)x(t-i)+a_j(t)$$

$$r_{j-1}<x(t-d)<r_j \quad (\mathrm{j}=1,2,3,\cdots,\mathrm{l}) \tag{1}$$

In formula (1), $a_i(t)$ is the white noise list of σ_i^2. σ_j^2 is variance. (i) is the auto-regressive coefficient of model in the threshold region. nj is the rank of model in the threshold region. The key difference between equation (1) and an AR model is that they distribute observation sequence $\{x(t)\}$ into different threshold ranges according to values of $\{x(t-d)\}$ and adopt a different R model to describe all $x(t)$ in each range. becomes an AR model when the value of l equals to 1 and the value of d equals to 0.

Equation (1) indicates that it builds up an $AR(n_j)$ model for n sequential data between $x(t)$ and $x(t-n_j)$ when the value of $x(t-d)$ is in the range of (r_{i-1},r_i), where t is cursor. If the number is K and the value of is in the range of (r_{j-1},r_j), we can use

K groups of data that have n_j+1 sequential data to establish $AR(n_j)$ model. In other words, we may ascertain the AR model at the time of t according to the range of the value of $x(t-d)$.

3 Modeling on Threshold Auto-Regressive Model

Because Threshold Auto-Regressive Model is sectional AR model, it can be adopted for parameter estimating method and model inspection criterion of the AR model during modeling. At present, the least square method of model parameter estimate and AIC criterion of model adaptability inspection has been widely applied. The difficulty of modeling $SETAR$ is to ascertain the number of threshold range l, threshold value $r_1, r_2, \cdots, r_{l-1}$ and retardant steps d. In theory, this is the multi-dimension optimizing problem for l, $r_1, r_2, \cdots, r_{l-1}$ and d. If we adopt AIC criterion to ascertain the model steps ($n_1, n_2, \cdots, n_l$) in each threshold range and the objective function about l, $r_1, r_2, \cdots, r_{l-1}$ and d, AIC value should be the function that has $2l+1$ parameters. That is:

$$AIC \quad {}_2; \quad r \quad)$$

AIC values of the model should be the space shown in the upper formula. This article will combine H. Tong method and D.D.C method established the $SETAR$ model (Yang, 1996; Jin, 2000; Ding, 1988; 1998; Du, 1991).

3.1 Drawing dot figure by D.D.C method (Yang, 1996)

D.D.C method was put forward by Jinpei Wu. Its idea is with drawing dot figure to ascertain the number of threshold l and search range of threshold value $r_1, r_2, \cdots, r_l$; with duplication method to estimate model parameter and with cross-validation method to confirm retardance steps . The duplication method is to recur the least square method for the parameter matrix of the AR model.

The first step of modeling is to ascertain the number of threshold and the search range of threshold value $r_1, r_2, \cdots, r_{l-1}$.

For time series, we can divide axis $x(t-d)$ into s sections evenly according to the data $(x(t), x(t-d))$(1,2,3 . If the number of $x(t-d)$ in the first section is N, the mean value of $x(t)$

$$\hat{E}(x(t)/x(t-d))_i = \frac{1}{N_i} \qquad (\mathrm{i}=1,2,\cdots,\mathrm{s};\ \mathrm{d}=1,2,\cdots). \quad (2)$$

The dot figure can be acquired through drawing the dot $\hat{E}(x(t)/x(t-d))_i$ in the center of each section with the horizontal axis $x(t-$ and vertical axis $\hat{E}(x(t)/x(t-d))$. When the dots show linear distribution in the dot figure, we can use the sectional linear model to describe the time series. This is the basic idea of the $SETAR$ model. Thus, the dot figure can not only judge the property of the model but also provide two notes for the $SETAR$ model: firstly, to ascertain the number of the threshold range according to the number of subsection and decrease a layer nesting in Tong method because it is unnecessary for l to optimize; secondly, to turn the large scale optimization of the threshold to local optimization when ascertain the search range of each threshold value r_1, in the turning point of sectional linearity. Thus, the modeling of D.D.C method has three steps: ① dot figure drawing; ② ascertain l and the search range of $\cdots, r_{l-1}$ according to the dot figure; ③ optimize for $\cdots, r_{l-1}$ with any optimizing theory. The article adopts the golden section method and searches the optimum value of $r_1, r_2, \cdots, r_{l-1}$ in three to five steps.

3.2 Optimum retard steps d, r_j and $\varphi_j(i)$ by tong method (Yang, 1996)

Tong method is the method that optimizes in one-dimensional space and layer upon layer nesting for d, l and r_j ($\mathrm{j}=1,2,3,\cdots \mathrm{l}-1$). Its basic idea is as:

① acquire a $SETAR$ model through fixing a group of d, l, r_j ($\mathrm{j}=1,2,3,\cdots \mathrm{l}-1$), establishing the AR model in each range respectively and ascertaining the applied model of each range according to AIC criterion; ② change the value of d, l and r_j ($\mathrm{j}=1,2,3,\cdots \mathrm{l}-1$) respectively and acquire a $SETAR$ model according the first step; ③ compare with the AIC value of the $SETAR$ model established by d, l and r_j ($\mathrm{j}=1,2,3,\cdots \mathrm{l}-1$) and consider the model with the minimal AIC value as applied model. Because threshold range has been ascertained by the dot figure, a layer nesting can be decreased. That is to say that l is a known value. The steps in detail are as followed:

①Suppose that retardant steps d equal to one and ascertain the search range of threshold value r_j ($\mathrm{j}=1,2,3,\cdots \mathrm{l}-1$) by dot figure method. Then divide

time series $\{x(t-d)\}(t=d+1,d+2,\cdots N)$ into l subsections according to the range it belongs to among $(-\infty, r_1], (r_1, r_2], \cdots, (r_{l-1}, +\infty)$.

② Establish the AR model in each threshold range. Confirm the form of the model by auto-correlation analysis and ascertain the steps n_j of the model primarily through bias-correlation analysis. For example, if for any series the AR model is established, its auto-correlation coefficient is:

$$\rho(k)=\frac{\sum_{t=1}^{n-k}x(t)x(t+k)-\frac{1}{n-k}(\sum_{t=1}^{n-k}x(t))(\sum_{t=1}^{n-k}x(t+k))}{\left[\sum_{t=1}^{n-k}x^2(t)-\frac{1}{n-k}(\sum_{t=1}^{n-k}x(t))^2\right]^{\frac{1}{2}}\left[\sum_{t=1}^{n-k}x^2(t+k)-\frac{1}{n-k}(\sum_{t=1}^{n-k}x(t+k))^2\right]^{\frac{1}{2}}}$$

Where time delay k equals to 0,1,2,…m. When n is bigger than 50 ($n>50$), m must be less than n/4 and m equals to n/10 usually. Draw the allowable range that confidence level of auto-correlation coefficient is 95% in the auto-correlation figure. If α equals to 0.05, allowable range of auto-correlation coefficient $\rho(k)$ is

$$\rho(k)(\alpha=0.05)=\frac{-1\pm1.96\sqrt{n-k-1}}{n-k}$$

If p-step correlation coefficient is prominent to independent sequence, the former random sequence is a mean square contingency sequence and the $AR(p)$ model can be adopted.

The main way of confirming the steps p is to do the statistical analysis for bias-correlation coefficient. The bias-correlation coefficient φ_k can be acquired by recurrence algorithm (Ding, 1988; 1998; Du, 1991).

The same as the former theory, we can establish the AR model of each threshold range respectively. Then inspect each model by AIC criterion:

$$AIC=N_j\ ln\sigma_j^2+2(n_j+1)\quad (j=1,2,3,\cdots,l)$$

By all appearances, when the value of d , l and r_j (j=1,2,3,⋯l-1) has been known, AIC value is only the function of model steps n_j. When AIC value is the minimal one, the model is the applied model of each section. Its AIC value is:

$$AIC(n_j)=\min_{1\le n_j\le M}\{N_j\ ln\sigma_j^2+2(n_j+1)\}\quad (j=1,2,3,\cdots,l)$$

where M is the uppermost steps.

③ Acquire the $SETAR$ model by combining the applied model $AR^{(j)}(n_j)$ (j=1,2,3,⋯,l) of each threshold range. AIC value of each section model add up to the AIC value of the model. That is as the

$$AIC(l \qquad (3)$$

Because we acquire the model and the AIC value in the case of l parameters unchanged from d , l and , the AIC value in equation (3)is the function of the l parameters.

④ Fix d and and optimize for threshold value r_j (j=1,2,3, in the known search range by adopting golden section method or accelerating genetic algorithm. Then repeat the former steps and calculate AIC value according to equation (3). Finally confirm the group of whose value is the minimal one as the best threshold value in the case of known d and . The objective function of threshold optimization is:

$$AIC \quad \hat{r}_1 = \underset{-\infty<r_1<}{} \{ \quad {}_{-1} \quad {}_1)\} \qquad (4)$$

⑤ Fix l and repeat the former steps when d is from d+1 to D, which is the maximal search steps. Then ascertain the best retardant steps d when the AIC value is the minimal one. Because in fact the data of modeling only have N , where $max\{d,M\}$, the AIC value should adopt standard value. That is:

$$\overline{AIC}(l \quad {}_2, \quad {}_{l-1}) \qquad (5)$$

Calculate different AIC value for each d according to equation(5). Then confirm the $\hat{d}$ when the AIC value is the minimal one as the best retardant steps in the case of known . The objective function of d optimization is:

$$\overline{AIC}(l \quad \hat{r}_2,\cdots,\hat{r}_{l-1})=\min_{1\le d\le D}\{\overline{AIC}(l;d;\hat{r}_1,\hat{r}_2,\cdots,\hat{r}_{l-1})\}$$

Thus, the process of parameter optimization has finished and the $d,n_1,n_2)$ model has been established.

3.3 SETAR model forecast (the best forecast) (Yang, 1996)

As the model, the best forecast of threshold auto-regressive model is also the forecast with the least

variance of forecast error. The best-forecast value $\hat{x}_k(t)$ at time t for next k step equals to the conditional mathematics expectation $E[x(t+k)]$ at time t in time $t=t+k$. That is: $\hat{x}_k(t)=E[x(t+k)]$. The formula of the best forecast of threshold auto-regress-
ive model is:

$$\hat{x}_k(t)=\begin{cases}\varphi_j(0)+\sum_{i=1}^{n_j}\varphi_j(i)x(t+k-i) & (k=1)\\ \varphi_j(0)+\sum_{i=1}^{k-1}\varphi_j(i)\hat{x}_{k-i}(t)+\sum_{i=k}^{n_j}\varphi_j(i)x(t+k-i) & (k\le n_j)\\ \varphi_j(0)+\sum_{i=1}^{n_j}\varphi_j(i)\hat{x}_{k-i}(t) & (k>n_j)\\ & (r_{j-1}<x(t+k-d)\le r_j, j=1,2,3,\cdots,l)\end{cases} \quad (6)$$

4 A Case Study

The Sanjiang Plain is an important crop commodity base in China. By the end of 1998, 80% of irrigation water for rice was believed to be drawn from groundwater. Since people have excessively exploited ground water the ground water tables have fallen beneath the depth of farmers wells. In the spring of 1996, the Jiansanjiang administration bureau had recorded the incidence of more than 600 of such dry wells. This ground water resources crisis has constrained further development in the Sanjiang Plain. Precise forecasting of water requirements is expected to have a significant effect on establishing reasonable water use, thereby saving ground water resources and renewing a sustainable ground water balance that still benefits agriculture in the Sanjiang Plain.

Using the fifteen-year observation data (1984-1998) in Fu Jin, which is the hinterland in the Sanjiang Plain, the well irrigation to rice can be divided into six phases according to its breeding period. Rice planting was around May 20 every year based on climate records in past years in San Jin Plain. Therefore, the rice growth phases are: rice planting stage (May 20-May 29, 10 days in total), turning green stage (May 30-June 5, 7 days in total), tillering stage（6.6～7.10，35 days in total）, booting stage (July 11-July 20, 10 days in total), spiking and blooming stage (July 21-July 27, 7 days in total) and grain filling and mature stage (July 28-Agust 31, 35 days in total) (Fu, 2000).

Table 1 Water requirements rice of Fu Jin City in the Sanjiang Plain (daily mean, mm)

Year	rice planting stage	returning green stage	Tillering	booting stage	spiking and blooming stage	grain filling and mature stage
1984	4.86	7.32	8.18	9.54	7.34	5.71
1985	5.28	7.62	9.88	10.20	12.89	5.93
1986	4.10	5.93	9.77	10.03	11.35	5.08
1987	5.44	5.85	10.02	11.52	12.45	6.05
1988	4.90	5.16	7.77	10.82	8.26	7.28
1989	4.60	5.55	8.53	12.78	9.97	5.99
1990	5.48	5.14	7.55	9.85	7.14	5.50
1991	4.25	5.14	9.64	12.06	9.83	6.04
1992	4.87	4.12	9.06	12.23	6.80	4.91
1993	4.88	5.29	6.72	11.21	10.30	6.26
1994	3.53	5.60	8.27	10.21	8.70	5.52
1995	4.58	6.20	6.90	10.25	9.88	5.65
1996	5.18	6.12	9.06	10.05	10.46	6.90
1997	4.50	6.53	8.35	12.96	9.46	5.72
1998	4.59	5.15	9.90	12.64	11.27	7.54

4.1 Drawing dot figure

Firstly, consider $x(t-d)(d=1,2,3,\cdots 6)$ as the horizontal axis and $\hat{E}(x(t)/x(t-d))$ as the vertical axis and divide the horizontal axis into fifteen sections. Then

line out the dot $\hat{E}(x(t)/x(t-d))_i$ in the center of each section and draw the dot figure for water requirement sequence of well irrigation rice when retardant steps are from one to six. Finally, ascertain the number of threshold range and the search range of threshold value. Because the dot figure is two-section linear distribution from Figure 1 to Figure 6, the number of threshold range is two. From the turning point of two straight lines in Figure 1 to Figure 6, the search range of threshold value r is between seven and eight approximately. So, golden section method can be used to optimize.

4.2 Optimizing step by step

Firstly, suppose that the retardant steps d are one to six and the search range of threshold value r is between seven and eight. Then calculate the AIC value in the different case respectively by adopting golden section method, applying two-layer cycle mechanically and utilizing Matlab 5.3 software program. Consequently ascertain the best threshold value r and retardant steps d (Table 2, Figure 7). It is known from Table 2 that AIC value is the minimal one when d equals to 6.0 and the best threshold value r equals to 7.55. In the case, there are three AR model steps correspondingly. AIC inspection of the AR model is in Table 2 and Table 3.

The independent inspection of the AR model is:

$AR(n_1)$: $Q=6.5899<\chi^2_{0.05}=9.488$

$AR(n_2)$: $Q=3.3696<\chi^2_{0.05}=9.488$

All of them pass the independent inspection.

Table 2 Step by step optimize ($l=2$)

	d =1	d =2	d =3	d =4	d =5	d =6
AIC	115.4904	108.9723	86.7864	120.2671	108.5283	60.9523
Threshold Value r	7.60	7.57	7.55	7.58	7.58	7.55
Model Steps n_1, n_2	3，3	3，3	2，2	2，3	2，5	3，3

Table 3 AIC Testing of $AR(n_1)$ model

$AIC(0)$	$AIC(1)$	$AIC(2)$	$AIC(3)$	$AIC(4)$	$AIC(5)$	$AIC(6)$	$AIC(7)$
	20.4682	15.3375	12.4302	16.2228	13.2245	15.2274	18.6218

Table 4 AIC Testing of $AR(n_2)$ model

$AIC(0)$	$AIC(1)$	$AIC(2)$	$AIC(3)$	$AIC(4)$	$AIC(5)$	$AIC(6)$	$AIC(7)$
	58.3743	56.2078	54.5222	57.1001	59.0141	60.0505	61.0984

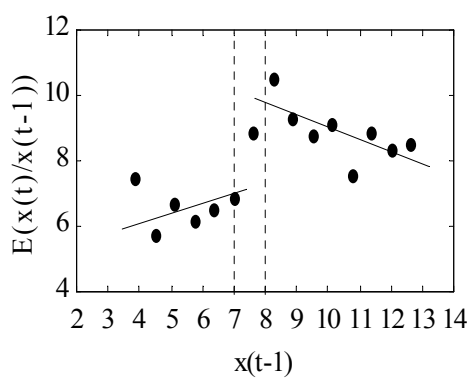

Figure 1 Dot Figure (d =1)

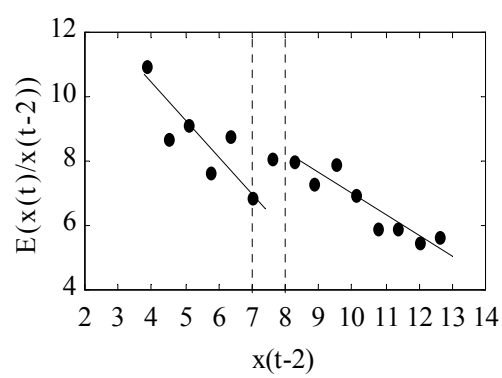

Figure 2 Dot Figure (d =2)

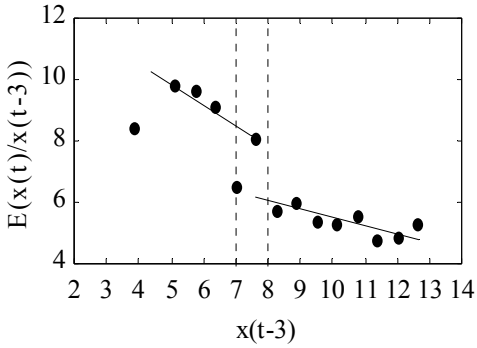

Figure 3 Dot Figure (d =3)

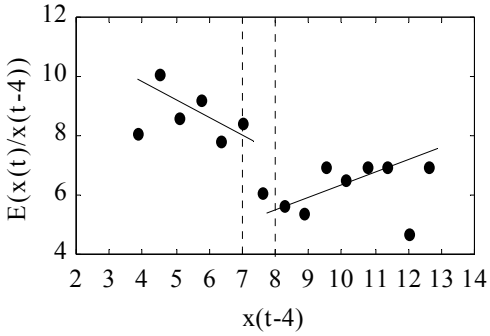

Figure 4 Dot Figure (d =4)

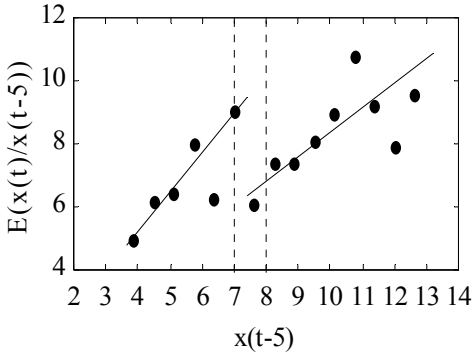

Figure 5 Dot Figure (d =5)

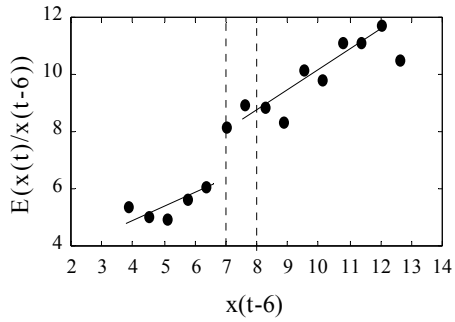

Figure 6 Dot Figure (d =6)

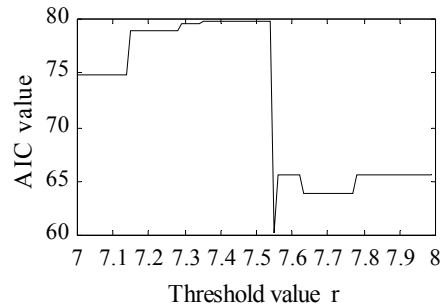

Figure 7 Seeking the Optimum Value of r (d =6, l =2)

4.3 Establish the threshold auto-regressive model of water requirement

$$x(t)=\begin{cases} aver\ 1+\varphi(1,1)(x(t-1)-aver\ 1) \\ +\varphi(1,2)(x(t-2)-aver\ 1) \\ +\varphi(1,3)(x(t-3)-aver\ 1) \quad \mathrm{x(t\ -6)} \le \mathrm{r} \\ aver\ 2+\varphi(2,1)(x(t-1)-aver\ 2) \\ +\varphi(2,2)(x(t-2)-aver\ 2) \\ +\varphi(2,3)(x(t-3)-aver\ 2) \quad \mathrm{x(t\ -6)} > \mathrm{r} \end{cases}$$

where $aver1$ is the mean of $AR(n_1)$ model and $aver2$ is the mean of $AR(n_2)$ model. $\varphi(1,1),\varphi(1,2),\varphi(1,3)$ is the auto-regressive coefficient of $AR(n_1)$ model and $\varphi(2,1),\varphi(2,2),\varphi(2,3)$ is the auto-regressive coefficient of $AR(n_2)$ model. r is threshold value. The optimizing value of each parameter is shown in Table 5.

Table 5 Optimizing the parameters of $SETAR$ model (r =7.55, d =6, l =2)

	$\varphi(1,1)$	$\varphi(1,2)$	$\varphi(1,3)$	$aver1$
$AR(n_1)$	-0.3657	-0.5268	0.2906	5.6466
	$\varphi(2,1)$	$\varphi(2,2)$	$\varphi(2,3)$	$aver2$
$AR(n_2)$	-0.3736	-0.2786	0.1758	10.0922

4.4 Rice water requirement forecast

According to the former theory, forecast water requirement of well irrigation rice during each phase in Fu Jin in 1999 and 2000 and compare with the observed value (Figure 6). Forecast precision of the model is very high and its mean relative error is in 10% (Table 6).

Table 6 Using SETAR Model to forecast the mean daily water requirement of well irrigation rice during each phase in Fu Jin City in 2000

Year	Item	rice planting stage	returning green stage	Tillering stage	booting stage	spiking and blooming stage	grain filling and mature stage
1999	Observed value	4.85	5.98	9.72	10.15	11.04	6.12
	Forecast value	4.82	6.17	9.85	9.75	10.46	5.96
	Absolute error	-0.03	+0.19	+0.13	-0.40	-0.58	-0.16
	Relative error（%）	-0.62	+3.18	+1.34	-3.94	-5.25	-2.61
2000	Observed value	5.20	6.06	9.85	10.54	11.01	6.35
	Forecast value	5.23	5.70	10.06	10.04	10.14	5.88
	Absolute error	+0.03	-0.36	+0.21	-0.50	-0.87	-0.77
	Relative error（%）	+0.58	-5.94	+2.13	-4.74	-7.90	-7.4

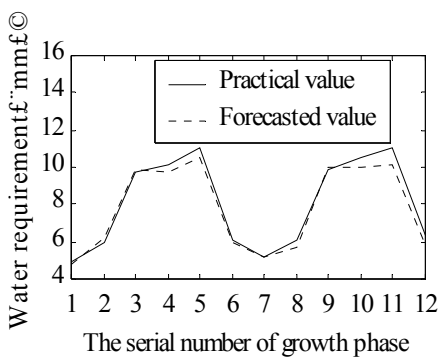

Figure 8 The Water Requirement Curve Fitted by SETAR Model

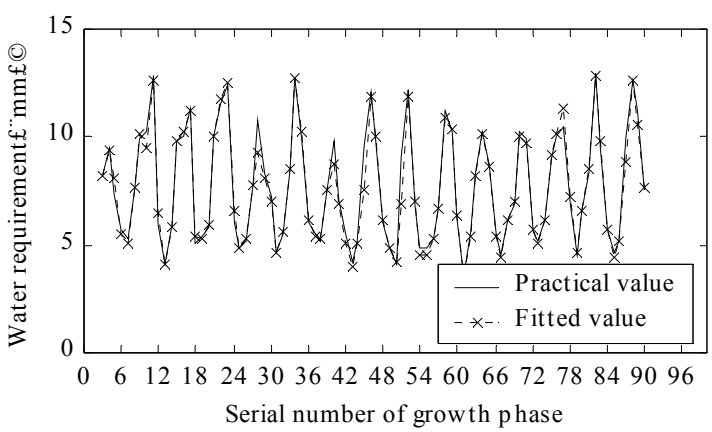

Figure 9 The Contrast Curve Between Practical Value and Forecasting Value Calculated by SETAR Model

5 Conclusion

This article applies the *SETAR* model in well irrigation rice water requirement forecast. It is divided according to the breeding phase through analyzing its property of water requirement. Establish threshold auto-regressive model of daily mean water requirement by optimizing parameters of the model, such as threshold value, threshold range, retardant steps and auto-regressive coefficient etc. Because the control of threshold has its effect, it is possible to describe effectively the non-linear dynamic system of well irrigation rice daily mean water requirement in each phase by using interdependent property of water requirement in retardant steps of one step, two steps and three steps. The high forecast precision shows that the capability of the *SETAR* model is steady and can be applied in irrigation water widely.

Acknowledgement

The financial support provided by Chinese National "863" High-Technique Programme (No. 2002AA2Z4251-09).

Correspondence author:

Qiang Fu

School of Water Conservancy & Civil Engineering
Northeast Agriculture University
Harbin, Heilongjiang 150030, China
Telephone: 01186-451-55190298 (O)
Cellular phone: 01186-13936246215
E-mail: fuqiang100@371.net

References

[1] Ding J, Deng Y. Stochastic Hydrology. Publishing Company of Sichuan University, Chengdu, China , 1988 , 125-36

[2] Ding Y, Jiang Z. Signal Treatment on Time Sequence of Meteorological Data. Weather Publishing Company, Beijing, China , 1998 , 32-7.

[3] Du J, Xiang J. Time Sequence Analysis in the Application of Modeling and Forecasting. Anhui Education Publishing Company, Hefei, China , 1991 , 98-106.

[4] Fu Q. Synthesis Study on Save Water Technology and Optimization in the Course of Water Irrigation Rice Filed Production in Sanjiang Plain. NorthEast Agriculture University, Harbin, China , 2000 , 58-62.

[5] Jin J, Ding J. Genetic Algorithm and Its Applications to Water Science. Publishing Company of Sichuan University, Chengdu, China, 2000 , 51-5.

Fuzzy Analysis on Water Resources of Heilongjiang State Farms

Yongsheng Ma

(School of Water Conservancy & Civil Engineering, Northeast Agricultural University, Harbin, Heilongjiang 150030, China, ysma66@yahoo.com.cn)

Abstract: Fuzzy clustering deals with many topics. Applying Fuzzy clustering, the article analyzed water resources distribution and optimum utilization in State farms. The article studied 9 administration bureaus of State Farms, selected 10 fuzzy factors according to hydrological, meteorological and geographic conditions, and classified them into 3 different districts. The results proposed by the article basically accord with the cases of water resources distribution and agricultural practice in each district. The article can be a reference to agricultural planning and opening water resources decision making. [Nature and Science, 2004,2(1):44-47].

Key words: Fuzzy Analysis; Water Resources; State Farm

1 Introduction

In Heilongjiang State Farms, there are 9 administration bureaus, are located in vast area of Three River Plain, Xing An Maintain areas and Song Nen Plain (Wu, 1986). Owing to different location and hydrological conditions, agricultural productions in every administration bureau are different (Ma, 1993). In order to understand the situation of agricultural production and water resources effect on agriculture, it is important to study the characteristics of water resources and agriculture of the bureaus, so that take measures and decisions of water conservancy fundament construction.

2 Fuzzy Clustering Analysis

Applying Fuzzy clustering methyods the article analyzed agricultural and natural conditions of 9 administration bureaus and then classified districts. The model includes 10 fuzzy factors that are roughly divided into three types: (1) definite factors, (2) Overall index, (3) Non-definite factors (Ma, 1993).

2.1 Definite factors

Grain production, annual average principal, annual average evaporation, accumulate heat, the water quantity in unit farmland are all the definite factors.

2.2 Overall indexes

The overall indexes are concerning with those comprehensive factors including the rate of land using, drought coefficient etc. For example, the drought coefficient is a comprehensive coefficient to show the annual drought level. It is a time product by spring drought, summer drought and the dry hazard.

Based on agricultural climate types, the drought indexes and dry hazard appearances of the 9 bureaus have shown in Table 1. The comprehensive drought factors shown in table 3 and calculated by formula 1.

$$Y = (K_{Spr} + K_{Sum})V_{dr} / 2 \qquad (1)$$

In which:

Y = drought comprehensive coefficient;
K_{spr} = Drought index in spring season;
K_{Sum}= Drought index in summer season;
V_{dr} = The rate of arid hazard appearance.

2.3 Non-definite factors

Non-definite factors are factors without definite values. Such as, soil and soil erosion indexes which the value should be given by evaluation. The soil quality indexes are given by soil types time the weighted value of soil distribution. In the article, the black clay soil has been taken as the best quality soil and the value is assumed as 1.0. Folium white slurry soil (Baijiang Soil) is lowest quality soil and the value is assumed as 0.2. Then the soils have been arranged as the series Black loamy clay, brown loamy clay, peat duck brown loamy clay, marshland soil, and Folium white slurry soil (Baijiang Soil) (Ma, 2003). The Figure 1 showed the value of each soil. The data of agriculture and natural

condition of State Farms have been shown in Table 1, and soil classified factors have been shown in Table 3.The soil erosion indexes are also non-definite factors. According to soil erosion degree, the article classified the soil erosion in three classes: very strong erosion, strong erosion and general erosion. The index value is determined also by Fuzzy clustering method and shown in Table 2 and Table 3. The Quantitative analyses of drought factors have been calculate in Table 4.

In the article, the grain productivity was average of 1985 and 1990 two years production per Mu*. The data of annual precipitation and annual evaporation were obtained from Heilongjiang hydrological isograms (Ma, 1991).

Calculate resembling coefficient and set up resemble matrix:

$$R = (r_{ij}) \tag{2}$$

The resembling coefficient is calculated with the formula (3).

$$r_{ij} = \frac{|\sum_{k=1}^{n} X_{ik} X_{jk}|}{\sqrt{\sum_{k=1}^{n}(x_{ik}^2)\sum_{k=1}^{n}(x_{jk}^2)}} \tag{3}$$

To run the matrix model on computer to calculate equal value matrix (Fu, 2003) as shown in Table 5.

Table 1 The agricultural and natural factors

No	Bureau	Yield / Mu	Water / Mu	Land Use (%)	Ann. Prec. (mm)	Ann. Evap. (mm)	Non-Frost	Accum. Heat
1	Jiusan	222	280	35.9	491.6	381	121	2183
2	Bei'an	173	260	26.9	543	417	112	2164
3	Nenjiang	244	300	43.4	445.3	449	121	2610
4	Suihua	160	275	31.7	554.8	500	129	2206
5	Harbin	194	270	43.2	604.6	442	145	2600
6	Hongxinglong	221	204	45.7	534	539	142	2545
7	Baoquanling	180	331	45.5	553	485	129	2445
8	Jiansanjiang	160	346	31	592	446	130	2402
9	Mudanjiang	215	341	31.6	566	454	148	2517

Table 2 Soil component, Erosion and Land use factors

No.	Bureau	Type of soil	Land Use %	Soil erosion	Fuzzy value
1	Jiusan	Bl, Br, DB	35.9	HS	1.0
2	Bei'an	Bl, Br, DBr	26.9	HS	1.0
3	Nenjiang	BGr , Gr, Sd	43.4	HS	1.0
4	Suihua	Bl, Gr, Ml	31.7	S	0.6
5	Harbin	Bl, Gr, Ml	43.2	S	0.6
6	Hongxinglong	Bl, Gr, Ml, Ws	45.7	G	0.3
7	Baoquanling	Br, Db, Gr, Ml	45.5	G	0.3
8	Jiansanjiang	Bl,Br,Gr,Ml	31	G	0.3
9	Mudanjiang	Br,Gr,Ml,Ws	31.6	HS	1.0

Table 3 Soil type and soil quality evaluation

Bureaus	Black soil (Blk) (%)	brown soil (Br) (%)	Eroded dark & brown soil (DB) (%)	Gully latent raised meadow soil (Gr, Ml) (%)	Folium white slurry soil (Ws) (%)	Degree of Soil quality (%)
Jiusan	73.5	23	3.5			94
Bei'an	60	30.2	9.8			90
Nenjiang			72.3 (chernozem soil)	25 (Saline Soil)	3 (Arenaceous meadow soil)	68.4
Suihua	57			35.9	7.1	74.2
Harbin	51.1			35.9	13	70.3
Hongxinglong	41.6			39.6	18.8	61.2
Baoquanling		45	10	36	9	58.2
Jiansanjiang	6	34.6		35	19	51.5
Mudanjiang		22		28	50	38.8

Table 4 Quantitative analysis of drought indexes and coefficient

No	Bureaus	Ann. Precip. (mm)	Ann. Evap. (mm)	Drought Index		Drought Appr (%)	Logging Appr. (%)	Drought Coef.
				Spr	Sum			
1	Jiusan	491.6	1181	1.37	2.58	30	60	0.59
2	Bei'an	543	1117	1.18	1.89	30	58.6	0.46
3	Nenjiang	445.3	1449	2.04	3.6	80	52	2.26
4	Suihua	554.8	1200	1.33	2.29	40	64	0.72
5	Harbin	604.6	1142	1.17	1.82	60	58	0.9
6	Hongxinglong	534	1239	1.34	1.94	30	70	0.49
7	Baoquanling	553	1185	1.23	1.8	30	70	0.45
8	Jiansanjiang	592	1146	1.19	1.17	20	78	0.29
9	Mudanjiang	566	1134	1.23	1.69	30	80	0.44

Table 5 The Fuzzy similarity matrix of farm bureaus

	Farm Bureaus								
Farm Bureaus	1	0.917	0.947	0.917	0.944	0.904	0.904	0.904	0.904
	0.917	1	0.917	0.96	0.904	0.904	0.904	0.904	0.904
	0.947	0.917	1	0.917	0.96	0.904	0.904	0.904	0.904
	0.917	0.96	0.917	1	0.904	0.904	0.904	0.904	0.904
	0.944	0.904	0.904	0.904	1	0.924	0.924	0.924	0.924
	0.904	0.904	0.904	0.904	0.924	1	0.963	0.963	0.93
	0.904	0.904	0.904	0.904	0.904	0.924	1	0.966	0.93
	0.904	0.904	0.904	0.904	0.924	0.963	0.966	1	0.93
	0.904	0.904	0.904	0.904	0.924	0.963	0.93	0.93	1

According to natural condition of each administration bureau and matrix analysis, the threshold value l was calculated into 3 levels by statistical quantity, and 9 farm bureaus are divided into 3 groups they have similar agricultural, natural conditions to open water resources respectively, that are:

The threshold value is: l=0.94;

Second class group: II (6,7,8,9)

The threshold value is: l= 0.93

Third class group: III (2,4,5)

The threshold value is: l = 0.92

First class group: I (1, 3)

3 The Results of Fuzzy Clustering

Upon classification are basically fit to the agricultural production, geographic condition, hydrology and meteorological characteristic of local bureaus. The results show that Jiusan and Nenjian farm bureau have same geographic and meteorolo-gycal condition owing to be located in the western of the province; the second group is three river plain districts.

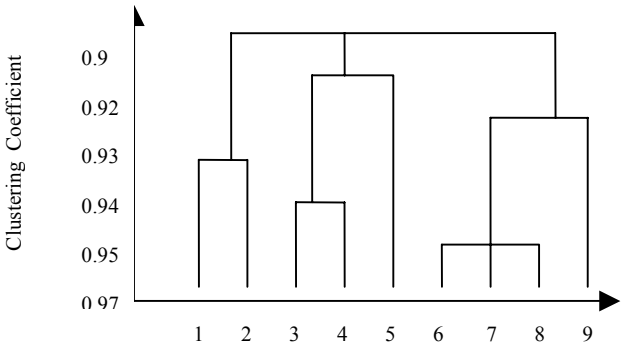

Figure 1 Fuzzy Clustering of Agricultural Water resources of State Farms

By means of Fuzzy clustering, those eastern 4 bureaus (Hongxinglong (6), Baoquanling (7), Jiansanjiang (8) and Mudanjiang (9) Bureaus) have been cl- assified into one group is reasonable result; Bei An (2), Suihua (4) and Harbin (5) bureaus are all located in Songnen Plain and Xing An Hilly area, they have similar weather conditions, the annual precipitation, drought and water logging problems are basically same, therefore belong to one group.

4 Conclusion

Fuzzy clustering analysis has been applied broadly to system demarcating problems. There are many different methods may demarcating the system data. Since Fuzzy method systematically takes consideration of factors, the results are closed to practice. According to State farm natural and agricultural conditions, the article applied Fuzzy clustering method analyzed water resources of 9 Farm administration bureaus and classified them into three groups. The results conform to the local practice situation.

References

[1] Wu Y. China watwer resources utilization, Hydraulic and Electric Planning and Design Academy of China, 1986, 30-32.

[2] Ma X. Heilongjiang Water Resources Research, Heilongjiang Hydrology Bureau, 1991.

[3] Fu Q, Xie Y. Application of projection pursuit evaluation model based on real-coded accelerating genetic algorithm in evaluating wetland soil quality variation in the Sanjiang Plain. China Pedosphere, 2003,13(3):249-56.

[4] Ma Y. Water Resources Analysis of Heilongjiang State Farms. The journal of economic management of state farms, ISSN 1002-2635, 45-47.

[5] Ma X, Fu Q. Applying Self-Organizing Competition Artificial Neural Networks to Classify the soil. Nature and Science, 2003,1(1):75-81.

Application of a New Hybrid Model to Predicting Daily Runoffin a Week

Beilei Qin [1], Wensheng Wang [1], Jing Ding [1], Qiang Fu [2]

（1. Department of Hydrology and Water Resources, Hydraulic School of Sichuan University, Chengdu, Sichuan 610065, China, 1207qbl@sohu.com;
2. School of Water Conservancy & Civil Engineering, Northeast Agricultural University, Harbin, Heilongjiang 150030, China, fuqiang100@371.net）

Abstract: A new hybrid model is presented for predicting daily runoff in a week, which is combined by threshold regressive model and nearest neighbor bootstrapping disaggregation model. In this hybrid model, firstly, threshold regressive model is used to predict weekly runoff. Secondly, nearest neighbor bootstrapping disaggregation model is used to disaggregate this weekly runoff, and then daily runoff in the week is obtained. Analysis and examples indicate that this new hybrid model is practical, efficient and has prominent merit. [Nature and Science, 2004,2(1):48-52].

Key words: threshold regressive model; nearest neighbor bootstrapping disaggregation model; prediction; disaggregation

1 Introduction

Now, inflow prediction of next week must be obtained in order to constitute correct weekly dispatching plan of one hydroelectric plant. For the sake of satisfying hydroelectric plant's demand, predicting daily runoff in a week is tried in this paper. Predicting daily runoff in a week refers to that daily runoff in the next week is predicted according to the historical runoff (or rainfall) data of the river basin.

Traditional hydrology prediction method usually gives one mathematical model with certain prediction period. If traditional hydrology prediction method is used to predict daily runoff in a week, it means that seven mathematical models with different prediction period (from 1d to 7d) must be constituted, and prediction accuracy may descend remarkably with the increase of prediction period. In order to obtain relatively stable prediction accuracy, a new hybrid model is presented, which first predicts weekly runoff and then disaggregates weekly runoff into daily runoff.

In the first part of the hybrid model, threshold regressive model (TR) is used to predict weekly runoff, owing to that, not only can TR model take non-linear characteristic of weekly runoff which is a complex dynamic phenomenon into account, but also consider linear correlation of weekly runoff as its special example, and TR model can ensure good stability and prediction accuracy of the model by controlling threshold values. In the disaggregation part of the hybrid model, nearest neighbor bootstrapping disaggregation model (NNBD) is applied, because compared with traditional classical disaggregation model, NNBD model considers much more historical information.

The principle and algorithm of TR model and NNBD model, and the constitution and application of the hybrid model, are introduced respectively as following sections.

2 Threshold Regressive Model

2.1 The principle and algorithm of TR model

The principle of TR model is，that non-linear correlation between dependent variable and independent variable is described by several linear regressive models with different threshold values. Its general formula is as follows:

$$\hat{W}_t = b(j,0) + \sum_{i=1}^{P} b(j,i) Q_{t-i} + e_t(j)$$

$$As Q_{t-k} \in [r(j-1), r(j)] \qquad (1)$$

where, $r(0) = -\infty$, $r(L) = +\infty$, $r(j)$ ($j = 1,2,\cdots,L-1$) is threshold value, L is the number of threshold intervals,

$b(j,i)$ is regressive coefficient of threshold interval number j, $\hat{W}_t$ is independent variable series (for example weekly runoff), Q_{t-i} is dependent variable series (for example daily runoff), Q_{t-k} is threshold variable, P is the number of dependent variables, and $e_t(j)$ is stochastic series, which is independent series. As the mean of $e_t(j)$ series is zero, $E\ [e_t(j)] = 0$, it can be neglected when predicting.

2.2 Parameter estimation of TR model

Constituting TR model substantially is that estimating its parameters, the number of threshold intervals L, threshold value $r(j)$ (j =1,2,⋯,L－1) and aggressive coefficient $b(j,i)$. Till now, there still isn't one specific method to confirm these parameters. So, choosing initial parameters, threshold variable, L and $r(j)$ (j =1,2,⋯,L－1), is usually based on correlation of independent variable and dependent variables. Then through trial method, threshold variable, L and $r(j)$ (j =1,2,⋯,L－1) are confirmed. And last, aggressive coefficient $b(j,i)$ is calculated through one optimization method.

3 Nearest Neighbor Bootstrapping Disaggregation Model

Traditional classic disaggregation is usually based on similarity principle and a typical module is chosen to disaggregate water volume. But this kind of method doesn't make use of the historical information fully. NNBD model is quoted in the hybrid model in order to improve the accuracy of disaggregation. NNBD model has clear concept and single structure, and avoids the assumption of the form of dependence and probability function. Taking the characteristic of components into account and several typical modules required to constitute an expected disaggregation module when confirming disaggregation module, are its prominent merits. Thus ensures full use of information and stable result.

3.1 The principle and algorithm of NNBD model

Let the observed daily runoff be represented by $\{Q_t\}_n$, where n is the number of daily runoff series. If the number of variables studied is m, let vector X_t=（Q_t，Q_{t+1}，⋯，Q_{t+m-1}）, and we can suppose

$$W_t = \sum_{i=0}^{m-1} Q_{t+i}$$

(if m=7, then W_t represents weekly runoff). Generally, there exists correlation between hydrology phenomena along time scale. So, to some extent, X_t depends on the historical daily runoff Q_{t-1}, Q_{t-2}, ⋯, Q_{t-P}. Make D_t= (Q_{t-1}, Q_{t-2}, ⋯, Q_{t-P}) and name it as eigenvector of the daily runoff series. Then, X_t=（Q_t，Q_{t+1}，⋯，Q_{t+m-1}）(t=P+1，P+2，⋯，n-m+1) can be defined as the succeeding value of D_t.

Among D_t（t= P+1，P+2，⋯，n） which are constituted by $\{Q_t\}_n$, there must be some eigenvectors nearest neighbor to current eigenvector D_i. Suppose the number of nearest neighbor eigenvectors is K, and represented by $D_{1(i)}$，$D_{2(i)}$，⋯，$D_{K(i)}$. $X_{1(i)}$，$X_{2(i)}$，⋯，$X_{K(i)}$ must be the succeeding values of each corresponding eigenvector. The nearest neighbor is judged by the difference between D_i and D_t, which is defined as:

$$r_{t(i)} = (\sum_{j=1}^{P}(d_{ij} - d_{tj})^2)^{\frac{1}{2}} \tag{2}$$

where, $r_{t(i)}$ represents the difference between D_i and D_t, d_{ij} and d_{tj} are number j variable of D_i and D_t respectively, and P is the dimension of eigenvector. Then, $r_{j(i)}$ (j=1,2,…,K) is denoted as the difference between $D_{j(i)}$ and D_i, and it should be mentioned that $r_{1(i)}<r_{2(i)}<\cdots<r_{K(i)}$ (the number j is ordered according to the value of $r_{j(i)}$). The less $r_{j(i)}$ is, the nearer D_i and $D_{j(i)}$ will be and X_i is more similar to $X_{j(i)}$. Let $G_{j(i)}$ be the nearest neighbor bootstrapping weight of $X_{j(i)}$, which shows similarity between X_i and $X_{j(i)}$. Obviously, $G_{j(i)}$ is related to $r_{j(i)}$.

As discussed above, $X_{j(i)}$ (l) / $W_{j(i)}$, the relative value of number l variable of number j nearest neighbor succeeding vector $X_{j(i)}$, is known. Number l variable of current succeeding vector X_i can be obtained through multiplying predicted weekly runoff $\hat{W}_i$ by weighted average of $X_{j(i)}$ (l) / $W_{j(i)}$. So, the ultimate formula of NNBD model can be written as:

$$X_i(l) = \left(\sum_{j=1}^{K} G_{j(i)} \, X_{j(i)}(l) \Big/ W_{j(i)}\right)\hat{W}_i,$$

$$(l=1,2,\cdots,m), \tag{3}$$

where, X_i (l) refers to number l variable of current succeeding vector X_i, $\hat{W}_i$ is the corresponding gross of X_i calculated according to equation (1), $X_{j(i)}$ (l) is number l variable of number j nearest neighbor succeeding vector $X_{j(i)}$, $W_{j(i)}$ is the corresponding gross of $X_{j(i)}$, and $G_{j(i)}$ is the nearest neighbor bootstrapping weight of $X_{j(i)}$.

3.2 Parameter estimation of NNBD model

NNBD model is confirmed, on the condition that the number of nearest neighbor K, the dimension of eigenvector P, and the nearest neighbor bootstrapping

weight $G_{j(i)}$ are estimated.

Generally, $K = \text{int}(\sqrt{n-P})$ is taken. On the condition of $P \geqslant 2$, the dimension of eigenvector P can be estimated by runoff auto-correlation graph or partial-correlation graph. But the ultimate value of K and P should be estimated suited to the instance through trial method.

There are a number of methods to estimate bootstrapping weight $G_{j(i)}$. When estimating, first of all, its restraint condition

$$\sum_{j=1}^{k} G_{j(i)} = 1.0$$

must be satisfied, and then bootstrapping weight $G_{j(i)}$ should be related to $r_{j(i)}$, and the bootstrapping weight function should be a simple one. As the number j is ordered according to the value of $r_{j(i)}$, in this paper, the following formula is adopted.

$$G_{j(i)} = \frac{1/j}{\sum_{l=1}^{K} 1/l}, \quad (j=1,2,\cdots,K) \tag{4}$$

When K is confirmed, we can only calculate Gj(i) once.

4 Case Study

4.1 Constitution of the hybrid model

5-year daily runoff of Jinsha River is used to demonstrate how to constitute the hybrid model and apply it to practice. Let Q_t be observed daily runoff, and weekly runoff can be denoted as

$$W_t = \sum_{i=0}^{6} Q_{t+i}$$

Figure 1 shows the hydrograph of observed daily runoff at Pingshan station, Jinsha river. Table 1 shows correlation coefficient between daily runoff and its succeeding weekly runoff.

According to correlation coefficient between weekly runoff and its nearest neighbor historical runoff showed above, it is proposed that P=3. So weekly runoff prediction TR model is constituted, considering Q_{t-1}、Q_{t-2} and Q_{t-3} as dependent variables (correlation coefficient between them and their succeeding weekly runoff is above 0.9) and their succeeding weekly runoff

$$W_t = \sum_{i=0}^{6} Q_{t+i}$$

as independent variable. And then, NNBD model is adopted, letting eigenvector $D_t = (Q_{t-1}, Q_{t-2}, \cdots, Q_{t-3})$. and succeeding value $X_t = (Q_t, Q_{t+1}, \cdots, Q_{t+6})$. According to equation (3), the predicted weekly runoff $\hat{W}_t$ is disaggregated into daily runoff in the week.

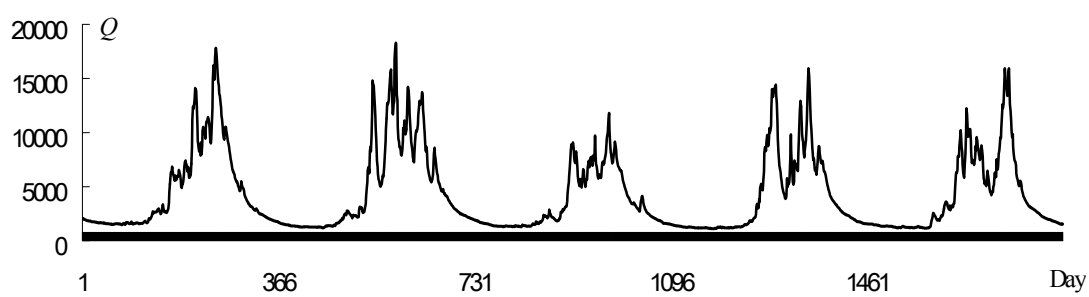

Figure 1 The hydrograph of observed daily runoff at Pingshan station, Jinsha river

Table 1 The correlation coefficient between daily runoff and its succeeding weekly runoff at Pingshan station, Jinsha river

$R(W_t, Q_{t-i})$	i=1	i=2	i=3	I=4	i=5	i=6
W_t	0.95	0.93	0.91	0.89	0.87	0.86

4.2 Weekly runoff prediction

The first four years runoff series is used for fitting of TR model, and the remaining one-year data is used for prediction or testing purpose. In this research, the number of samples during fitting phase and prediction phase should be 1443 and 365, respectively.

Since the correlation coefficient between $Q_{t\text{-}1}$ and W_t is the most one, $Q_{t\text{-}1}$ is chosen to be the threshold variable. The number of threshold interval L and threshold value $r(j)$ (j =1,2,⋯,L－1) can be confirmed based on correlation graph of W_t and $Q_{t\text{-}1}$ and the optimization method chosen by TR model. Weekly runoff prediction TR model is obtained. The formula is showed below, and Tab.2 shows the accuracy of weekly runoff prediction:

$$\hat{W}_t = \begin{cases} 40.3 - 0.03Q_{t-3} - 2.27Q_{t-2} + 9.31Q_{t-1}, Q_{t-1} < 1630 \\ -1561.9 - 3.58Q_{t-3} - 3.25Q_{t-2} + 14.68Q_{t-1}, 1630 \le Q_{t-1} < 5540 \\ 18335.6 - 0.67Q_{t-3} - 4.50Q_{t-2} + 10.04Q_{t-1}, 5540 < Q_{t-1} \end{cases} \quad (5)$$

From the result of weekly runoff prediction, we can see that accuracy in fitting phase is accordant to that in prediction phase, owing to TR model's superiority.

At the same while, the rate of relative error less than 20% is over 80% both in fitting phase and prediction phase. The result is satisfied.

4.3 Daily runoff prediction

According to the main idea of NNBD model, K ＝10 and P＝3 are taken after calculation and comparison, then the first four years runoff series is used for constituting eigenvector D_t＝($Q_{t\text{-}1}$, $Q_{t\text{-}2}$, ⋯, $Q_{t\text{-}3}$) (t=1,2, ⋯ ,1443), just like weekly runoff prediction part, and last, the predicted weekly runoff $\hat{W}_t$ from equation (5) in prediction phase can be disaggregated into daily runoff in the week. Table 3 shows the accuracy of daily runoff predicted by hybrid model.

Table 2 The accuracy of weekly runoff prediction

Relative error	<10%	<20%	<30%	*MAE*	*MSE*
Fitting phase	64.73	86.35	95.36	563	1030
Prediction phase	69.32	85.48	93.97	517	899

Note: *MAE* is mean absolute error, and *MSE* is mean square error.

Table 3 The accuracy of daily runoff predicted by hybrid model

Relative error	<10%	<20%	<30%	*MAE*	*MSE*
1d	83.29	97.81	100	290	512
2d	75.89	92.05	98.08	389	714
3d	70.41	86.85	94.52	497	918
4d	64.93	81.92	92.05	584	1080
5d	60.82	79.45	88.77	670	1220
6d	58.08	76.16	86.03	755	1350
7d	53.42	72.88	83.56	834	1440

Note: *MAE* is mean absolute error, and *MSE* is mean square error.

From the result of daily runoff prediction in a week, it can be found that the hybrid model can give satisfied prediction accuracy for shorter prediction period. With the increase of prediction period, prediction accuracy decreases gradually. But the rate of decrease isn't prominent. Even when prediction period gets to 7d, the rate of relative error less than 20% can get to 76.16%. So, it can be concluded that prediction accuracy of this hybrid model is relatively more stable.

5 Summary

A new hybrid model that effectively blends the

merits of TR model and NNBD model has been firstly presented for predicting daily runoff in a week. Analysis and examples indicate that this hybrid model can be well applied to predicting daily runoff in a week and it has following characteristics: (1) Taking the advantage of TR model, no matter the characteristic of runoff is linear or non-linear, the hybrid model can give finer runoff prediction. (2) Substituting NNBD model for traditional classical disaggregation model to choose distribution module, the hybrid model improves disaggregation accuracy effectively. (3) The hybrid model has strong adaptability. It not only can be applied to daily runoff prediction in a week, but also can be applied to daily runoff prediction in ten-day or in a month, etc.

Correspondence to:

Beilei Qin
Hydraulic School of Sichuan University
Chengdu, Sichuan 610065, China
Telephone: 01186-28-8541-0803
Cellular Phone: 01186-13036660654
E-mail: 1207qbl@sohu.com

References

[1] Srinivas VV, Srinivasan K. A hybrid stochastic model for multiseason streamflow simulation. Journal of Water Resources Research in India 2001;37(10):2537-2549.

[2] Wang WS, Xiang HL, Ding J. Prediction of hydrology and water resources with nearest neighbor bootstrapping regressive model. Journal of Hydroelectric Energy in China 2001;19(2):8-10,14.

[3] Jin JL, Yang XH, Jin BM, Ding J. Application of threshold regressive model to predicting annual runoff. Journal of Glaciology and Geocryology in China 2000;22(3):230-234.

[4] Ding J, Liu QS. Stochatis Hydrology, Chinese Water resource and Hydroelectricity Press, 1997.

[5] Wang HW. Partial least-squares regression-method and application. Chinese Natural Defense Industry Press, 1999.

[6] Jin JL, Wei YM, Ding J. Application of projection pursuit threshold regressive model for predicting annual runoff. Journal of Scientia Geographica Sinica in China 2002;22(2):171-175.

[7] Liu SY, Liao JP. The theory and method of non-linear application of runoff. Journal of Hubei Polytechnic University in China 2003;18(1):42-49.

[8] Jin JL, Wei YM, Ding J. Nearest neighbor bootstrapping model for predicting daily flow process. Journal of System Simulation in China 2002;14(11):1494-1496.

A Novel H_∞ Output Feedback Controller Design for LPV Systems with a State-delay

Junling Wang [1], Changhong Wang [1], Wei Yuan [2]

（1. Department of Control Science and Engineering, Harbin Institute of Technology, Harbin, Heolongjiang 150001, China, E-mail: jun_ling2003@yahoo.com.cn
2. Education Department of Heilongjiang Province, Harbin, Heolongjiang 150001, China）

Abstract: A H_∞ control for linear parameter-varying (LPV) systems with a parameter-varying state delay is described. A new parameter-dependent H_∞ performance criterion is first established by the introduction of a slack variable, which exhibits a kind of decoupling between Lyapunov functions and system matrices. This kind of decoupling enables us to obtain a more easily tractable condition for analysis and synthesis problems. Then, the corresponding output feedback controller design is investigated upon this new performance criterion, with sufficient conditions obtained for the existence of admissible controllers in terms of parameterized linear matrix inequalities (PLMIs) and a non-convex constraint set. The cone complement linearization idea is employed to convert the controller design into a convex optimization problem. A numerical example is provided to illustrate the feasibility and advantage of the proposed controller design procedure. [Nature and Science, 2004,2(1):53-60].

Key words: linear parameter-varying system; parameterized linear matrix inequality; time delay; H_∞ control.

1 Introduction

Linear parameter-varying (LPV) systems have recently much attention because they provide a systematic means of computing gain-scheduled controllers (Shamma, 1990; Apkarian, 1995, 1998). LPV systems are characterized as linear systems that depend on time-varying real parameters. These parameters are assumed to be exogenous signals that are unknown in advance but are constrained a priori to lie in some known, bounded set, and can be measured in real time. Recently, many researchers examined the stability analysis and gain scheduling control of LPV systems extensively and a great number of important results have been reported to the literature (see, for instance, (Shamma, 1990; Apkarian, 1995, 1998; Wu, 2001; Tan, 2000, 2003; Zhang, 2001, 2002; Bara, 2001a, 2001b) and the references therein).

On the other hand, time delays are often present in engineering systems, which have been generally regarded as a main source of instability and poor performance. Therefore, recent research effort is focused more on the analysis and synthesis problems of LPV time-delay systems. To mention a few, (Wu, 2001; Tan, 2003; Tan, 2000) investigated control problems for LPV systems with parameter-varying delays, and (Zhang, 2001, 2002) with a fixed delay size.

In this note, we extend the results in (Wu, 2001) to output feedback control synthesis problems for LPV systems with a parameter-varying state-delay. We seek to develop controllers that are scheduled based on the measurement of the parameters to guarantee stability and the desired H_∞ performance specification. Firstly, a parameter-dependent H_∞ performance criterion is established based on the Lyapunov approach. Secondly, we further improve the obtained performance by decoupling the product terms involving the positive definite matrices, which is enabled the introduction of an additional slack variable. This resulting new performance condition is more easily tractable for analysis and synthesis problems. Thirdly, upon this new criterion, the corresponding parameter-varying dynamic output feedback controllers are designed, which guarantee the closed-loop system to be asymptotically stable with a prescribed H_∞ disturbance attenuation level. Since the sufficient conditions for the existence of such controllers are not expressed as parameterized linear matrix inequalities (PLMIs), an iterative algorithm involving convex optimization is proposed. Numerical

example shows that the effectiveness of the proposed methods. The results obtained in this note can be easily extended to LPV systems with multiple delays.

Notations: Throughout this note the superscript T stands for matrix transposition, R^n denotes the n dimensional Euclidean space, $R^{m\times n}$ is the set of all $m\times n$ real matrices, and the notation $P>0$ for $P\in R^{n\times n}$ means that P is symmetric and positive definite. In addition, in symmetric block matrices or long matrix expressions, we use * as an ellipsis for the terms that are induced by symmetry, $diag\{\cdots\}$ stands for a block-diagonal matrix, and $trace\{H\}$ denotes the trace of the matrix H.

2 Problem Set-up

Consider the following LPV system with a parameter-varying delay:

$$\begin{aligned}\dot{x}(t) &= A(\rho(t))x(t)+A_h(\rho(t))x(t-h(\rho(t)))+B_1(\rho(t))\omega(t)+B_2(\rho(t))u(t)\\ z(t) &= C_1(\rho(t))x(t)+C_{1h}(\rho(t))x(t-h(\rho(t)))+D_{11}(\rho(t))\omega(t)+D_{12}(\rho(t))u(t)\\ y(t) &= C_2(\rho(t))x(t)+C_{2h}(\rho(t))x(t-h(\rho(t)))+D_{21}(\rho(t))\omega(t)\end{aligned} \tag{1}$$

with initial condition

$$x(\theta)=\phi(\theta),\ \ \forall\theta\in[-h(\rho(0)),0] \tag{2}$$

where $x(t)\in R^n$ is the state vector; $y(t)\in R^m$ is the measured output vector; $\omega(t)\in R^l$ is the exogenous disturbance signal; $z(t)\in R^p$ is the control output vector; $u(t)\in R^q$ is control input. The state-space matrices $A(\cdot)$, $A_h(\cdot)$, $B_1(\cdot)$, $B_2(\cdot)$, $C_1(\cdot)$, $C_2(\cdot)$, $C_{1h}(\cdot)$, $C_{2h}(\cdot)$ $D_{11}(\cdot)$, $D_{12}(\cdot)$, $D_{21}(\cdot)$ and the delay $h(\cdot)$ are assumed to be bounded continuous functions of a time-varying parameter vector $\rho(t)\in\Re_\psi^v$. The set $\Re_\psi^v$ is the set of allowable parameter trajectories

$$\Re_\psi^v=\{\rho:\rho(t)\in\psi,|\dot{\rho}_i|\le\upsilon_i,i=1,2,\cdots,s,\forall t\in R_+\} \tag{3}$$

where ψ is a compact set of R^s, $\{\upsilon_i\}_{i=1}^s$ are nonnegative numbers and it is assumed that the parameter trajectories are bounded with bounded variation rates. And the delay $h(\cdot)$ is assumed to be a differentiable function such that $0<h(t)\le H<\infty$, $\dot{h}(t)\le\sigma<1$, $\forall t\ge 0$ .For simplicity, ρ denotes time-varying parameters $\rho(t)$ respectively throughout this note.

Construct a dynamic output feedback LPV controller described by

$$\begin{aligned}\dot{x}_c(t) &= A_c(\rho)x_c(t)+B_c(\rho)y(t)\\ u(t) &= C_c(\rho)x_c(t)+D_c(\rho)y(t)\end{aligned} \tag{4}$$

where $x_c(t)\in R^n$ is the state vector and $A_c(\rho)$, $B_c(\rho)$, $C_c(\rho)$, $D_c(\rho)$ are to be determined parameter-varying matrices.

The feedback connection of the system (1) with the controller (4) produces a closed-loop system described by

$$\begin{aligned}\dot{\xi}(t) &= \bar{A}(\rho)\xi(t)+\bar{A}_h(\rho)E\xi(t-h(\rho))+\bar{B}(\rho)\omega(t)\\ z(t) &= \bar{C}(\rho)\xi(t)+\bar{C}_h(\rho)E\xi(t-h(\rho))+\bar{D}(\rho)\omega(t)\end{aligned} \tag{5}$$

where

$$\begin{aligned}&\xi(t)=\begin{bmatrix}x(t)\\ x_c(t)\end{bmatrix},\ \bar{A}(\rho)=\begin{bmatrix}A(\rho)+B_2(\rho)D_c(\rho)C_2(\rho) & B_2(\rho)C_c(\rho)\\ B_c(\rho)C_2(\rho) & A_c(\rho)\end{bmatrix},\\ &\bar{A}_h(\rho)=\begin{bmatrix}A_h(\rho)+B_2(\rho)D_c(\rho)C_{2h}(\rho)\\ B_c(\rho)C_{2h}(\rho)\end{bmatrix},\quad \bar{B}(\rho)=\begin{bmatrix}B_1(\rho)+B_2(\rho)D_c(\rho)D_{21}(\rho)\\ B_c(\rho)D_{21}(\rho)\end{bmatrix},\\ &\bar{C}(\rho)=\begin{bmatrix}C_1(\rho)+D_{12}(\rho)D_c(\rho)C_2(\rho) & D_{12}(\rho)C_c(\rho)\end{bmatrix},\quad \bar{C}_h(\rho)=C_{1h}(\rho)+D_{12}(\rho)D_c(\rho)C_{2h}(\rho),\\ &\bar{D}(\rho)=D_{11}(\rho)+D_{12}(\rho)D_c(\rho)D_{21}(\rho),\quad E=\begin{bmatrix}I & 0\end{bmatrix}.\end{aligned} \tag{6}$$

Our objective is to seek an output feedback controller that asymptotically stabilizes the closed-loop system and guarantees a prescribed H_∞ performance, that is, it should be guaranteed that

$$\|z\|_2^2 < \gamma^2 \|\omega\|_2^2 \tag{7}$$

for all nonzero $\omega \in l_2[0,\infty)$ under zero initial conditions, where γ is a positive scalar,

$$\|\omega\|_2^2 = \int_0^\infty \omega^T(t)\omega(t)dt \ , \ \|z\|_2^2 = \int_0^\infty z^T(t)z(t)dt \ .$$

3 H_∞ Performance Criterion

In this section, we will establish the H_∞ performance criterion for time-delayed LPV systems.

Lemma 1: Consider system (1) and suppose γ is a given positive constant. Then the closed-loop system (5) is asymptotically stable and has an H_∞ performance level less than γ if there exists a matrix function $0 < P(\rho) = P^T(\rho) \in R^{2n\times 2n}$ and a matrix $0 < Q = Q^T \in R^{n\times n}$ such that for all $\rho \in \Re_\psi^v$ and $|\tau_i| \le \upsilon_i$ the following inequality holds

$$\begin{bmatrix} \bar{A}^T(\rho)P(\rho)+P(\rho)\bar{A}(\rho)+\sum_{i=1}^{S}(\tau_i\frac{\partial P}{\partial \rho_i})+E^TQE & P(\rho)\bar{A}_h(\rho) & P(\rho)\bar{B}(\rho) & \bar{C}^T(\rho) \\ * & -(1-\sum_{i=1}^{S}(\tau_i\frac{\partial h}{\partial \rho_i}))Q & 0 & \bar{C}_h^T(\rho) \\ * & * & -\gamma I & \bar{D}^T(\rho) \\ * & * & * & -\gamma I \end{bmatrix} < 0 \tag{8}$$

***Remark* 1:** The above lemma will be obtained by the similar way to (Wu, 2001) using different Lyapunov-Krasovskii type functional

$$V(\xi(t),\rho(t)) = \xi^T(t)P(\rho)\xi(t) + \int_{t-h(\rho)}^{t} \xi^T(s)E^TQE\xi(s)ds \tag{9}$$

where $0 < P(\rho) = P^T(\rho) \in R^{2n\times 2n}$ and $0 < Q = Q^T \in R^{n\times n}$.

***Remark* 2:** It should be noted that the condition presented in *Lemma 1* contain product terms between Lyapunov matrices and system matrices, such that condition (8) is a bilinear matrix inequality when (6) is considered. In the following, we will present an improved version of *Lemma 1* by introducing a slack variable to decouple these product terms, which is more easily tractable for controller synthesis problems.

***Theorem* 1:** Consider system (1) and suppose γ is a given positive constant. Then the closed-loop system (5) is asymptotically stable and has an H_∞ performance level less than γ if there exists matrix function $0 < P(\rho) = P^T(\rho) \in R^{2n\times 2n}$ and three matrices $0 < Q = Q^T \in R^{n\times n}, 0 < Z = Z^T \in R^{n\times n}, W \in R^{2n\times 2n}$ such that for all $\rho \in \Re_\psi^v$ and $|\tau_i| \le \upsilon_i$ the following inequality and an non-convex condition hold

$$\begin{bmatrix} -(W+W^T) & W^T\bar{A}(\rho)+P(\rho) & W^T\bar{A}_h(\rho) & W^T\bar{B}(\rho) & 0 & 0 & W^T \\ * & -P(\rho)+\sum_{i=1}^{S}(\tau_i\frac{\partial P}{\partial \rho_i}) & 0 & 0 & \bar{C}^T(\rho) & E^T & 0 \\ * & * & -(1-\sum_{i=1}^{S}(\tau_i\frac{\partial h}{\partial \rho_i}))Q & 0 & \bar{C}_h^T(\rho) & 0 & 0 \\ * & * & * & -\gamma I & \bar{D}^T(\rho) & 0 & 0 \\ * & * & * & * & -\gamma I & 0 & 0 \\ * & * & * & * & * & -Z & 0 \\ * & * & * & * & * & * & -P(\rho) \end{bmatrix} < 0 \tag{10}$$

$$QZ = I \tag{11}$$

Proof **:** The proof is based on the generalization of the stability results of (Apkarian, 2001). The inequality (10) is equivalent to:

$$\begin{bmatrix} 0 & P(\rho) & 0 & 0 & 0 & 0 & 0 \\ * & -P(\rho)+\sum_{i=1}^{S}(\tau_i \frac{\partial P}{\partial \rho_i}) & 0 & 0 & \bar{C}^T(\rho) & E^T & 0 \\ * & * & -(1-\sum_{i=1}^{S}(\tau_i \frac{\partial h}{\partial \rho_i}))Q & 0 & \bar{C}_h^T(\rho) & 0 & 0 \\ * & * & * & -\gamma I & \bar{D}^T(\rho) & 0 & 0 \\ * & * & * & * & -\gamma I & 0 & 0 \\ * & * & * & * & * & -Z & 0 \\ * & * & * & * & * & * & -P(\rho) \end{bmatrix} + \begin{bmatrix} -I \\ \bar{A}^T(\rho) \\ \bar{A}_h^T(\rho) \\ \bar{B}^T(\rho) \\ 0 \\ 0 \\ I \end{bmatrix} W \begin{bmatrix} I & 0 & 0 & 0 & 0 & 0 & 0 \end{bmatrix} + (*) < 0$$

Now we can drop the matrix W by using the Projection Lemma. The null-spaces of $\begin{bmatrix} I & 0 & 0 & 0 & 0 & 0 & 0 \end{bmatrix}$ and $\begin{bmatrix} I & \bar{A}(\rho) & \bar{A}_h(\rho) & \bar{B}(\rho) & 0 & 0 & I \end{bmatrix}$ are respectively

$$\begin{bmatrix} 0 & 0 & 0 & 0 & 0 & 0 \\ I & 0 & 0 & 0 & 0 & 0 \\ * & I & 0 & 0 & 0 & 0 \\ * & * & I & 0 & 0 & 0 \\ * & * & * & I & 0 & 0 \\ * & * & * & * & I & 0 \\ * & * & * & * & * & I \end{bmatrix} \quad \text{and} \quad \begin{bmatrix} \bar{A}(\rho) & \bar{A}_h(\rho) & \bar{B}(\rho) & 0 & 0 & I \\ I & 0 & 0 & 0 & 0 & 0 \\ * & I & 0 & 0 & 0 & 0 \\ * & * & I & 0 & 0 & 0 \\ * & * & * & I & 0 & 0 \\ * & * & * & * & I & 0 \\ * & * & * & * & * & I \end{bmatrix},$$

thus the projection conditions yield to:

$$\begin{bmatrix} -P(\rho)+\sum_{i=1}^{S}(\tau_i \frac{\partial P}{\partial \rho_i}) & 0 & 0 & \bar{C}^T(\rho) & E^T & 0 \\ * & -(1-\sum_{i=1}^{S}(\tau_i \frac{\partial h}{\partial \rho_i}))Q & 0 & \bar{C}_h^T(\rho) & 0 & 0 \\ * & * & -\gamma I & \bar{D}^T(\rho) & 0 & 0 \\ * & * & * & -\gamma I & 0 & 0 \\ * & * & * & * & -Z & 0 \\ * & * & * & * & * & -P(\rho) \end{bmatrix} < 0 \tag{12}$$

$$\begin{bmatrix} P(\rho)\bar{A}(\rho)+\bar{A}^T(\rho)P(\rho)-P(\rho)+\sum_{i=1}^{S}(\tau_i \frac{\partial P}{\partial \rho_i}) & P(\rho)\bar{A}_h(\rho) & P(\rho)\bar{B}(\rho) & \bar{C}^T(\rho) & E^T & P(\rho) \\ * & -(1-\sum_{i=1}^{S}(\tau_i \frac{\partial h}{\partial \rho_i}))Q & 0 & \bar{C}_h^T(\rho) & 0 & 0 \\ * & * & -\gamma I & \bar{D}^T(\rho) & 0 & 0 \\ * & * & * & -\gamma I & 0 & 0 \\ * & * & * & * & -Z & 0 \\ * & * & * & * & * & -P(\rho) \end{bmatrix} < 0 \tag{13}$$

By Schur complement (Boyd, 1994), the inequality (13) is equivalent to (8), and (12) is equivalent to the constraint $-P(\rho)+\sum_{i=1}^{S}(\tau_i\frac{\partial P}{\partial\rho_i})<0,\quad (1-\sum_{i=1}^{S}(\tau_i\frac{\partial h}{\partial\rho_i}))>0$

This means that the domain of solution given by (10-11) is included in the domain of solutions satisfying (8) and thus the condition (10-11) is sufficient to ensure the closed-loop system asymptotically stable and guarantee the prescribed H_∞ performance level.

4 H_∞ Output Feedback Synthesis

In this section, the H_∞ performance criterion presented in the above section will be used to design the parameter-dependent H_∞ output feedback controllers.

First we introduce a partition of the slack matrix W and its inverse $V=W^{-1}$ in the form

$$W=\begin{bmatrix}W_{11} & W_{12}\\ W_{21} & W_{22}\end{bmatrix},\quad V=W^{-1}=\begin{bmatrix}V_{11} & V_{12}\\ V_{21} & V_{22}\end{bmatrix} \tag{14}$$

There is no loss of generality in assuming that V_{21} and W_{21} are invertible. Then we introduce the notation

$$J_W=\begin{bmatrix}W_{11} & I\\ W_{21} & 0\end{bmatrix},\quad J_V=\begin{bmatrix}I & V_{11}\\ 0 & V_{21}\end{bmatrix} \tag{15}$$

then $WJ_V=J_W, VJ_W=J_V$. Multiplying the righthand and left-hand sides of the inequality (10) by $J=diag\{J_V,J_V,I,I,I,I,J_V\}$ and its transpose, respectively, we obtain:

$$\begin{bmatrix}
-J_V^TJ_W-J_W^TJ_V & J_W^T\bar{A}(\rho)J_V+J_V^TP(\rho)J_V & J_W^T\bar{A}_h(\rho) & J_W^T\bar{B}(\rho) & 0 & 0 & J_W^TJ_V\\
* & J_V^T(-P(\rho)+\sum_{i=1}^{S}(\tau_i\frac{\partial P}{\partial\rho_i}))J_V & 0 & 0 & J_V^T\bar{C}^T(\rho) & J_V^TE^T & 0\\
* & * & -(1-\sum_{i=1}^{S}(\tau_i\frac{\partial h}{\partial\rho_i}))Q & 0 & J_V^T\bar{C}_h^T(\rho) & 0 & 0\\
* & * & * & -\gamma I & J_V^T\bar{D}^T(\rho) & 0 & 0\\
* & * & * & * & -\gamma I & 0 & 0\\
* & * & * & * & * & -Z & 0\\
* & * & * & * & * & * & -J_V^TP(\rho)J_V
\end{bmatrix}<0 \tag{16}$$

Defining the following matrices

$$\begin{aligned}
&X(\rho)=J_V^TP(\rho)J_V,\quad R=W_{11},\quad F=V_{11},\quad U=W_{11}^TV_{11}+W_{21}^TV_{21},\\
&\tilde{A}(\rho)=W_{11}^TA(\rho)V_{11}+W_{21}^TA_c(\rho)V_{21}+W_{21}^TB_c(\rho)C_2(\rho)V_{11}+W_{11}^TB_2(\rho)C_c(\rho)V_{21}\\
&\qquad +W_{11}^TB_2(\rho)D_c(\rho)C_2(\rho)V_{11},\\
&\tilde{B}(\rho)=W_{21}^TB_c(\rho)+W_{11}^TB_2(\rho)D_c(\rho)\\
&\tilde{C}(\rho)=D_c(\rho)C_2(\rho)V_{11}+C_c(\rho)V_{21}\\
&\tilde{D}(\rho)=D_c(\rho)
\end{aligned} \tag{17}$$

and considering (6) and (15), we have

$$\begin{bmatrix} -(R+R^T) & -(I+U) & X_1(\rho)+R^TA(\rho)+\tilde{B}(\rho)C_2(\rho) & \tilde{A}(\rho)+X_2(\rho) & R^TA_h(\rho)+\tilde{B}(\rho)C_{2h}(\rho) & R^TB_1(\rho)+\tilde{B}(\rho)D_{21}(\rho) & 0 & 0 & R^T & U \\ * & -(F+F^T) & X_2^T(\rho)+A(\rho)+B_2(\rho)\tilde{D}(\rho)C_2(\rho) & X_3(\rho)+A(\rho)F+B_2(\rho)\tilde{C}(\rho) & A_h(\rho)+B_2(\rho)\tilde{D}(\rho)C_{2h}(\rho) & B_1(\rho)+B_2(\rho)\tilde{D}(\rho)D_{21}(\rho) & 0 & 0 & I & F \\ * & * & -X_1(\rho)+\sum_{i=1}^{S}(\tau_i\frac{\partial X_1}{\partial\rho_i}) & -X_2(\rho)+\sum_{i=1}^{S}(\tau_i\frac{\partial X_2}{\partial\rho_i}) & 0 & 0 & C_1^T(\rho)+C_2^T(\rho)\tilde{D}^T(\rho)D_{12}^T(\rho) & I & 0 & 0 \\ * & * & * & -X_3(\rho)+\sum_{i=1}^{S}(\tau_i\frac{\partial X_3}{\partial\rho_i}) & 0 & 0 & F^TC_1^T(\rho)+\tilde{C}^T(\rho)D_{12}^T(\rho) & F^T & 0 & 0 \\ * & * & * & * & -(1-\sum_{i=1}^{S}(\tau_i\frac{\partial h}{\partial\rho_i}))Q & 0 & C_{1h}^T(\rho)+C_{2h}^T(\rho)\tilde{D}^T(\rho)D_{12}^T(\rho) & 0 & 0 & 0 \\ * & * & * & * & * & -\gamma I & D_{11}^T(\rho)+D_{21}^T(\rho)\tilde{D}^T(\rho)D_{12}^T(\rho) & 0 & 0 & 0 \\ * & * & * & * & * & * & -\gamma I & 0 & 0 & 0 \\ * & * & * & * & * & * & * & -Z & 0 & 0 \\ * & * & * & * & * & * & * & * & -X_1(\rho) & -X_2(\rho) \\ * & * & * & * & * & * & * & * & * & -X_3(\rho) \end{bmatrix} < 0 \tag{18}$$

$$\begin{bmatrix} X_1(\rho) & X_2(\rho) \\ * & X_3(\rho) \end{bmatrix} > 0 \tag{19}$$

Summarizing the above way, we can derive the following theorem.

Theorem 2: Consider system (1) and suppose γ is a given positive constant. Then an admissible H_∞ output feedback controller exists if there exist matrices functions

$0 < X_1(\rho) = X_1^T(\rho) \in R^{n\times n}$, $X_2(\rho) \in R^{n\times n}$, $0 < X_3(\rho) = X_3^T(\rho) \in R^{n\times n}$, $\tilde{A}(\rho) \in R^{n\times n}$, $\tilde{B}(\rho) \in R^{n\times m}$, $\tilde{C}(\rho) \in R^{q\times n}$, $\tilde{D}(\rho) \in R^{q\times m}$ and matrices $R \in R^{n\times n}$, $F \in R^{n\times n}$, $U \in R^{n\times n}$ such that for all $\rho \in \Re_\psi^\nu$ and $|\tau_i| \le \upsilon_i$ (11), (18) and (19) hold.

Furthermore, if (11), (18) and (19) have feasible solution, an admissible output feedback can be carried out by two steps:

a. Compute a factorization $V_{21}^TW_{21}$ of $U - V_{11}^TW_{11}$ and deduce V_{21} and W_{21}.

b. Compute the controller data $A_c(\rho), B_c(\rho), C_c(\rho), D_c(\rho)$ by reversing the formulas in (17).

Remark 3: Notice that the PLMI conditions (18) and (19) correspond to infinite-dimensional convex problems due to their parametric dependence. Using the gridding technique and the appropriate basis functions (Apkarian, 1998; Wu, 2001; Tan, 2000, 2003), infinite-dimensional PLMIs can be transformed to finite-dimensional ones, which can be solved numerically using convex optimization techniques. We choose the appropriate basis functions as $\sum_{j=1}^{n_j} f_j(\rho)$, then, for example, we have

$$X_1(\rho) = \sum_{j=1}^{n_f} f_j(\rho) X_{1j} \tag{20}$$

Remark 4: The condition (11) is a non-convex constraint. We can readily modify the algorithm proposed in (El Ghaoui, 1997) to solve the above nonlinear problem to obtain the suboptimal minimum H_∞ performance level γ.

Algorithm 1:

i) Find a feasible solution to (18-21). Set

$$k = 0, \gamma_0 = \gamma. \quad \text{where} \begin{bmatrix} Q & I \\ I & Z \end{bmatrix} \geq 0 \tag{21}$$

ii) Find a feasible set $(R, F, U, X_1, X_2, X_3, \tilde{A}_1, \tilde{A}_2, \cdots \tilde{A}_{nf}, \tilde{B}_1, \tilde{B}_2, \cdots \tilde{B}_{nf}, \tilde{C}_1, \tilde{C}_2, \cdots \tilde{C}_{nf}, \tilde{D}_1, \tilde{D}_2, \cdots \tilde{D}_{nf})^0$.

iii) Choose a sufficiently small initial $0 < \varepsilon \ll 1$ and solve the following LMI problem.

Minimize $Trace(QZ^k + Q^k Z)$ subject to (18-21) .

Set
$$\begin{aligned}&(R,F,U,X_1,X_2,X_3,\tilde{A}_1,\tilde{A}_2,\cdots\tilde{A}_{n_f},\tilde{B}_1,\tilde{B}_2,\cdots\tilde{B}_{n_f},\tilde{C}_1,\tilde{C}_2,\cdots\tilde{C}_{n_f},\tilde{D}_1,\tilde{D}_2,\cdots\tilde{D}_{n_f})^k \\ &=(R,F,U,X_1,X_2,X_3,\tilde{A}_1,\tilde{A}_2,\cdots\tilde{A}_{n_f},\tilde{B}_1,\tilde{B}_2,\cdots\tilde{B}_{n_f},\tilde{C}_1,\tilde{C}_2,\cdots\tilde{C}_{n_f},\tilde{D}_1,\tilde{D}_2,\cdots\tilde{D}_{n_f})\end{aligned}$$

iv) If $Trace(QZ) \leq n + \varepsilon$ holds, then set $\gamma_0 = \gamma$ and return to ii) after decreasing γ to some extent. If $Trace(QZ) > n + \varepsilon$ within a specified number of iterations, then exit. Otherwise, set $k = k + 1$, and go to iii).

5 Numerical Example

Consider the following time-delay LPV system:

$$\begin{aligned}\dot{x}(t) &= \begin{bmatrix} 0 & 1+0.2\rho(t) \\ -2 & -3+0.1\rho(t) \end{bmatrix} x(t) + \begin{bmatrix} 0.2\rho(t) & 0.1 \\ -0.2+0.1\rho(t) & -0.3 \end{bmatrix} x(t-(1+0.5\rho(t)) + \begin{bmatrix} 0.2 \\ 0.2 \end{bmatrix} \omega(t) + \begin{bmatrix} 1 \\ 0.2 \end{bmatrix} u(t) \\ z(t) &= \begin{bmatrix} 0 & 1 \\ 0 & 0 \end{bmatrix} x(t) + \begin{bmatrix} 0 \\ 1 \end{bmatrix} u(t) \\ y(t) &= \begin{bmatrix} 0 & 1 \end{bmatrix} x(t)\end{aligned} \tag{22}$$

where $\rho(t) = \sin(t)$ satisfies $\rho(t) \in [-1,1], \dot{\rho}(t) \in [-1,1]$ and the time delay $h(\rho(t)) = 1 + 0.5\rho(t)$ is varying from 0.5 to 1.5 and the condition $dh/dt < 1$ holds. To design a parameter-dependent output feedback controller to guarantee a prescribed H_∞ performance level γ, we choose appropriate basis functions

$$f_1(\rho(t)) = 1, \quad f_2(\rho(t)) = \rho(t)$$

and grid the parameter space using 9 points grid. By Algorithm 1, for $\gamma = 0.4061$, an admissible parameter--dependent output feedback controller is given by

$$A_c(\rho(t)) = \begin{bmatrix} -277.6489 - 0.1781\rho(t) & 89.7425 + 0.0921\rho(t) \\ -44.6239 - 0.5853\rho(t) & 14.7158 + 0.0273\rho(t) \end{bmatrix}, \quad B_c(\rho(t)) = \begin{bmatrix} -345.9074 - 0.2329\rho(t) \\ -60.4045 - 0.8487\rho(t) \end{bmatrix},$$
$$C_c(\rho(t)) = \begin{bmatrix} 0.0965 + 0.0062\rho(t) & 0.2957 - 0.0050\rho(t) \end{bmatrix}, \quad D_c(\rho(t)) = -0.1054 - 0.0313\rho(t)$$

and for $\gamma = 0.4141$, the controller is described by

$$A_c(\rho(t)) = \begin{bmatrix} -264.9895 - 0.1852\rho(t) & 85.8323 + 0.0946\rho(t) \\ -39.3147 - 0.5791\rho(t) & 12.9948 + 0.0282\rho(t) \end{bmatrix}, \quad B_c(\rho(t)) = \begin{bmatrix} -325.8208 - 0.2406\rho(t) \\ -53.0215 - 0.8355\rho(t) \end{bmatrix},$$

$$C_c(\rho(t)) = \begin{bmatrix} 0.0975 + 0.0064\rho(t) & 0.3014 - 0.0051\rho(t) \end{bmatrix}, \quad D_c(\rho(t)) = -0.1057 - 0.0315\rho(t)$$

Even for $\gamma = 0.105$ and $\varepsilon = 0.0008$, we can still find feasible output feedback controller which produces relatively larger gain than the above results. Therefore, we can choose appropriate γ to design feasible output feedback controller.

6 Concluding Remarks

In this note, a new H_∞ performance criterion for time-delayed LPV systems is presented, upon which the parameter-dependent H_∞ output feedback controller design problem is investigated. An iterative output feedback controller design procedure is described. A numerical example has shown the feasibility and applicability of the proposed designs.

References

[1] Apkarian P, Adams RJ. Advanced gain-scheduling techniques for uncertain systems. IEEE Trans Control System Technology , 1998, 6:21-32.

[2] Apkarian P, Adams RJ. Continuous-time analysis, eigen-structure assignment, and H_2 synthesis with enhanced linear matrix inequalities (LMI) characterizations. IEEE Trans Automatic Control , 2001, 12:1941-6.

[3] Apkarian P, Gahinet PA. Convex characterization of gain-scheduled H_∞ controllers. IEEE Trans Automatic Control , 1995 , 40:853-64.

[4] Bara G.I, Daafouz J, Kratz F. Advanced gain scheduling techniques for the design of parameter-dependent observers [A]. Proceedings of the 40th Conference on Decision & Control, Florida USA, 2001a , 3892-7.

[5] Bara G.I, Daafouz J, Kratz F. Parameter-dependent control with γ -performance for affine LPV systems [A]. Proceedings of the 40th Conference on Decision & Control, Florida USA, 2001b , 2378-9.

[6] Boyd SP, El Ghaoui L, Feron E, Balakrishnan V. Linear matrix inequalities in system and control theory. Philadelphia: SIAM, 1994.

[7] El Ghaoui L, Oustry F, Rami A. A cone complementarity linearization algorithm for static output-feedback and related problems. IEEE Trans Automat Control , 1997 , 42(8):1171-6.

[8] Shamma JS, Athans M. Analysis of gain scheduled control for nonlinear plants. IEEE Trans Automatic Control, 1990, 35:898-907.

[9] Tan K, Grigoriadis KM, L_2-L_2 and L_2-L_∞ output feedback control of time-delayed LPV systems. Proceedings of the 39th IEEE Conference on Decision and Control, Sydney, Australia, 2000 , 4422-7.

[10] Tan K, Grigoriadis KM, Wu F. H_∞ and L_2-to-L_∞ gain control of linear parameter-varying systems with parameter-varying delays. IEE Proc Control Theory Appl , 2003 , 150(5):509-17.

[11] Wu F, Grigoriadis KM. LPV systems with parameter-varying time delays: analysis and control. Automatica , 2001 , 37:221-9.

[12] Zhang LW, Guo LS, Liu XP. H_∞ control for a class of linear parameter-varying systems with time-delay. Control and Decision , 2001 , 5:595-8.

[13] Zhang XP, Tsiotras P, Knospe C. Stability analysis of LPV time-delayed systems. *International Journal on control* , 2002 , 75:538-58.

Study on the Mathematic Model of Product Modular System Orienting the Modular Design

Shisheng Zhong[1], Jiang Li[1], Jin Liu[2], Lin Lin[1]

(1. College of Mechatronic Engineering, Harbin Institute of Technology,
Harbin, Heilongjiang 150001, China, lijiang@hit.edu.cn;
2. Third Department of Aerospace Industry Company, Beijing 100074, China)

Abstract: Modular design is a key technology of implementing virtual organization and mass customization. Orienting the modular design a mathematic model of modular system is presented and is used to realize the mathematic description of modular decomposing "Top-Down" process. Extending Boolean matrix of modular interface relationship is gotten by reverse reasoning strategy of modular interface relationship. The application based on the mathematic model of modular system and extending Boolean matrix of modular interface relationship is concluded, which provides theory foundation for the researching of modular design software system. [Nature and Science, 2004,2(1):61-67].

Keywords: modularization; modular design; modular interface; mass customization

1 Introduction

Modular design technology, as the advanced form of standardization, is a key technology of implementing virtual organization and mass customization. At present, the research of modular design is concentrating on the realization of design, production, assembly and maintaining of the specific product using modular design, and doesn't pay attention to the theory study. As a result, modular design is still a philosophy discussion and a thinking perfection, and can't form a general theory that instruct industry to implementing modular design. Through researching on the process of modular design, this paper presents a mathematical model of product modular system and realizes the mathematical description of the Top-Down module partition process. The application based on the mathematic model of modular system and extending Boolean matrix of modular interface relationship is concluded, which provides theory foundation for the researching of modular design software system (Tong, 2000; Huang, 2000).

2 Product Modular System Modeling

2.1 Product modular system mathematical model

Modular product consisted of basic modules, which have independent function, independent structure and suitable granularity (Figure 1). Basic module refers to the most basic unit that constitutes modular product

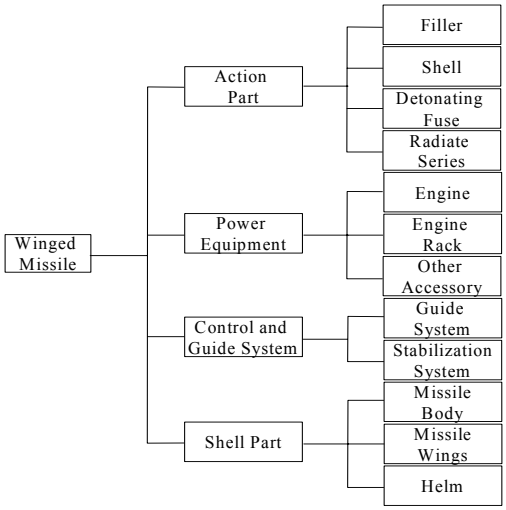

Fig. 1. Modular tree of winged missile

and constructional relationship, or the route of input and output of stream, energy, information, and so on. The superiority of modular design is using existing standard modules to manufacture new product by interchange and combination. From the point of view of systems engineering if we take the basic modules make up of the product as input of the modular design and take the

modular product as the output of modular design, modular product is a system in which basic modules associating and effecting each other in a certain exterior environment (Chen, 1988). We call it product modular system, and its mathematical model can be:

$$P = f(M_n, W_{n\times n}) \quad (1)$$

Where P represents the product modular system, M_n represents the basic modular vector which make up of the modular product, $M_n = (m_1, m_2, \cdots, m_n)$. $W_{n\times n}$ represents the Boolean matrix of interfaces relationship in basic modules, which shows the relationship of the product basic modules. $W_{n\times n} = (\omega_{kl})_{n\times n}$, where $k, l = 1,2,\cdots,n$, and correlative coefficient ω_{kl} determines if there is a relationship between m_k and m_l,

$$\omega_{kl} = \omega_{lk} = \begin{cases} 0, & k = l \\ 0, & k \neq l,\ m_k \text{ and } m_l \text{ have not relationship} \\ 1, & k \neq l,\ m_k \text{ and } m_l \text{ have relationship} \end{cases}$$

We name formula (1) as mathematical model of product modular system. The meaning of the model is that it abstracts the product modular system as a module's netty architecture, which takes the modules selection and the definition of their correlative as system input, and takes the product function and its structure as system output. And this makes the modular design easier to understand.

The mathematical model of product modular system can be used to describe the process of partitioning product modules. The process of partitioning product modules can be descript as: product →first class module→second class module→ ⋯ → basic module, we call the modules that is not the top product and can be partitioned again, such as first class module, second module and etc, as middle module, the process can be described as product→middle module→ basic module.

If mid_v^u represents the module v(v=1,2,⋯) in u(u=1,2,⋯) class, the second module in the first class, power equipment, will be showed as mid_2^1. Suppose mid_v^u can be partitioned into s(s=1,2,⋯) modules, and these modules make up of module vector $Ch_v^u M_s = (ch_v^u m_1, ch_v^u m_2, \cdots, ch_v^u m_s)$. According to formula (1), middle module mid_v^u can be described as:

$$mid_v^u = f(Ch_v^u M_s, Ch_v^u W_{s\times s}) \quad (2)$$

Where $Ch_v^u W_{s\times s} = (\omega_{fg})_{s\times s}$, f,g=1,2,⋯,s, and ω_{fg} has the same way as ω_{kl} to get its value.

Through formula (1) and (2), the process of partitioning product modules be described as a series of module vectors and Boolean matrices of interfaces relationship in modules. Combining with modular tree, these module vectors and Boolean matrices describe the structure and the hiberarchy and netty architecture of product system at the same time.

But through the module vectors and Boolean matrices of interfaces relationship in modules we cannot get the Boolean matrix of interfaces relationship in basic modules directly. The process of partitioning of product modules is Top-Down and classified. In each partitioning action we get the son modules of the middle module or product and the relationship among them, for example, action part, power equipment, control and guide system and shell part are partitioned from winged missile product by a partitioning action, and at the same time the relationship among them and Boolean matrix of their interfaces relationship is determined (Figure. 2 (a)). But we cannot get the correlative among the modules belong to different father modules but at the same class, for instance, the correlative between stabilization system in control and guide system and helm in shell part, or engine rack in power equipment and missile body in shell part, etc. This paper presents extending Boolean matrix of modular interface relationship and reverse reasoning strategy of modular interface relationship to solve the problem.

2.2 Extending boolean matrix of modular interface relationship and reverse reasoning strategy of modular interface relationship

Modular interface relationship can be divided into inter interface relationship and outer interface relationship. The inter interface relationship refers to the interface relationship among the modules belong to a same superior module, for instance, the relationship between stabilization system and control and guide system; the outer interface relationship refers to the interface relationship among the modules belong to different superior module or between the module and the environment, for example, the correlative between stabilization system in control and guide system, and helm in shell part, or engine rack in power equipment and missile body in shell part. Especially, we define the relationship between

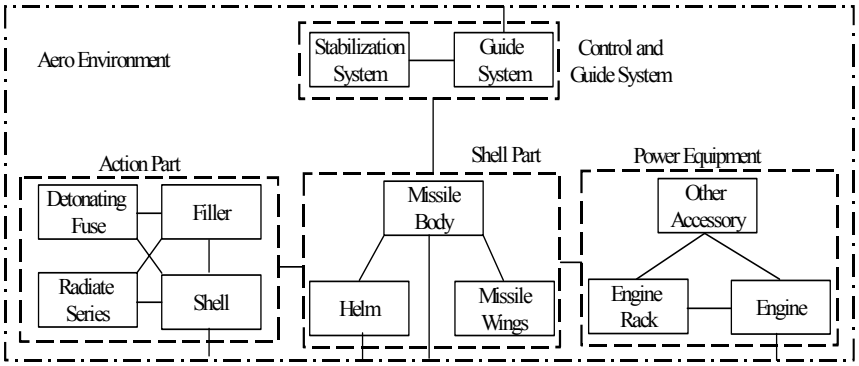

(a) Modular relationship in partitioning

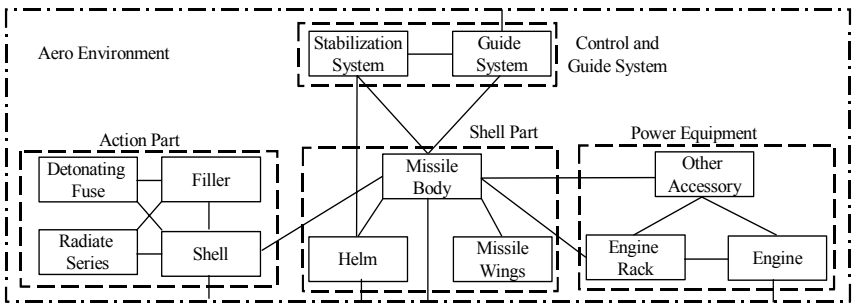

(b) Real modular relationship

Figure 2 Modular relationship in partitioning and real modular relationship

module and the outer system environment as system interface relationship. This relationship belongs to outer interface relationship.

Boolean matrix of modular interface relationship only describes the inter interface relationship and cannot show the outer interface relationship.

In order to describe the process of the modular partitioning process and the structure of product modular system, we introduce the extending subordinate modular vector

$ExCh_v^u M_{s+1} = (ch_v^u m_1, ch_v^u m_2, \cdots, ch_v^u m_s, om)$,

om represents outer module that don't belong to a same superior module in the same class or be the outer environment. Based on the extending subordinate modular vector, extending Boolean matrix of interface relationship in the subordinate modules of the middle module can be showed as

$$ExCh_v^u W_{(s+1)\times(s+1)} = (\psi_{bc})_{(s+1)\times(s+1)},$$

where $b, c = 1,2,\cdots,s+1$. When $b, c = 1,2,\cdots,s$, ψ_{bc} and ω_{fg} have the same way to get there values. They show if module $ch_v^u m_b$ and module $ch_v^u m_c$ have interface relationship, and we call them inter correlative coefficient. When $b = s+1$ or $c = s+1$, ψ_{bc} shows that if module $ch_v^u m_c$ or $ch_v^u m_b$ have the interface relationship with om, we call it outer correlative coefficient. If an interface relationship is exist between b and c, then $\psi_{bc} = \psi_{cb} = 1$, else $\psi_{bc} = \psi_{cb} = 0$. If $Exmid_v^u$ is used to represent the middle module that its outer interface relationship is defined, the extending mathematical model of middle module can be described as

$$Exmid_v^u = f(ExCh_v^u M_{s+1}, ExCh_v^u W_{(s+1)\times(s+1)}) \quad (3)$$

Accordingly, if we use

$$ExM_{n+1} = (m_1, m_2, \cdots, m_n, om)$$

to represent extending basic modular vector of product modular system, and use

$$ExW_{(n+1)\times(n+1)} = (\psi_{eq})_{(n+1)\times(n+1)}$$

$(e, q = 1,2,\cdots,n+1)$to describe the interface relationship

among basic modules or between basic module and system environment, and utilize ExP to represent the product system, then extending mathematical model of product modular system can be described as

$$ExP = f(ExM_{n+1}, ExW_{(n+1)\times(n+1)}) \quad (4)$$

The extending mathematical model of product modular system not only shows the relationship of system basic modules, but also defines the correlative of basic modules and the environment. The model further uncovers the essence of product modular system, and can be used to describe the process of partitioning product modules, which is the coming into being process of the modules and the extending Boolean matrices of their relationship. This paper presents the reverse reasoning strategy of modular interface relationship to get the relationship of basic modules, that is to say, the extending Boolean matrices of interface relationship in basic modules.

Reverse reasoning strategy of modular interface relationship is that using the modular tree and the extending Boolean matrices of modular interface relationship formed in partitioning process, and through interface matching to superpose the extending Boolean matrices of modular interface relationship of every class to the last class by breaking up the interface relationship in middle modules and transforming it to the interface relationship in basic modules, in the end obtaining the extending Boolean matrix of interface relationship in product basic modules. In order to put in force the reverse reasoning strategy of modular interface relationship, and realize the coming into being of the extending Boolean matrix of interface relationship in basic modules automatically, the product modular design system must have the ability:

(1) The outer interface relationship can be transferred and their information is equal. That is to say, the outer interface relationship can be divided and distributed to the outer interface relationship in the subordinate modules, and parameters of the interface will not change.

(2) Descript and definition of modular interface information can be queried and distinguished. So we can confirm if the modular interface relationship is matching according to the qualitative and quantitative information.

The reverse reasoning strategy of modular interface relationship can be described as next five steps:

(1) According to principle of partitioning modules, the product is broken up to suitable classes. Partitioning process of middle modules includes confirming subordinate modules number, describing basic information of subordinate modules, defining interface relationship (including inter interface relationship and outer interface relationship) of subordinate modules and describing interface information of subordinate modules. We get the extending Boolean matrices of interface relationship in the subordinate modules of product and middle modules, and at same time we get the modular tree that shows the hiberarchy of product system. Suppose that the max class of modular tree is z, if array num(u) (u=1,2,⋯,z) represents the module number of the class u, chn(u)(v) represents the subordinate module number of the module v(v=1,2,⋯,num(u)) in class u, then according to formula (3), the middle module of every class can be showed as

$$mid_v^u = f(ExCh_v^u M_{chn(u)(v)+1}, ExCh_v^u W_{(chn(u)(v)+1)\times(chn(u)(v)+1)})$$

where

$$ExCh_v^u M_{chn(u)(v)+1} = (ch_v^u m_1, ch_v^u m_2, \cdots, ch_v^u m_{chn(u)(v)}, om)$$

$$ExCh_v^u W_{(chn(u)(v)+1)\times(chn(u)(v)+1)} = (\psi_{(row,col)})_{(chn(u)(v)+1)\times(ch(u)(v)+1)}$$

$row, col = 1,2,\cdots,chn(u)(v)+1$.Then the subordinate module of class u is the module of module u+1, and $ch_v^u m_j = mid_{vi+j}^{u+1}(vi = \sum_{x=1}^{v-1} chn(u)(x)\ ,\ j = 1,2,\cdots,chn(u)(v))$.

Especially, when a basic module appears in middle classes, it will be taken as the subordinate module of itself.

(2) Suppose that the module number of last class is n, then $num(z) = n$. We arrange the basic modules of the product to the basic vector of the product modular system according to their top-down sequence in modular tree. Combing with the outer module, the basic vector is extended to the extending basic vector $(m_1, m_2, \cdots, m_n, om)$ (where $m_i = mid_i^z$, and $i = 1,2,\cdots,n$).The extending basic vector determines the columns and the rows of the extending Boolean matrix of interface relationship in basic modules. Let

correlative coefficient be zero, that is to say,

$$ExW_{(n+1)\times(n+1)} = (\psi_{eq})_{(n+1)(n+1)} = (0)_{(n+1)(n+1)}.$$

Table 1 is an extending Boolean matrix of interface relationship in winged missile basic modules.

(3) For $mid_v^{z-1}(v = 1,2,\cdots,num(z-1))$, if mid_v^{z-1} is a middle module, then its subordinate modules must be basic modules. Suppose that $row,col = 1,2,\cdots,chn(z-1)(v)$, then $\psi_{(row,col)}$ in $Exch_v^{z-1}W_{(chn(z-1)(v)+1)\times(chn(z-1)(v)+1)}$ and $\psi_{(vi+row,vi+col)}$ in $ExW_{(n+1)\times(n+1)}$ are equal. According to inter correlative coefficient of the extending Boolean matrices of interface relationship in the subordinate modules of middle modules, we may get inter correlative coefficient of the extending Boolean matrix of interface relationship in basic modules, and these inter correlative coefficients are close to the diagonal of the extending Boolean matrix of interface relationship in basic modules, see the part of Figure 1. For example, we can get inter correlative coefficients of basic module missile body, missile wings and helm in shell part through the extending Boolean matrix of interface relationship in the subordinate modules of module shell part.

(4) For module $mid_v^{z-2}(v = 1,2,\cdots, num(z-2))$ in class z-2, if mid_v^{z-2} is a middle module and its subordinate modules are basic modules, then we replace inter correlative coefficients of the basic modules with inter correlative coefficients of the subordinate modules of module mid_v^{z-2} following the step 3. If the subordinate modules of mid_v^{z-2} are middle modules, we suppose that $row,col = 1,2,\cdots,chn(z-2)(v)$ and seeing about the middle module $ch_v^{z-2}m_{row}$ and $ch_v^{z-2}m_{col}$ in $Exch_v^{z-1}W_{(chn(z-2)(v)+1)\times(chn(z-2)(v)+1)}$ where $\psi_{(row,col)} = 1$.

According to the characters of modular design, the inter interface relationship in the father modules is the outer interface relationship in their son modules, so if module $ch_v^{z-2}m_{row}$ and $ch_v^{z-2}m_{col}$ have a inter interface relationship, it means that there are outer interface relationships in their son modules. In this situation, in the extending Boolean matrices of interface relationship in their son modules we should find out the basic modules that their outer correlative coefficients are 1. According to the ability that the interface information can be queried and distinguished, and the character that the interface relationship can be transferred and its quantity is equal, we can find the basic modules that are the subordinate modules and have interface relationship by the type of interface relationship, the main parameters of interface relationship and the condition that the middle modules are partitioned. And we define the correlative coefficients accordingly as 1. For example, the confirming of $\psi_{2,6}$ and $\psi_{6,10}$, and so on in Table 1. When subordinate modules of mid_v^{z-2} are middle modules or basic modules, the management is same as above, and at this time, if basic module and the subordinate modules of middle module have a interface relationship, that is to say, the relationship is the inter interface relationship of basic module and the outer interface relationship of the subordinate module.

(5) Repeat step 4, and transfer the inter interface relationship in every middle modules to outer interface relationship in their subordinate modules, so interface relationships are transferred downwards and finally turn into the interface relationship of basic modules. And the system interface relationship of product also can be transferred to the outer interface relationship in basic modules. See the outer interface relationship of m_5 and m_8 in Table 1. The whole extending Boolean matrix of interface relationship in product basic modules is established.

Reverse reasoning strategy of modular interface relationship realizes establish of the extending Boolean matrix of interface relationship in product basic modules. The matrix shows the relationship in basic modules and in basic modules and the environment. Combining with the modular definition model, we can realize the auto form of the extending Boolean matrix of interface relationship in basic modules.

3 Application of the Model

Through the mathematics of product modular system we can know the interface relationship of every two basic modules. If we use $R_k\,(k = 1,2,\cdots,n)$ to express the basic modules aggregate which have relationship with the basic module m_k, then

$$R_k = \{r_l \mid r_l = m_l \times \omega_{lk} \ and \ r_l \neq 0, l = 1,2,\cdots,n\} \quad (5)$$

Where $r_l = m_l \times \omega_{lk} = \begin{cases} 0, & \omega_{lk} = 0 \\ m_l, & \omega_{lk} = 1 \end{cases}$.

Table 1 The extending Boolean matrix of interface relationship in product basic modules of Figure 1

	m_1	m_2	m_3	m_4	m_5	m_6	m_7	m_8	m_9	m_{10}	m_{11}	m_{12}	Om
M_1	0	1	1	1									
M_2	1	0	1							1			1
M_3	1	1	0										
M_4	1			0									
M_5					0	1	1						1
M_6					1	0	1			1			
M_7					1	1	0			1			
M_8								0	1	1			1
M_9								1	0	1		1	
M_{10}		1				1	1	1	1	0	1	1	1
M_{11}										1	0		1
M_{12}									1	1		0	1
om		1			1			1		1	1	1	0

Note: the space in the Table is 0.

And we can know if basic module m_k has relationship with outer environment through judging the value of $\omega_{(n+1)k}$ and $\omega_{k(n+1)}$. The basic modules aggregate that relates with outer environment is

$$R_{n+1} = \{r_l \mid r_l = m_l \times \omega_{l(n+1)}, and \quad r_l \neq 0, l = 1,2,\cdots,n\}$$

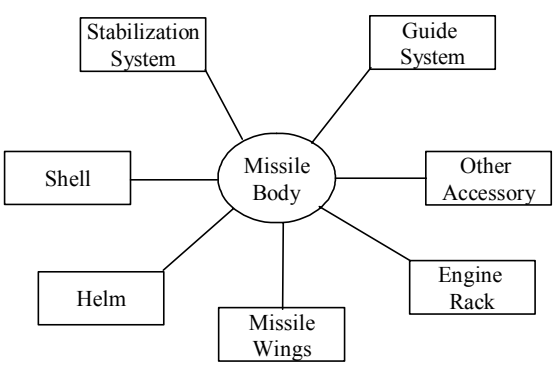

Fig. 3. Relationship figure of Missile Body

For example, R_{10} is a basic modules aggregate that relate to the basic module m_{10}. According to Table 1 and formulation (5), we can get

$$R_{10} = \{m_2, m_6, m_7, m_8, m_9, m_{11}, m_{12}\}.$$

Specific relationship is showed in Figure 3.

According to the relationship in basic modules, the hierarchy and inclusive relationship between basic modules and middle modules, we can judge if there is a relationship between random two modules (middle modules or basic modules). The judgment of the relationship in modules provides a possibility of partitioning the task of modular design and demonstrates which two companies have relationship in the process of product concurrent design.

The application of the mathematic model of product modular system also can be researched and discussed as follow:

(1) Realize the automatization and intelligentization of product modular synthesis using the

technology of neural net. We can take product basic modular vector and the extending Boolean matrix of interface relationship in basic modules as input and take product function and structure as output, using the technology of neural net to realize modular synthesis.

(2) Judge if the modular partition is reasonable by the extending Boolean matrix of interface relationship in basic modules. The degree of the product modularization relates to the interface numbers of product basic modules directly. We can Judge if the modular partition is reasonable by computing interface numbers in the extending Boolean matrix of interface relationship. Denmark scholar Juliana Hsuan has done some research (Hsuan, 1999).

(3) Application of the extending Boolean matrix's variation. The extending Boolean matrix of interface relationship in basic modules describes the common interface relationship in basic modules. We can map the matrix to different departments of the company, such as design, product, assemble, and so on.

4 Conclusion

Orienting the modular design a mathematic model of modular system is presented and is used to realize the mathematic description of modular decomposing "Top-Down" process. Base on the model, mathematic expression of the product interface relationship is discussed. Extending Boolean matrix of modular interface relationship is gotten by reverse reasoning strategy of modular interface relationship. The application based on the mathematic model of modular system and extending Boolean matrix of modular interface relationship is concluded, which provides theory foundation for the researching of modular design software system.

Acknowledge

This research is supported by the High-Tech Research and Development Program of China (No. 2001AA412210).

References

[1] Chen L, Lu J. Theory and application of systems engineering. Academic Magazine Publishing Company, Beijing, China, 1988 .

[2] Huang C. Overview of modular product development. Proc Natl Sci Counc ROC(A), 2000 , 24:149-65.

[3] Hsuan J. Impacts of supplier–buyer relationships on modularization in new product development, European Journal of Purchasing and Supply Management , 1999 , 197－209.

[4] Tong S. Modular principle, design method and application., Standard Publishing Company of China，Beijing, China , 2000.

L-THIA: A Useful Hydrologic Impact Assessment Model

Yongsheng Ma

(Research Scholar, Institute of Water Research, Michigan State University, MI 48823)

[Nature and Science, 2004,2(1):68-73]

1 Introduction

L-THIA (Long-Term Hydrologic Impact Assessment) has been developed by Purdue University (contact persons: Bernie Engel, and Jon Harbor) as a straightforward analysis tool that provides estimates of changes in runoff, recharge and non-point source pollution resulting from past or proposed land use changes. L-THIA was initially designed for planners and natural resource managers because they are familiar with land use change in a particular area, have perhaps the best access to land use information, and are often interested in environmental impacts. Whether it be past, present, or projected land use development scenarios, establishing land use areas and determ- ining CNs as input variables to runoff estimation is a task well-suited to planners and resource managers. L-THIA and many other models determine runoff from precipitation data and a land use / soils index, the Curve Number (CN), developed from real-world data by the United States Department of Agriculture, Soil Conservation Service (USDA, 1986).

It is important to consider the effects land use changes have on surface runoff, stream flow, and groundwater recharge. Expansion of urban areas significantly impacts the environment in terms of ground water recharge, water pollution, and storm water drainage. Urbanization leads to creation of impervious surfaces, which lead to an increase in surface runoff volume, this in turn contributes to downstream flooding and a net loss in groundwater recharge. Eventually loss of recharge affects residential and municipal water supplies. Minimizing the disturban- ce on an urbanizing watershed is one way of ensuring continued water supply. Since each land use has a different level of impact, careful physical planning can minimize these impacts. Although the impacts of urban sprawl on groundwater recharge and surface water quantity and quality are of considerable importance, many planners, city managers and water resource professionals lack the ability to provide estimates of the potential hydro- logic impacts of land use change.

L-THIA was developed as a straigh- tforward analysis tool to provide estimates of changes in runoff, recharge and non-point source pollution resulting from past or proposed land use changes. It gives long-term average annual runoff for a land use configuration, based on actual long-term climate data for that area. By using many years of climate data in the analysis, L-THIA focuses on the average impact, rather than an extreme year or storm.

The SCS CN method, which is a core component of many traditional hydrologic models, has been used in a straightforward simple fashion to assess the long-term hydrological impacts of land use change.

Ref. web sites:

http://www.ecn.purdue.edu/runoff/documentation/about.html

What is L-THIA?

http://www.ecn.purdue.edu/runoff/documentation/downloads/whislthia.ppt

Why use L-THIA?

http://www.ecn.purdue.edu/runoff/documentation/downloads/yuselthia.ppt

How L-THIA works?

http://www.ecn.purdue.edu/runoff/documentation/how%20works.html

2 Runoff Basics

Runoff is that portion of precipitation that flows over land surfaces toward larger bodies of water. Before runoff can occur, rainfall must satisfy the immediate demands of infiltration, evaporation, interception, surface storage, and surface detention and/or channel detention. Some are very minor losses, *e.g.,* interception by a corn crop is only about 0.02 inches. However, in a forested area interception may not be minor, accounting for up to 25 percent of the rainfall. For short time periods (storms) on agricultural lands:

rainfall - runoff = infiltration

This can be illustrated by a hydrograph with a steady rainfall input:

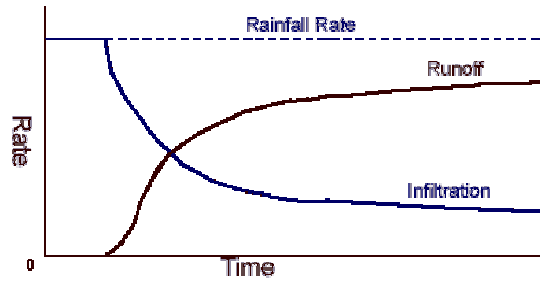

Notice that runoff is an approximate mirror image of infiltration (with some additional time-lag for overland flow travel lag).

3 Factors Affecting Runoff

There are two broad categories of factors that control runoff: rainfall (storm) characteristics and watershed physical conditions. Important rainfall character- istics include duration, amount, intensity and distribution. Key watershed factors are:

Size

For a fixed return interval, as watershed size increases, the runoff per unit area decreases. This occurs primarily because **average** rainfall amount decreases with increasing area; secondarily, increa- sed travel time for runoff allows more infiltration and other losses.

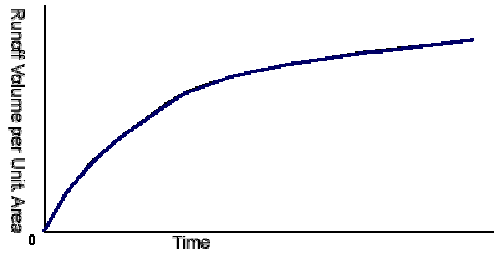

Shape

For equal sized watersheds, runoff decreases as overland flow length incr- eases. This results from the increased time of concentration. Longer duration storms, needed to produce runoff from all points in watershed, have lower average intens- ities.

Topography

Surface slopes and roughness greatly influence runoff. Seep slopes reduce time of concentration and detention volume. Roughness increases surface storage and promotes greater infiltration, both of which decrease runoff.

Soils

Watershed soils influence infiltration and deep seepage rates. Infiltration must be satisfied before runoff begins.

Surface culture

Modern agricultural practices prom- ote infiltration, slow runoff and reduce the antecedent water content of soils prior to a storm event.

Runoff hydrograph

A graph of runoff rate vs. time is called a runoff hydrograph. The shape of a hydrograph depends on the time distribution of rainfall and upon watershed flow characteristics. However, most hydr- ographs bear some resemblance to the "typical shape" shown below:

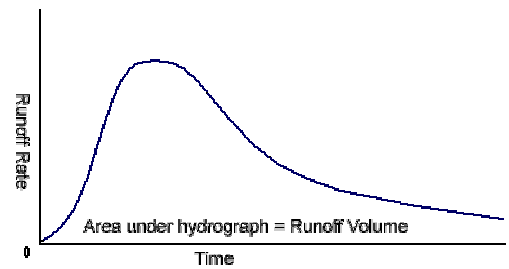

The receding limb of a hydrograph usually extends over a longer period of time than the rising limb. The area under the curve gives the volume runoff (volume/time x time = volume). In this course, we will primarily use the peak runoff rate in our problems. Since hydrographs of previous storm events are seldom available for small watersheds, estimates of peak rates and/or volume must be made using computational models rather than from statistical analyses of past records.

Ref web site:

http://www.ecn.purdue.edu/runoff/documentation/runoff.htm

4 The SCS Curve Number Method

The SCS curve number method is a simple, widely used and efficient method for determining the approximate amount of runoff from a rainfall even in a particular area. Although the method is designed for a single storm event, it can be scaled to find average annual runoff values. The start requirements for this method are very low, rainfall amount and curve number. The curve number is based on the area's hydrologic soil group, land use, treatment and hydrologic condition. The 2 former being of greatest are importance.

For detail:

http://www.ecn.purdue.edu/runoff/documentation/scs.htm

The concept of a limited recharge capacity, which is determined by ant-ecedent moisture conditions and by the physical characteristics of the drainage basin, has been elaborated by the U.S. Soil Conservation Service to a preconceived multiple correlation model in which the partial correlations are expressed in tabular form. This method is described in the S.C.S. National Engineering Handbook (1964; SCHULZE, 1966). It takes its name from the curve number

$$CN = 1000 / (10 + S) \qquad (1)$$

Where S is the recharge capacity or "potential maximum retention" at a certain time. The curve number is found from tables as a function of antecedent rainfall, land use, density of pant cover, soil type, and not readily applicable in other parts of the world. If used outside the U.S.A., they will first have to be adjusted to local conditions.

The underlying concept of the model is: $I_a = 0.2S$ is an initial quantity of interception, depression storage, and initial infiltration that must be satisfied by any rainfall before runoff can occur.

The ratio of direct runoff Q and the precipitation minus the initial loss $P - I_a$ equals the ratio of the actual recharge minus initial loss, $P - Q - I_a$ and the mathematical model could be based.

$$Q / (P - I_a) = (P - Q - I_a) / S \qquad (2)$$

or $Q = (P - I_a)^2 / (P - I_a + S)$

And since $I_a = 0.2S$ it follows that:

$$Q = (P - 0.2S)^2 / (P + 0.8S) \qquad (3)$$

The curve expressing the relation of Q and P depending on the parameter S (and $I_a = 0.2S$) is the only parameter in this model that determines the relationship between the amount of rainfall in one day and the corresponding daily amount of rainfall excess that will subsequently.A heterogeneous basin may be divided into sub-areas with different curve numbers. The total rainfall excess is then obtained by adding up the amounts that have been computed for the sub-areas. The basic assumption, which has been expressed in Eq. 2, is certainly open to criticism. For high values of P and Q the left hand side of Eq. 2 approaches unity, whereas the right hand side cannot exceed the value of 0.8, unless the actual recharge P-Q exceeds the recharge capacity S. This, of course, is in contradiction with the concept of recharge capacity. Substitution of Q = P - S in Eq. 3 shows that the limit is reached for P = 4.2 S. Therefore the U.S. Soil conservation Service introduced the limits $P > I_a$ and $S > I_a + F$, where $F = P - I_a - Q$. It follows that $S > P - Q$. For high curve numbers which go with a small recharge capacity, this could imply a definite restriction to the method's applicability.

Be transformed into direct runoff.

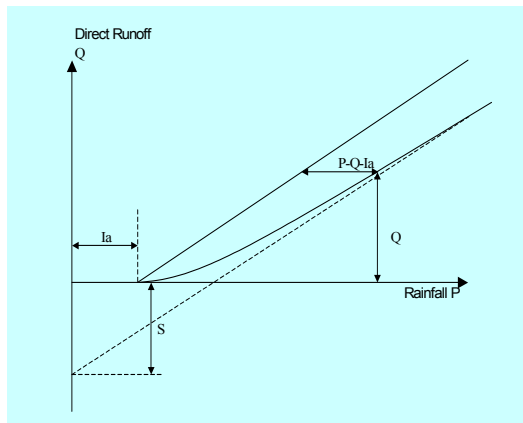

Curve number method: Relationship rainfall-direct runoff as dependent on the recharge capacity.

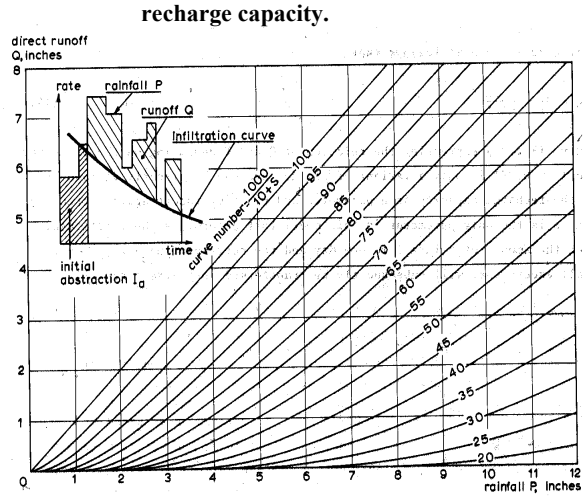

Solution of Eq.3 for various values of the recharge capacity, S. (U.S. Soil Conservation Service, 1964)

Although the underlying concept is not quite sound, the method is presented here because much work has been done to correlate the one parameter S with antecedent rainfall, seasonal effects, and certain

characteristics of the soil surface and plant cover.

Ref. web sites:

http://www.ilri.nl/publications/pub16.html

About ILRI:

http://www.ilri.nl/institute/ilri.html

http://www.ecn.purdue.edu/runoff/documentation/scs.htm

http://pasture.ecn.purdue.edu/~aggrass/agnps/runoff.html#curve%20number

Derivation of SCS Curve Number Method:
http://www.engr.udayton.edu/Civil/CIE%20333%20Winter%202002/SCS_CN.htm

About TR-55:

http://www.brc.tamus.edu/epic/documentation/tr55method.html

For detail:

http://www.ecn.purdue.edu/runoff/documentation/scs.htm

5 Non-Point Source Pollution and Hydrologic Soil Groups

NPS pollution comes from many diffuse sources. It is caused by rainfall or snowmelt moving over and through the ground. Runoff after rain events pick up and carry away natural and human-made pollutants, finally depositing them into lakes, rivers, wetlands, coastal waters, and even our underground sources of drinking water. NPS pollution remains the largest source of pollution of water bodies the United States. (EPA, 1997).

For detail**:**

http://www.ecn.purdue.edu/runoff/documentation/nps/nps.htm

NPS Pollution - Common Sources:

http://www.ecn.purdue.edu/runoff/documentation/nps/common_nps.htm

NPS Pollution - Reducing Sources:
http://www.ecn.purdue.edu/runoff/documentation/nps/reducing_nps.htm

Soils are classified by the Natural Resource Conservation Service into four Hydrologic Soil Groups based on the soil's runoff potential. The four Hydrologic Soils Groups are A, B, C and D. Where A's generally have the smallest runoff potential and Ds the greatest.

Details of this classification can be found in 'Urban Hydrology for Small Watersheds' published by the Engineering Division of the Natural Resource Cons- ervation Service, United States Depar- tment of Agriculture, Technical Release–55.

Group A is sand, loamy sand or sandy loam types of soils. It has low runoff potential and high infiltration rates even when thoroughly wetted. They consist chiefly of deep, well to excessively drained sands or gravels and have a high rate of water transmission.

Group B is silt loam or loam. It has a moderate infiltration rate when thoroughly wetted and consists chiefly or moderately deep to deep, moderately well to well drained soils with moderately fine to moderately coarse textures.

Group C soils are sandy clay loam. They have low infiltration rates when thoroughly wetted and consist chiefly of soils with a layer that impedes downward movement of water and soils with moderately fine to fine structure.

Group D soils are clay loam, silt clay loam, sandy clay, silt clay or clay. This HSG has the highest runoff potential. They have very low infiltration rates when thoroughly wetted and consist chiefly of clay soils with a high swelling potential, soils with a permanent high water table, soils with a clay pan or clay layer at or near the surface and shallow soils over nearly impervious material.

For detail:

http://www.ecn.purdue.edu/runoff/documentation/hsg.html

6 Getting Started - A Tutorial for L-THIA

This document describes how to get started in using the L-THIA WWW system. An example application of L-THIA WWW is presented to describe how to use the system.

For detail:

http://www.ecn.purdue.edu/runoff/documentation/tutorial.htm

The model runs can be made by selecting the input option from the menu on the left to return to the input form. There are several options of input: the basic input, detailed input, advanced input, and impervious area input.

7 L-THIA Input

To begin using L-THIA WWW, select the arrow to the left of the input option from the menu on the left.

Scenario Name

The scenario name will be used in tracking your L-THIA analysis.

Location

Select the location of the area being analyzed (State and County) from pull down menus. The location information is used to select the appropriate rainfall data for running L-THIA.

Units

Select the units that will be used in describing the area you are analyzing.

Land Use

The land uses considered are selected from the SELECT LANDUSE menus. Be sure that all of the columns add to the same amount of land. You may need to click on another entry box for the last value entered to the included in the totals.

Hydrologic Soil Groups

Hydrologic soil group is a soil property that characterizes the runoff tendency of the soil. If you do not know the hydrologic soil group for an area you wish to analyze, this information can be obtained after selecting the state of interest in state field.

If the detailed input was selected, the user can define a custom land use. In the land use drop down menu, choose the custom option. In the pop-up box, enter a name for the land use and the appropriate curve number separated by a comma. The last column of the input sheet is labeled "SELECT Land Use Similar to the Custom Land Use for NPS Estimation". In this column select the land use that most closely represents the custom land use for the approximation of NPS pollution.

Ref web sites: L-THIA WWW: A short tour:

http://www.ecn.purdue.edu/runoff/documentation/downloads/lthiawww1.ppt

(1) The basic input and detailed input

You can select either basic or detailed input. With the basic input the user can chose from 8 different land use types. This input form is for involved community people who many not have a background in land use planning but are concerned with development in their area. The detailed input has 13 different land use choices plus a custom field. If the custom field is chosen the user can create a new land use by defining the appropriate curve number. Land use planners, deve- lopers; landscape architects and consu- ltants are the intended users of this type of input.

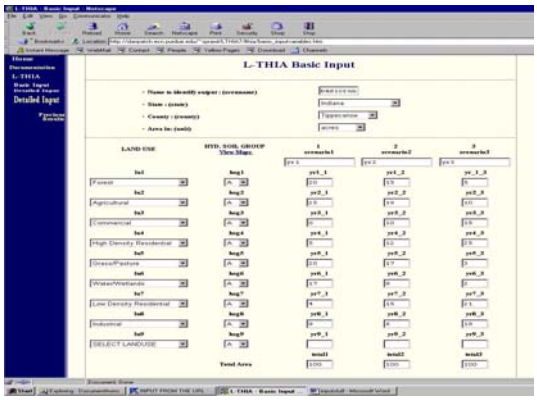

Link to L-THIA Basic Input and Detail Input:

L-THIA Basic Input:

http://www.ecn.purdue.edu/runoff/lthia/basic_input.htm

L-THIA Detailed Input:

http://www.ecn.purdue.edu/runoff/lthia/detailed_input.htm

(2) The advanced input page

The Advanced input page should be used in one or more of the following situations.

a. The user wants to calculate the NPS pollution for pollutants other than the standard pollutants

b.The user wants to enter pollutant expected mean concentration (EMC) values other than the default values for these pollutants.

c.The user wants to specify a LAND USE other than the default LAND USES for a given land area.

Link to L-THIA Advanced Input:

http://www.ecn.purdue.edu/runoff/lthia/advanced_input.htm

(3) The impervious area input

The 'Percent Impervious Area Input' of L-THIA is best suited for urban land use change analysis. The Curve Number (CN) Value calculated by the model for this particular input is based on the assumption that the pervious area is 'grass' in 'fair' condition.

In case the pervious area is agricu- ltural or forest for example the CN value and consequently the runoff generated will be very different. Land uses such as agriculture, also generate runoff and impact the long-term hydrology of the watershed. Converting agricultural land to urban use generates less difference in the amount of runoff than if grassland or forest is converted to higher intensity uses such as commercial or high density residential.

Link to L-THIA Impervious Input:

http://www.ecn.purdue.edu/runoff/lthia/impervious_input.htm

For how using L-THIA first to visit:

http://www.ecn.purdue.edu/runoff/documentation/lthiaurllink.htm

8 L-THIA Output

Once L-THIA runs (a few seconds), the results will appear in the WWW browser. The average annual depth of runoff for each land use and soil combination is also reported as shown.

Runoff

Average annual runoff volumes are also reported in tabular form in this section. Volumes are reported for each time period analyzed.

If you are going to want to review your data later, provide a user name and password at the bottom of the page.

The runoff depth and volume results can also be viewed in graphical form by selecting the bar chart or pie chart option from the menu on the left side of the web browser window.

Non-Point Source Pollution

Non-point source (NPS) pollution results can be obtained by selecting NPS in the menu on the left (use the mouse to click on the triangle symbol beside NPS). A list of NPS outputs will be made available as shown in the figure at the right. Select the NPS pollutant of interest and then select the format that you wish to use when viewing the data.

9 Conclusion

L-THIA results can be used to aid land use planners in a variety of ways. For instance, a planner may decide to change the land use based on soil type, to minimize impact in a given area. That is because the same land use located on different hydrologic soil types has different impacts. Also, since the amount of runoff generated by different land uses is a function of the hydrologic soil type and the land use, relocating land uses based on the hydrologic soil type can in some cases significantly reduce the long-term impact of the development.

Ref. web sites:

Advanced GIS version:

http://www.ecn.purdue.edu/runoff/documentation/downloads/lthiagiswww111.avi

Field Evaluation of permeable pave- ments for storm water management:

http://www.ecn.purdue.edu/runoff/documentation/downloads/perm.pdf

Street storage for combined sewer surcharge control:

http://www.ecn.purdue.edu/runoff/documentation/downloads/street.pdf

Low impact development (LID):

http://www.ecn.purdue.edu/runoff/documentation/downloads/effect.pdf

Low impact development hydrolo-gy analysis:

http://www.ecn.purdue.edu/runoff/documentation/downloads/LID_HYDR.PDF

Chaotic Analysis on Precipitation Time Series of Sichuan Middle Part in Upper Region of Yangtze

Baohui Men [1, 2], Chuan Liang [2], Xiejing Zhao [1]

(1.Agricultural Department, Key Open Laboratory of Agriculture Resource and Environment in Yangtze River Upper Reaches, Chengdu, Sichuan 610066, China, bhmen1973@sohu.com;
2.College of Hydraulic Engineering, Sichuan University, Chengdu, Sichuan 610065, China)

Abstract: Based on the introduction of main quantitative indexes (correlation dimension D_2 and Kolmogorov entropy) in reconstruction phase-space technique, according to precipitation time series of Sichuan middle part in upper regions of Yangtze, relationship between embedding dimension m and correlation dimension D_2 is discussed and saturation correlation dimension, minimum embedding dimension and Kolmogorov entropy are calculated, that is, $D_2 = 5.11$, $m = 10$ and $k = 0.338$. Meanwhile, primary component analytic method (PCA) is applied to validate its chaotic character and result shows forecasting length for this precipitation time series should be less than 2.96 years. Thus, chaotic analysis on precipitation time series provides a scientific gist for precipitation forecasting. [Nature and Science, 2004,2(1):74-78].

Key words: correlation dimension; Upper regions of Yangtze; Primary component analysis (PCA); Kolmogorov entropy

1 Introduction

Mainly focusing on those anomalistic and noperiodic macroscopical spatio-temporal phenomenon, chaotic theory is about research of special muddle behavior in dynamic system evolving, which reveals the underlying regulations of those appearing stochastic and out-of-order behavior. Chaotic theory, as a newly development of nonbalancable Stat – physics, comes up with new methods of researching some special and muddleheaded phenomenon.

Amount of yearly precipitation has direct effect on water resource exploitation and utility and is also closely related to occurrence and evolution of drought and flood. Therefore, precise forecast of annual precipitation provides not only scientific gist for water resource exploitation but also guidance for calamity precaution and salvage. Considering precipitation is uncertain or stochastic, we need form scientific and reasonable predicting models as well as probe system causing precipitation as uncertain and stochastic and determine effective phase-space, providing foundation for making dynamical forecasting models.

Fractal theory, aiming at researching fractal characteristic of complex system and determining state space of time series, is an efficient tool for explaining complicated dynamical system and is widely used in field of physics, chemistry, biology, medicine, geology, weather, hydrology etc. In this thesis, according to precipitation time series of Sichuan middle part in upper regions of Yangtze, from 1953 to 2002 (Figure 1), from the view of correlation dimension D_2 and Kolmogorov entropy, regulation of precipitation formation and evolution is discussed, and then PCA is applied to validate chaotic feature of precipitation time series.

2 Chaotic Systems

Out-of-order in chaotic theory refers to those appearing disorder but not simply and normal chaos. For this reason, before there is ripe identifying method in describing features of attractor, we can recognize chaos from the point of correlation dimension D_2 and Kolmogorov entropy.

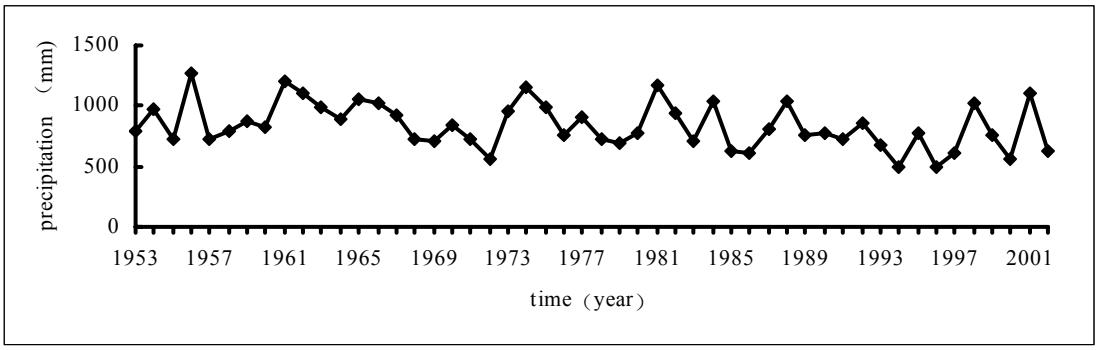

Figure 1 Precipitation Series in Middle Region Sichuan Province of Yangtze Rive Up Reaches

2.1 Phase-space reconstruct technique

Ruelle proposes to change system phase-space with a new n dimensional phase-space (embedding phase-space) resulting from time series x_t and its continual movement $x_{t+\tau}, x_{t+2\tau}, \cdots, x_{t+(n-1)\tau}$, and points out dimension of reconstruction phase-space m should be more than or equal to two times plus 1 of state space, that is

$$m \geq 2d + 1 \tag{1}$$

Take a scalar time series $x_1, x_2, \cdots, x_n$ in system phase-space as an example. Supposing its dimension d is 1, its dimension of embedding phase-space should be 3. If here $m = 4$, x_1, x_2, x_3, x_4 forms the first vector Y_1 of a four-dimensional state space and then moving right one step, x_2, x_3, x_4, x_5 forms the second vector Y_2. Just do in the same way, $Y_1, Y_2, Y_3, \cdots, Y_l$ forms the time series of reconstruction phase-space.

2.2 Correlation dimension D_2

In time series of $Y_1, Y_2, Y_3, \cdots, Y_k$, supposing r_{ij} is the absolute value of difference between two sectors, namely,

$$r_{ij} = \left| Y_i - Y_j \right| \tag{2}$$

Then r_0 which is in the range of maximum and minimum r_{ij} is determined. With the justification of r_0, a group of value of $\ln r_0, \ln C(r)$ and correlation dimension can be calculated. The definition of correlation dimension is as follows:

$$D_2 = \lim_{r \to 0} \ln C(r) / \ln(r_0) \tag{3}$$

$$C(r) = \frac{1}{l^2} \sum_i^l \sum_j^l H\left(r_0 - \left| Y_i - Y_j \right|\right) = \frac{1}{l^2} \sum_i^l \sum_j^l H\left(r_0 - r_{ij}\right) \tag{4}$$

$$H(z) = \begin{cases} 1 & z > 0 \\ 0 & z \leq 0 \end{cases} \tag{5}$$

Where: l is the total number of state vectors Y, r_{ij} is sphere diameter with the center of Y_i or Y_j, $\left| Y_i - Y_j \right|$ is Euclid distance, H is the function of Heaviside step function.

Numbers in Table 1 come from (3),(4),(5), $r_0 = \{300, 400, \cdots, 1000\}$, embedding dimension $m = \{4, 5, \cdots, 13\}$.

Using numbers in Table 1, we can draw a plot of $\ln C(r) \sim \ln r_0$. If line part exits, we say this time series has the feature of fractal, and slope of line is the correlation dimension (correlation dimension of the attractor). Figure 2 shows the relation between $\ln C(r)$ and $\ln r_0$.

From Figure 2, we see in chart of $\ln C(r) \sim \ln r_0$, with different embedding dimension m, part of linear correlation does exit, that is, precipitation time series of Sichuan middle part in upper regions of Yangtze has fractal feature. Slope of line in each curve is the correlation dimension corresponding m. Figure 3 shows the relation between correlation dimension D_2 and different embedding dimension m.

In Figure 3, we see when $m = 10$, correlation dimension tends to be stable, namely saturate. So when $D_2 = 5.11$, we say minimum embedding dimension $m = 10$ represents effective freedom rate of dynamical system. That is, when embedding phase-space of precipitation time series is 10, correlation dimension of the attractor is 5.11. From this aspect, we can draw a conclusion that precipitation time series of middle part of Sichuan in upper regions of Yangtze has chaotic feature. In order to further organize chaotic feature of this time series, PCA is introduced.

Table 1 Data Calculation Table of r_0 ~ C(r) ~ m

C(r) \ r0 / n	300	400	500	600	700	800	900	1000
4	0.1290	0.2884	0.4903	0.7103	0.8841	0.9674	0.9946	1.0000
5	0.0766	0.1777	0.3526	0.5709	0.7949	0.9272	0.9839	0.9981
6	0.0499	0.1062	0.2415	0.4331	0.6948	0.8647	0.9644	0.9921
7	0.0351	0.0651	0.1581	0.3140	0.5733	0.7893	0.9298	0.9824
8	0.0330	0.0471	0.1011	0.2353	0.4451	0.7112	0.8821	0.9654
9	0.0317	0.0385	0.0646	0.1508	0.3333	0.6145	0.8175	0.9342
10	0.0291	0.0351	0.0506	0.1041	0.2374	0.5253	0.7537	0.9084
11	0.0275	0.0325	0.0425	0.0762	0.1725	0.4275	0.6963	0.8738
12	0.0256	0.0309	0.0401	0.0572	0.1256	0.3123	0.6292	0.8435

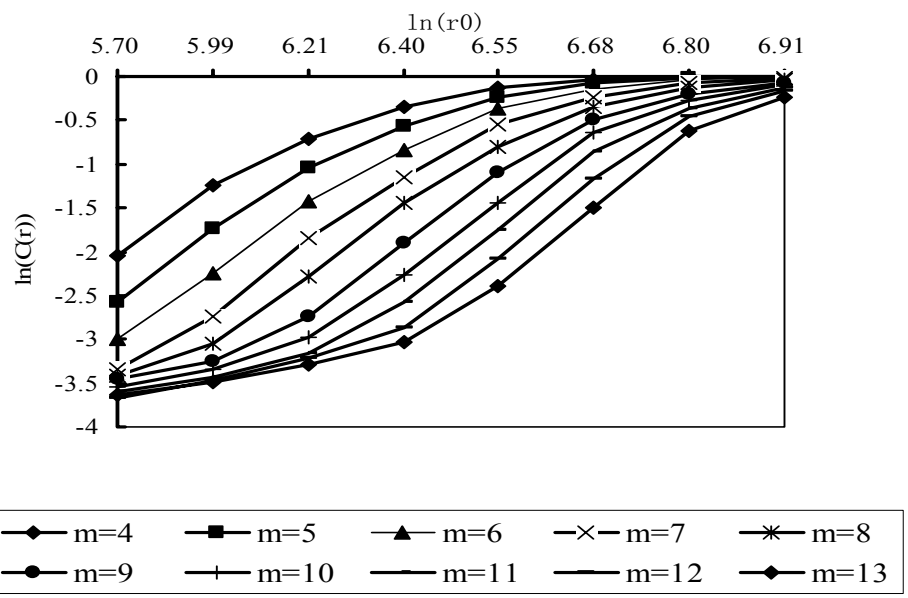

Figure 2 Relation between ln (r_0) and lnC (r)

2.3 Primary component analysis (Pca)

PCA is a newly proposed method in organizing noise and chaos. The step of this method is as follows:

Supposing a scalar time series is $x_1, x_2, \cdots, x_n$, after reconstructing phase-space (embedding dimension is m, and delay time is τ), matrix $Y_{l\times m}$ $(l = n-(d-1))$ is formed:

$$Y_{l\times m} = \frac{1}{l^{1/2}}\begin{bmatrix} x_1 & x_2 & \cdots & x_m \\ x_2 & x_3 & \cdots & x_{m+1} \\ \vdots & \vdots & \vdots & \vdots \\ x_l & x_{l+1} & \cdots & x_n \end{bmatrix} = \frac{1}{l^{1/2}}\begin{bmatrix} Y_1 \\ Y_2 \\ \vdots \\ Y_l \end{bmatrix}$$

Calculate covariance matrix $A_{d\times m} = \frac{1}{l} Y_{l\times m}^T Y_{l\times m}$

and its eigenvalue λ_i $(i=1,2,3,\cdots,m)$ and eigenvector U_i $(i=1,2,3,\cdots,m)$, then order them $\lambda_1 \geq \lambda_2 \geq \cdots \geq \lambda_m$ in descending sequence. Eigenvalue and eigenvector is called primary sector. Sum of all eigenvalue γ is $\gamma = \sum_{i=1}^{d} \lambda_i$. Chart of i and $\ln(\lambda_i / \gamma)$ is called primary spectrum. Primary spectrum of noise, which is parallel to x axis, is quite different from that of chaotic serial, which is a line across fixed dot with negative slope.

Figure 4 is the chart of primary spectrum. According to feature of spectrum of chaotic time series, we can further determine that precipitation time series has chaotic feature.

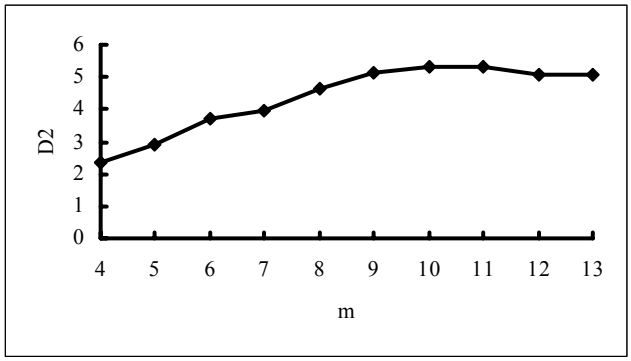

Figure 3 Relation between m and D_2

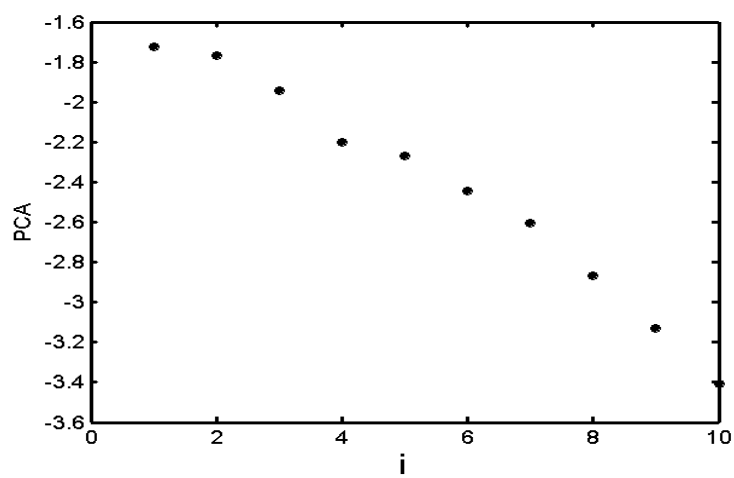

Figure 4 Relation between i and PCA

2.4 Kolmogorov entropy

Another important index of chaotic feature is Kolmogorov entropy, which provides upper and lower range of average amount of information in unit time. Generally, for a sequential system, $K=0$; for a stochastic system, $K=\infty$. When $0<K<\infty$, system is a chaotic system, and the bigger K is, the more serious the degree of chaos is. Formula proposed by Grassberger-Procaccia algorithm is:

$$K_2 = \frac{1}{\tau} \ln \frac{C_m(r)^2}{C_{m+1}(r)^2} \tag{4}$$

Where: τ is delay time, $C_m(r)$ is the value of $C(r)$ when embedding dimension of phase-space is m, $C_{m+1}(r)$ is the value of $C(r)$ when embedding dimension of phase-space is $m+1$.

Choice of τ and m is key to calculation of dimension, index and entropy. In application, we need to consider dimension of embedding phase-space as well as τ which has better simulating effect.

In theory, when $m \to \infty$, $K_2 \to K$. In fact, when m is somewhat value, K_2 tends to be stable and this stable value can be used as estimating value of K.

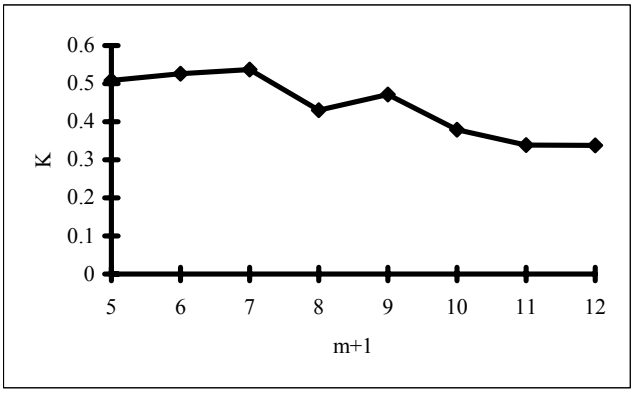

Figure 5 Relations between m+1 and K

Figure 5 shows the relation between k and $(m+1)$. From Figure 5, we know with the increase of m, k tends to be stable and when $(m+1)=11$, Kolmogorov entropy comes to saturation, that is, $K=0.338\ (>0)$. This data also indicates the chaotic feature of precipitation time series of Sichuan middle part in upper regions of Yangtze. $1/K$ shows predictable length of this system is 2.96 years.

3 Conclusion

Correlation dimension $D_2 = 5.11$ and Kolmogorov entropy $k = 0.338$ are achieved by reconstructing phase-space. Primary component analysis further validates the chaotic feature of precipitation time series of Sichuan middle part in upper regions of Yangtze and the reciprocal of Kolmogorov entropy tells us predicting length of precipitation time series should be 2 to 3 years instead of long-term prediction, which provides scientific gist for determining length of predicting period.

Acknowledgement

This study is supported by HI-TECH Research and Development Program of China 2002AA6Z3263.

References

[1] Bellie S, *et al.* Is correlation dimension a reliable indicator of low-dimensional chaos in short hydrological time series? Water resources research, 2002;38(2):3-1-3-8.

[2] Casdagli M. Nonlinear prediction of chaotic time series. Phys D, 1989,35:335-356.

[3] Chen YN, *et al.* Research on chaotic mechanism of glacier outburst floods. Journal of Natural Disasters, 1999,8(1):48-52.

[4] Grassberger P, *et al.* Estimation of the Kolomogorov entropy from a chaotic signal. Physic Rev A ,1983,28:2591-2593.

[5] Islam S, *et al.* A possible explanation for low correlation dimension estimates for the atmosphere, Journal of Appl Meteorol, 1993,32:203-208.

[6] Jayawardena A. Analysis and prediction of chaos in rainfall and streamflow time series, Journal of Hydrol, 1994;153:23-52.

[7] Lv JH, *et al.* Chaotic time series analysis and its application, Wuhan University press, Wuhan, China, 2002.

[8] Mandelbort BB. The fractal geometry of nature. San Franclso. W H, Freeman, 1983:15.

[9] Nicolis C. Is there a climate attractor? Nature 1984;311:529-532.

[10] Pool R. Is there something strange about the weather? Science, 1989,243:240-244.

[11] Sheng ZHH, *et al.* Analysis quote about nonlinear dynamical system, Science Press, Beijing, China, 2001.

[12] Wei YM, *et al.* The chaotic characteristics of annual precipitation series in Jiujiang, Jiangxi Science, 1998,16(3):141-145.

[13] Xin HW. Fractal theory and its application, China Sci-Tech University Press, Hefei, 1993.

Using RAGA for Multi-objective Planning of Soil and WaterConservation in a Small Watershed

Yankun Sun[1] , Qiang Fu[2]

(1. School of Resources & Environment, Northeast Agriculture University,
Harbin, Heilongjiang 150030, China ;
2. School of Water Conservancy & Civil Engineering, Northeast Agriculture University,
Harbin, Heilongjiang 150030, China, fuqiang100@371.net)

Abstract: Difficulties of optimizing many parameters at the same time were overcome by combining the optimized method named Real coded based Accelerating Genetic Algorithm (RAGA) with multi-objective planning techniques. Both partial optimization and quick convergence could be achieved. A multi-objective planning model was used to suggest soil and water conservation measures for a small watershed named Xinglong in the Song Nen Plain. [Nature and Science, 2004,2(1):79-84].

Keywords: RAGA, small watershed, soil and water conservation, multi-objection planning, model

1 Introduction

At present, there are many methods that have been used in small watershed soil and water conservation comprehensive planning. For example, multi-objective planning, empirical planning, computer aided planning, linear programming and objective planning. Because linear programming has the shortcoming of single object, and objective planning desires there must have expected value in every objective function, multi-objective planning can overcome both shortcoming and satisfy the multi-objective demand in small watershed soil and water conservation comprehensive planning. So, multi-objective planning has been applied widely. (Zhou. 1997) Also method of step by step (STEM) is usually adopted to calculate the problem of multi-objective planning and essential of this method is a iteration method or trial method. Since there are many parameters and restrict factors, and the interior relations are complex. Though it is easy to converge and mature early. But, it is easy only to seek the partial best value, and can't seek the overall best value. For these reasons, the author put forward to combine the GA (Genetic Algorithm) with multi-objective planning to deal with this kind of issue. the Xinglong small watershed soil and water conservation comprehensive planning in Songnen Plain, and build up the multi-objective comprehensive planning model based on GA.

2 Real Coding Based Accelerating Genetic Algorithm (RAGA)

Genetic Algorithm has been put forward by Professor Holland. (Michigan University, USA) The main operations include selection, crossover and mutation. (Jin, *et al*. 2000; Fu, *et al*. 2001; Yun. 2000; Xuan, *et al*. 2000)

The coding mode of traditional GA adopted binary system. But binary system coding mode has many abuses. So, inheriting the work by Jin in 2000, the author put forward a new method named RAGA, which includes 8 steps. (Jin, *et al*. 2000; Fu, *et al*. 2001).

3 A Case Study

Xinglong small watershed lies in the middle part in Heilongjiang Province of China. It has been dig up in 1900. The main soil style is chernozem. The depth of soil is 30mm to 40mm.

The whole area of 843.12 hm^2 , that accounts for 66.7 percent of the watershed, has been eroded. The

available soil depth is reducing in successive years. The soil fertility descends and the provision reduced. According to investigation, there are about 0.3 to 0.7 hm^2 sloping field have been nibbled. The soil and water loss is rather serious. So, it is necessary to carry through soil and water conservation comprehensive planning and set up synthetic optimum mode. Thus, we can advance the economy development of the watershed and prevent and cure the disaster of soil and water loss. (Zhou. 1997).

3.1 Select and treat with the objective function (Zhou. 1997; Yun, *et al*. 2000)

According to the natural economy rule and people's demand, we can define the objective function as follows.

(1) The maximum economy net income

$$\begin{aligned} Maxf_1(x) = {} & 134.5x_1 + 97x_2 + 59.5x_3 + 491x_4 + 391x_5 \\ & + 291x_6 + 423x_7 + 363x_8 + 231x_9 + 155x_{10} \\ & + 135x_{11} + 650x_{12} + 600x_{13} + 329x_{16} + 329x_{17} \\ & + 329x_{18} + 852x_{25} + 17.5x_{26} + 22.5x_{27} + 72x_{28} \\ & + 210x_{29} + 160x_{30} \end{aligned}$$

(2) The maximum provision yield

$$\begin{aligned} Maxf_2(x) = {} & 350x_1 + 300x_2 + 250x_3 + 1200x_4 + 1000x_5 \\ & + 800x_6 + 400x_7 + 350x_8 + 240x_9 + 200x_{10} + 180x_{11} \end{aligned}$$

(3) The minimum quantity of soil loss

$$\begin{aligned} M\inf_3(x) = {} & 0.333(x_1 + x_4 + x_7) + 0.017x_2 \\ & + 0.036(x_3 + x_5) + 0.1313x_6 + 0.164x_8 + 0.134x_9 \\ & + 0.073(x_{10} + x_{12}) + 0.153(x_{11} + x_{13}) \\ & + 0.25(x_{16} + x_{17} + x_{18} + x_{19} + x_{20} + x_{21} + x_{22} + x_{23} + x_{24}) \end{aligned}$$

We can adopt the method of linearity-weighted array to transform multi-objective function to single objective function.

$$\begin{aligned} MaxF = {} & \sum_{i=1}^{3} \alpha_i \cdot Maxf_i(x) = \alpha_1 \cdot Maxf_1(x) \\ & + \alpha_2 \cdot Maxf_2(x) + \alpha_3 \cdot M\inf_3(x) \end{aligned}$$

According to the experience of experts, we select the weight coefficients are as follows:

① The coefficient of the maximum economy net income is 0.55 ($\alpha_1 = 0.55$);

② The coefficient of the maximum provision yield is 0.35 ($\alpha_2 = 0.35$);

③ The coefficient of the minimum quantity of soil loss is 0.1 ($\alpha_3 = 0.1$).

3.2 Make the decision-making variable and restraint condition (Zhou. 1997)

According to the practical condition, we setup variables that have great influence and drop out variables that have little influence. At last, we select the 30 decision-making variables as follows. See also table 1.

Table 1 Table of decision-making parameters

Decision-making variable	Meanings of decision-making variable	Decision-making variable	Meanings of decision-making variable	Decision-making variable	Meanings of decision-making variable
x_1	Area of the first grade field for planting wheat.	x_{11}	Area of the third grade field for planting mixed grain through building sloping terrace	x_{21}	Area of the fourth grade field to planting timber
x_2	Area of the second grade field for planting wheat through building terrace	x_{12}	Area of the second grade field for planting economy crop through building terrace	x_{22}	Area of the second grade field to planting shrub
x_3	Area of the third grade field for planting wheat through building sloping terrace.	x_{13}	Area of the third grade for planting economy crop through building sloping terrace.	x_{23}	Area of the third grade field to planting shrub
x_4	Area of the first grade field for planting corn.	x_{14}	Area of the second grade field for planting artificial grazing	x_{24}	Area of the fourth grade field to planting shrub
x_5	Area of the second grade field for planting corn through building terrace	x_{15}	Area of the third grade field to planting artificial grazing	x_{25}	Number of milch cow
x_6	Area of the third grade field for planting wheat through building sloping terrace.	x_{16}	Area of the second grade field to planting economy woods.	x_{26}	Number of chicken
x_7	Area of the first grade field for planting soybean.	x_{17}	Area of the third grade field for planting economy woods.	x_{27}	Number of duck and goose
x_8	Area of the second grade field for planting soybean through building terrace	x_{18}	Area of the fourth grade field for planting economy woods.	x_{28}	Number of sheep
x_9	Area of the third grade field for planting soybean through building sloping terrace.	x_{19}	Area of the second grade field for planting timber	x_{29}	Number of pig
x_{10}	Area of the second grade field for planting mixed grain through building terrace	x_{20}	Area of the third grade field for planting timber	x_{30}	Number of big livestock

We can construct four kinds of restricted function according to many aspects. Such as soil resources, population, grain and oil, farming, feedstuff, dry firewood, yield, fertilizer, labor, yield development, people's demand and so on.

3.2.1 Soil restriction

(1) The first grade land restriction:

$$x_1 + x_4 + x_7 = 6849.25$$

(2) The second grade land restriction:

$$x_2 + x_5 + x_8 + x_{10} + x_{12} + x_{14} + x_{16} + x_{19} + x_{22} = 5499.4$$

(3)The third grade field restriction.:

$$x_3 + x_6 + x_9 + x_{11} + x_{13} + x_{15} + x_{17} + x_{20} + x_{23} = 4625.11$$

(4)The fourth grade land restriction:.

$$x_{18} + x_{21} + x_{24} = 331.64$$

3.2.2 Production development restriction.

(5) In order to satisfy the demand of commodity grain base for provision, the average area can't be less than 0.37hm^2. The total population is 2094.

$$x_1 + x_2 + x_3 + x_4 + x_5 + x_6 + x_7 + x_8 + x_9 + x_{10} + x_{11} \geq 12000$$

(6) The area of artificial grassland can't be less than 100 hm^2. $x_{14} + x_{15} \geq 1500$

(7) The bestrow rate by forest should be more than 20 percent.

$$x_{16} + x_{17} + x_{18} + x_{19} + x_{20} + x_{21} + x_{22} + x_{23} + x_{24} \geq 2651.9$$

(8) According to the national task, the total output can't be less than 1700000 kg.

$$350x_1 + 300x_2 + 250x_3 \geq 1700000$$

(9) The yield of soybean can't be less than 200000 kg. $400x_7 + 350x_8 + 240x_9 \geq 400000$

(10) The demand for other food grains can't be less than 2.5 kg per people.

$$200x_{10} + 180x_{11} \geq 10470$$

(11) According to exploited standard of small watershed, the area of economy wood can't be less than 20 percent of wood.

$$x_{16} + x_{17} + x_{18} \geq 20\% \begin{pmatrix} x_{14} + x_{15} + x_{16} + x_{17} + x_{18} + x_{19} \\ + x_{20} + x_{21} + x_{22} + x_{23} + x_{24} \end{pmatrix}$$

(12) The capital construction restriction.

$$\begin{aligned} & x_2 + x_5 + x_8 + x_{10} + x_{12} + x_{14} + x_{15} + x_{22} + x_{23} + x_{24} + \\ & 8(x_3 + x_6 + x_9 + x_{11} + x_{13}) + 3(x_{16} + x_{17} + x_{18}) \\ & + 4(x_{19} + x_{20} + x_{21}) \leq 51128 \end{aligned}$$

3.2.3 Balancing restriction.

(13) Balance restriction of forage grass.

$$\begin{aligned} & 175x_1 + 140x_2 + 105x_3 + 245x_4 + 210x_5 + 175x_6 \\ & + 175x_7 + 140x_8 + 112x_9 + 140x_{10} + 122x_{11} \\ & + 3000x_{14} + 3000x_{15} - 5000x_{25} - 1300x_{28} \\ & - 1800x_{29} - 4400x_{30} \geq 96000 \end{aligned} \quad (14)$$

Balance restriction of forage firewood.

$$\begin{aligned} & 325x_1 + 260x_2 + 195x_3 + 455x_4 + 390x_5 + 325x_6 \\ & + 325x_7 + 260x_8 + 208x_9 + 260x_{10} + 223x_{11} \\ & + 600x_{22} + 600x_{23} + 540x_{24} + 160x_{19} + 160x_{20} \\ & + 150x_{21} \geq 2292930 \end{aligned} \quad (15)$$

Balance restriction of organic fertilizer.

$$\begin{aligned} & 2500(x_1 + x_2) + 1500(x_4 + x_5 + x_{10} + x_{11} + x_{12} + x_{13}) \\ & + 2000x_3 + 1400x_6 + 1300(x_7 + x_8 + x_9) \\ & + 80(x_{16} + x_{17} + x_{18}) - 21900x_{25} - 500x_{26} - 900x_{27} \\ & - 2000x_{28} - 14400x_{29} - 21600x_{30} \leq 8376000 \end{aligned}$$

(16) Balance restriction of provision.

$$\begin{aligned} & 350x_1 + 300x_2 + 250x_3 + 1200x_4 + 1000x_5 \\ & + 800x_6 + 400x_7 + 350x_8 + 240x_9 + 200x_{10} \\ & + 180x_{11} - 1000x_{25} - 60x_{26} - 80x_{27} - 30x_{28} \\ & - 500x_{29} - 900x_{30} \geq 3141000 \end{aligned}$$

3.2.4 Balance restriction of stockbreeding

(17) Sheep: $x_{28} = 470$;

(18) Pig: $x_{29} \leq 1410$;

(19) Big livestock: $x_{30} = 470$;

(20) Milch cow: $x_{25} \geq 250$;

(21) Chicken: $x_{26} \leq 2350$;

(22) Duck and goose: $x_{27} \leq 1410$;

(23) $x_i \geq 0 \quad (\mathrm{i} = 1,2,\cdots 30)$.

3.3 Treat with the restricted function. (Jin, *et al.* 2000; Xuan, *et al.* 2000)

Because there are so many restricted conditions in the model, so, we should treat with the restricted conditions in order to ensure all the results are fit for every restricted condition. We can adopt the method of punished function. According to the method, we can add a punishment item in the objective function. Thus, we can obtain a generalized Thereby, we can seek the best value of the original issue based on the function of punishment item.

$$MaxF' = \alpha_1 \cdot Maxf_1(x) + \alpha_2 \cdot Maxf_2(x) + \alpha_3 \cdot M\inf_3(x) - \sum_{i=1}^{m} h_i(g_i(x))$$

$h_i(g_i(x))$ ——punish item.

When the restriction of $g_i(x)$ are satisfy the condition, the value of $g_i(x)$ equal zero, otherwise, give the $g_i(x)$ a big number M. (M=1000)

F' ——the optimum function

3.4 Seek the best parameters based on RAGA

Applying MATLAB 5.3 software, the author obtained the best value of these 30 parameters based on RAGA. During the course of RAGA, the parent generation scale is 400. ($n = 400$) The crossover probability is 0.80. (p_c =0.80) The mutation probability is 0.80. (p_m =0.80) The number of excellence individual is 20. α =0.05. Through accelerating 30 times, we can obtain the best project value. See also table 2.

Table 2 Optimizing the parameters based on RAGA

Variable	x_1	x_2	x_3	x_4	x_5	x_6	x_7	x_8	x_9	x_{10}
Optimum value (project 1)	3650.8	690.8	981.7	2261.3	832.7	672.2	937.1	741.9	571.1	376.5
Optimum value (project 2)	2643.4	710.6	754.2	3392.3	812.1	675.2	813.6	616.2	774.7	367.7
Variable	x_{11}	x_{12}	x_{13}	x_{14}	x_{15}	x_{16}	x_{17}	x_{18}	x_{19}	x_{20}
Optimum value (project 1)	517	608.9	269.6	682	837.5	668.3	291.7	107.1	292.7	262.1
Optimum value (project 2)	569.3	690.4	259.5	929.9	639.3	913.8	403.4	111.1	315.4	244.1
Variable	x_{21}	x_{22}	x_{23}	x_{24}	x_{25}	x_{26}	x_{27}	x_{28}	x_{29}	x_{30}
Optimum value (project 1)	95.9	605.5	222.1	128.6	392.5	977.6	329.7	470	1085.2	470
Optimum value (project 2)	110.8	143.3	305.4	109.7	460.5	1003.7	636.9	470	1015.3	470
Optimum value (project 1)	$MaxF' = 4.939\times10^6$ $Maxf_1(x) = 4.6823\times10^6$ Yuan $Maxf_2(x) = 6.7545\times10^6$ kg $Maxf_3(x) = 3.5051\times10^3$ t									
Optimum value (project 2)	$MaxF' = 5.548\times10^6$ $Maxf_1(x) = 5.2178\times10^6$ Yuan $Maxf_2(x) = 7.653\times10^6$ kg $Maxf_3(x) = 3.5111\times10^3$ t									

3.5 Analyze the optimum result

When the above 23 restricted conditions have been satisfied, the best result of net income is 4682300 Yuan, the total yield is 6754500 kg, the soil and water loss is 3505.1t. At the same time, the soil utility is much more reasonable. The soil used by agriculture reduces from 77.38% to 69.15. The original positive slope cultivation has been changed to transverse slope cultivation. Furthermore, sloping terrace and terrace have been build. Thus, we can combine the utilization soil with soil protection. The area of forestry changes from 6.01% to 14.1%. The bestrow rate by forest increases obviously. The environment has been improved. The layout of building economy wood and shrubbery is in reason and play a part. The system of soil and water conservation forest can control the soil and water loss effectively. The soil resources in the watershed have been developed greatly. The area of stockbreeding increases from 0.63% to 8%. The quality of grassland field has been improved, and the number of livestock increases much, the people's income increases obviously. The average income is 2236.1 Yuan (Three times than 700.4 Yuan before planning.), and the provision is 3225.6kg. (2.71 times than 1190.4kg before planning.) The erosion degree lighten, the covered rate enhance, the disaster of flood and waterlog lighten. The zoology benefit is good. After planning, the covered rate can reach 26.58%.

The soil distribution sees to table 3.

3.6 Discussion

If we adjust a part of restricted conditions properly, the total benefit will reach the better value. For example, if we reduce the demand of wheat, and increase the planting area of other crop (corn, soybean and economy crop.), the total benefit will much well.

$$350\ x_1 + 300\ x_2 + 250\ x_3 \geq 1300000$$

The optimum result sees to table 2. The soil distribution of every way sees to table 3 and figure 1.

From table 1 we can see that the total benefit enhance after adjusting the planting rate. The area of wheat reduces the area of corn, soybean and economy crop increase. That means the net income and total yield increase much, the quantity of soil loss varied a little. It is obvious that the project 1 is better than project 2 under the

Table 3 Soil distribution for each way

Item	Before adjustment.		Adjust project 1.		Adjust project 2.		Source of increasing field and reducing field
	Area before adjustment (hm^2)	Account for the total area. (%)	Area after adjustment (hm^2)	Account for the total area. (%)	Area after adjustment (hm^2)	Account for the total area. (%)	
Agriculture	14671.6	77.38	13111.6	69.15	13079.2	68.98	Forestry, stockbreeding, Garden.
Forestry	1140.1	6.01	2674	14.1	2657	14.01	Agriculture, wasteland
Stockbreeding	120	0.63	1519.5	8.0	1569.2	8.28	Agriculture, wasteland
Garden	0	0	850	4.48	850	4.48	Agriculture, wasteland
Wasteland	2873.8	15.16	654.4	3.45	650.1	3.43	Forestry, stockbreeding, garden, agriculture
Others	154.5	0.82	154.5	0.82	154.5	0.82	

condition of satisfying the provision supply. In fact, we can adjust any other some restricted conditions properly according to the concrete demand, then the total benefit will reach the best.

4 Conclusion

(1) The author improves the standard genetic arithmetic (SGA) and adopts the real code. Through reducing the region of the excellent individual step by step, the author puts forward a new method named RAGA. The method of RAGA can overcome many shortcomings in SGA. Furthermore, the author applies the RAGA to the model of multi-objective planning. The result is satisfactory.

(2) The author adopts the method of linearity weighted and builds the objective function. The issue of multi-objective function has been changed to single objective function. At the same time, through adopting the punish function, the author treats with many restricted conditions. The best result will be calculated under the condition of satisfying all the restricted conditions.

(3) The author builds up the model of multi-objective comprehensive planning of Xinglong small watershed in Songnen Plain based on RAGA. The result indicates the total benefit would reach much better if we adjusted some restricted conditions. Such as we can make the area rate of agriculture, forestry and stockbreeding from 77.38:6.01:0.63 to the rate in project 1 (69.15：14.1：8.00) or project 2 (68.98：14.01：8.28). Thus, the environment will be improved, soil and water loss will be prevented and cured effectively, the people's living standing will be enhanced.

(4) If we only adjusted the planting rate properly, the net income and total yield would increase obviously, and the quantity of soil loss would vary little. But the total benefit would be much better.

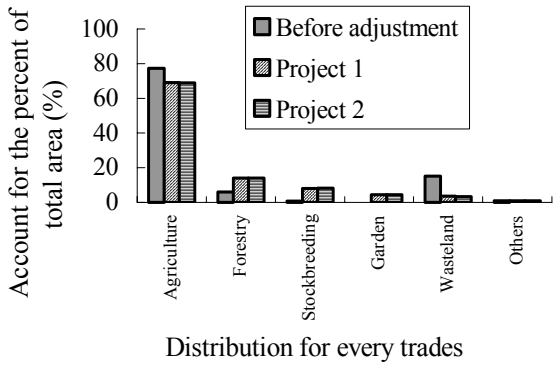

Fig.1 Soil distribution for each way between original and adjusted

References

[1] Fu Qiang,Liang Chuan. Technique of Modeling and Optimum about Water Saving Irrigation System. Chengdu: Publishing company of SiChuan Science and Technique, 2002.7:125 ~ 136

[2] Fu Qiang, Li Xiao Qiu, Xiao Jian Min. RAGA applied to calculate relation between discharge and water depth [J]. Water resources & Hydropower of northeast China: 2001, Vol.19, No. 10 1-4

[3] Jin Ju Liang, Ding Jing. Genetic arithmetic and its application to water science [M]. Chengdu: Si Chuan University publishing company: 2000, 42-47

[4] Xuan Guang Nan, Cheng Run Wei,. Genetic Arithmetic and Engineering Design[M]. Beijing: Science Publishing Company: 2000, 35-42

[5] Yun Qing Xia. Evolution Arithmetic [M]. Beijing: Metallurgy Industry Publishing Company: 2000, 60-61

[6] Zhou Jiang Hou. Study on the optimum model of Xinglong small watershed soil and water conservation comprehensive planning [D]. Harbin: Northeast Agricultural University, 1997.

[7] Zhou Ming, Sun Shu Dong. The theory of genetic arithmetic and its application [M]. Beijing: National defense industry publishing company: 2000, 4-7:37-38

Characterization of a New Species of Taxol-producing Fungus

Jingping Ge, Wenxiang Ping, Dongpo Zhou

(College of Life Sciences, Heilongjiang University, Harbin, Heilongjiang 150080, China,
gejingping9178@hotmail.com

Abstract: The macroscopic features of taxol-producing fungus G1353, as well as the microscopic features such as hyphae, conidiophores, and coridia, are sufficiently different from other members of the genus *Alternaria* that the strain constitutes a new species. The name *Alternaria taxi* is proposed. [Nature and Science, 2004,2(1):85-88].

Key words: taxol; anti-cancer; fungi; *Alternaria taxi*

1 Introduction

Taxol is a compound with anti-cancer properties, and it is proving to be particularly useful against mammary and ovarian cancers (McGuire, 1989). The most common source of Taxol is the bark of trees belonging to the *Taxus* family including Yew trees. Unfortunately, these trees tend to be rare, slow growing, and a large amount of bark may have to be processed to obtain a small amount of the drug. Alternative sources of Taxol have been sought, and Strobel *et al.,* were the first to isolate Taxol-producing fungi from the tree *Taxus brevifolia* (Strobel, 1993). Over the last decade there has been a great deal of interest in finding other fungi that produce Taxol (Zhou*.,* 2001). In the present study, a fungus was isolated from *T. cuspidatea* and shown to be able to produce the drug. Characterization of this fungus has shown it to be distinct from other species and a new name is thus proposed.

2 Materials and Methods

2.1 Strains

Two thousand fungal strains were separated from the bark of *T. cuspidatea* collected from HePing Forestry Centre, MuLing County, Heilongjiang Province, China in 2000. Each was screened for Taxol production by TLC and results were confirmed by HPLC where appropriate. Fungal strain G1353 was shown to produce taxol (data unpublished).

2.2 Culture media

PDA medium was prepared by adding potato (200g/L), glucose (20 g/L), and agar (20 g/L), to distilled water. The potato was first washed and cut into small pieces, boiled for 30 minutes, and filtered through gauze prior to addition of the glucose and agar.

Chase Medium was prepared by adding $NaNO_3$ 2 g, KH_2PO_4 1 g, KCl 0.5 g, $MgSO_4$ 0.5 g, $FeSO_4$ 0.01 g, sucrose 30 g, agar 20 g, to 1 litre of distilled water. The pH was adjusted to 7.0.

Martin Medium was prepared by adding glucose 10 g, peptone 5 g, KH_2PO_4 1 g, $MgSO_4.7H_2O$ 0.5 g, to 800 ml distilled water. After autoclaving streptomycin was added to a final concentration of 0.03%.

2.3 Microscopy

An XS-18 bright- field microscope (Jiang Nan), and an OLYMPUS BX51 fluorescent microscope were used to examine the microscopic features of the fungus. Strain G1353 was grown on PDA, Chase and Martin media at 28℃ and examined after 2, 3, 4, and 5 days. Hypha on the PDA plate were asceptically transferred to slides for cultivation (Shen, 2000).

3 Results

3.1 Colony morphology

G1353 grew fastest on the PDA medium (Table 1), and the diameter of the colony reached 6 cm after 5 days incubation at 28℃. The colony was flat, entire, and downy to woolly and was covered by brown, short, aerial hyphae in time. The surface was light brown at the start, later darkening to brown black with a light border. The reverse side was typically brown to black due to pigment production.

The height of colony was about 0.5 cm (Figures 1 and 2).

Table 1 Growth of G1353 on different media

Medium	Time of incubation (days)			
	2	3	4	5
PDA	1.8~2.2cm	3.0~3.5cm	4.5~4.9cm	6.0~6.4cm
Chase	1.0~1.2cm	1.2~1.4cm	1.4~1.6cm	1.8~2.2cm
Martin	0.8~1.7cm	2.5~3.2cm	3.2~3.5cm	3.8~4.6cm

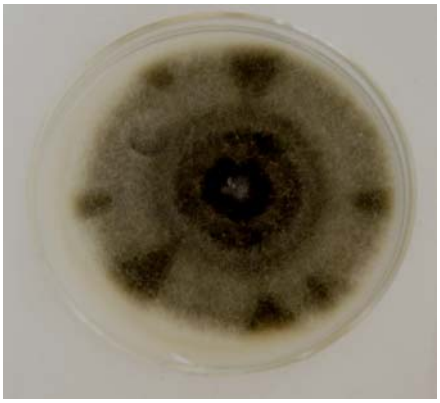

Figure 1 Face of G1353 colony on PDA media

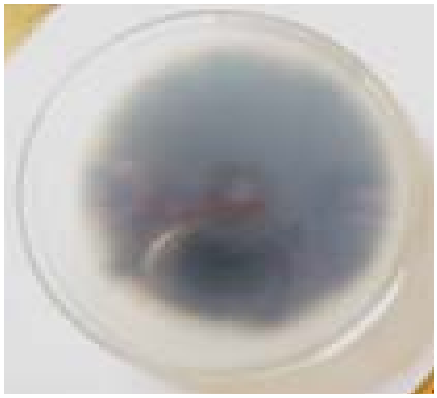

Figure 2 Reverse side of G1353 colony on PDA media

3.2 Structure (Figures 3-10)

Most of the hyphae grew on the surface of the PDA agar, but partially in the agar. They were septate, multi-offshoot, obviously having wart. The hyphae were brown in color, tapering to colorless at their ends and 2.5~5.0μm in diameter.

Conidiophores were brown to light brown, septate, and simple, with endlong or zigzag appearance. They were 12.5~27.4 × 2.5~5.0 μm in length.

Conidiogenous cells were tubular. Conidia were produced directly by hyphae cells, and were septate and brown / light brown in color. They were large (6.0~12.4 × 18.9~33.7 μm) with both transverse (3~8) and longitudinal (0~3) septations. These conidia were observed singly or in acropetal chains (2 or 3 conidia). They were ovoid to obclavate, darkly pigmented, muriform, and smooth. The end of the conidium nearest the conidiophore is round but it tapers towards the apex. This gives the typical beak or club-like appearance of the conidia (a few had no beak), and the beaks were 2.5~3.0 × 3.0~9.0μm in size.

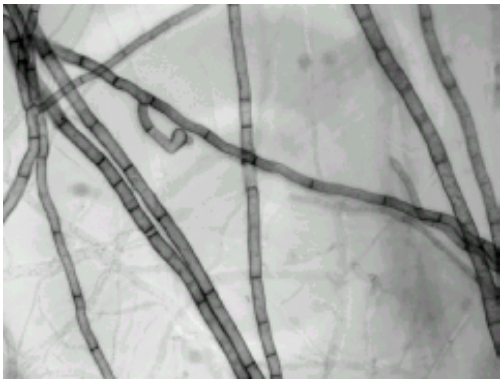

Figure 3 Hyphae of G1353 (Branch, sepate, 800×)

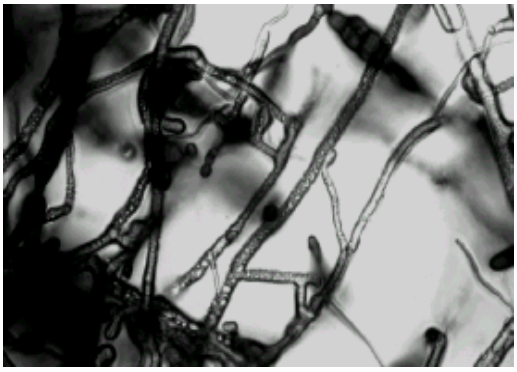

Figure 4 Wart on hyphae of G1353 (800×)

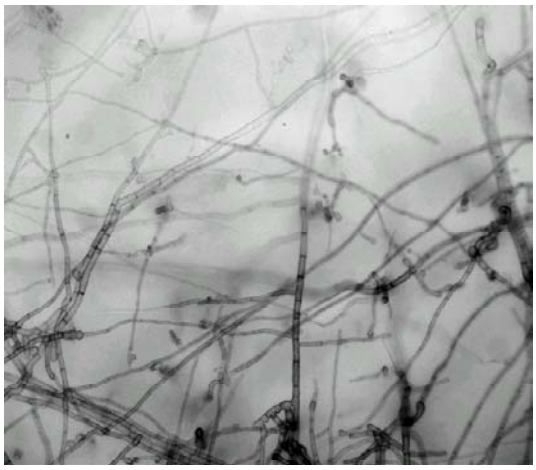

Figure 5 Color change of hyphae of G1353 (200 ×)

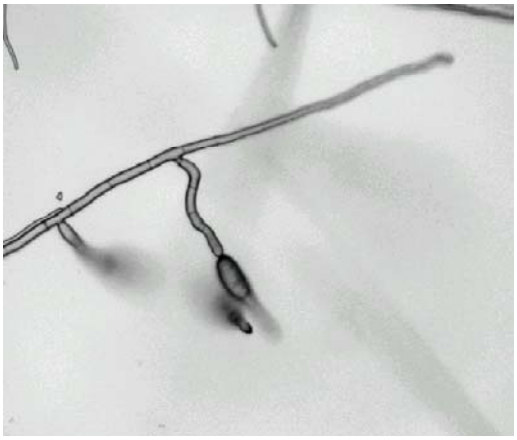

Figure 6 Conidiophores of G1353 (ziazag 800×)

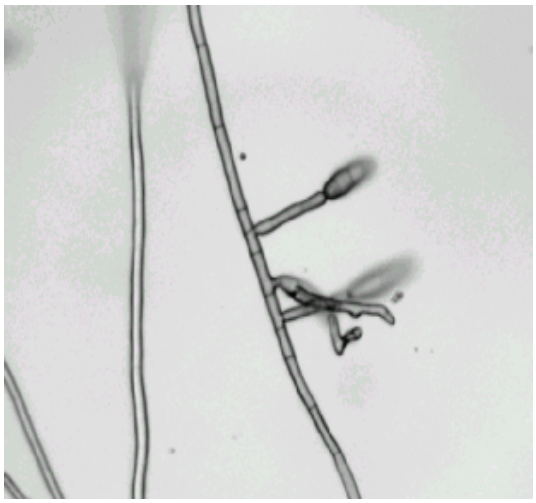

Figure 7 Conidiophores of G1353 (endlong 800×)

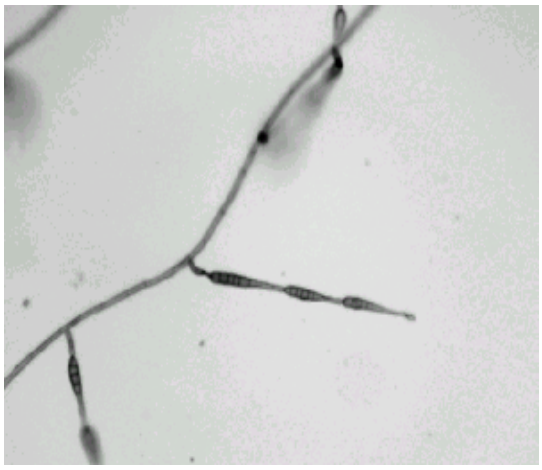

Figure8 Conidia and its location of G1353 (chain 800×)

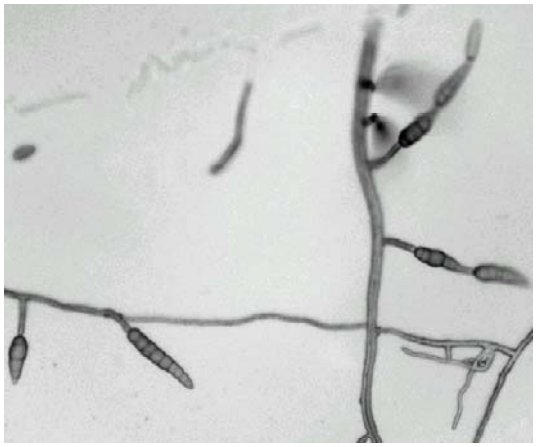

Figure 9 Conidia and its location on G1353 (800×)

Figure 10 Beak on the conidia of G1353 (800×)

4 Discussion

The colony of G1353 was flat on the surface of PDA medium. The hyphae were downy to woolly, white after two days but light brown or dark brown after five or six days. Both hyphae and conidiophores were septate. This strain bears simple large conidia, which have both transverse and longitudinal septations. These conidia were observed singly or in acropetal chains. They are ovoid to obclavate, darkly pigmented, muriform, and smooth. All of these characteristics were consistent with those of the Deuteromycotina, Hyphomycetes, Dematiaceae, *Alternaria* spp. (Colier, 1998; Larone, 1995; Germain, 1996). Thus, strain G1353 belongs to *Alternaria* spp., but has some unusual characteristics: 1) the conidiophores are simple, endlong or zigzag, 12.5~27.4 × 2.5~5.0 μm long. 2) Conidiophore cells are tubular and the conidia were directly produced by hyphae cells. 3) G1353 bears simple large conidia (6.0~12.4 × 18.9~33.7 μm) which have both transverse (3~8) and longitudinal (0~3) septations. These conidia were observed singly or in acropetal chains (2~3 conidia). They are ovoid to obclavate, darkly pigmented, muriform, smooth. 4) The end of the conidium nearest the conidiophore is round but it tapers towards the apex. This gives the typical beak or club-like appearance of the conidia (or no beak in some cases). From the above we conclude that strain G1353 is sufficiently different from other *Alternaria* spp. to be classified as a new species, and propose the name *Alternaria taxi.* Investigations into the production of taxol by this species are continuing, in the hope it can be used as a significant producer of this important anti-cancer drug.

Correspondence author:

Jingping Ge
74 Xuefu Road,
Nangang District,
College of Life Sciences, Heilongjiang University,
Harbin, Heilongjiang 150080, China
Office Telephone: 0086-451-86608586
Home telephone: 0086-451-86609178
Mobile phone: 0086-13836002907
E-mail: gejingping@0451.com Or gejingping9178@hotmail.com

References

[1] Colier L *et al.* Topley & Wilson Microbiology and Microbial Infections. 9th ed. Vol 4. London, Sydney, Auckland, New York, 1998.

[2] Germain G *et al.* Indetifying Filamentous Fungi—A Clinical Laboratory Handbook, 1st ed. Star Publishing Company, Belmont, California,1996.

[3] Larone DH *et al.* Medically Important Fungi—A Guide to Indentification, 3rd ed. ASM Press, Washington, D.C. ,1995.

[4] Shen P. Microbiology experiment (3 rd.). Beijing: Higher press, 2000.

[5] Strobel G *et al.* Mycotaxon. 1993; 47:71-80.

[6] Zhou DP *et al. Nolulisporium*, a genus new to China. Mycosystema, 2001, 20:148-150

Optimization of Water Allocation in Canal Systems of Chengai Irrigation Area

Zhiliang Wang, Zhenmin Zhou

(North China College of WRHP, Zhengzhou, Henan 450045, China)

Abstract: Chengai Yellow River Irrigation Area is situated in Liangshan County, Shandong Province, China. In history, no formalized irrigation regulations exist because of limitations on the project facilities and management capability. The utilization of water resources was unreasonable with serious waste of water and prolonged rotations and low irrigation benefits. Potential benefits have not been realized. With the development of agriculture production, it was considered urgently necessary to carry out research on the optimum water allocation in Chengai Yellow River Irrigation Area using system engineering methodology. Therefore, Based on the principle of system engineering and in accordance with the secondary main canal of the Chengai Yellow Irrigation Area, and taking the maximum irrigation benefits and minimum irrigation rotation as the objectives, the optimal crop pattern and irrigation water allocation models have been developed. Through calculations, the desirable optimal crop pattern and water allocation results were achieved. It proved in practice that the present research play very important role in water saving, irrigation and production improvement, and facilitation of irrigation area scientific management level.[Nature and Science, 2004;2(1):89-94].

Key words: irrigation canal systems; crop pattern; optimal water allocation model

1 Introduction

Chengai Yellow River Irrigation Area covers a total area of 542 km^2, of which 38000 ha are farmland, 20000 ha are gravity irrigated and 18000 ha lift irrigated. Main crops are wheat, maize, beans as well as other crops such as millet, sweet potatoes and sorghum, etc.

The irrigation area is situated in the warm temperature zone, with a continental monsoon climate. The average annual precipitation is only 647 mm, but evaporation reaches 1365 mm, which corresponds to semi-arid conditions. The distribution of rainfall is extremely uneven in time and space, resulting in serious water shortages. The principal source of water is the Yellow River supplementing groundwater. The annual diversion from the Yellow River is 150 million m^3 and the annual exploitation of groundwater amounts to 105 million m^3.

No formalized irrigation regulations exist because of limitations in the project facilities and in management capability. The utilization of water resources was unreasonable with serious waste of water and prolonged rotations. Potential benefits have not been realized. Therefore, it was considered urgently necessary to carry out research on optimum water allocation in Chengai Yellow River Irrigation Area using system engineering methodology.

The present research is based on the North Main Canal System in the gravity irrigation area, which includes 18 branch canals (Table 1). A mathematical model was established to determine the optimum crop patterns and water allocations with the minimum rotation times. Satisfactory results were obtained from the analysis and may be extended into the whole irrigation area.

2 Optimization Model for the Optimal Crop Pattern

In order to utilize the water resources reasonably, to match water supply and requirement and reach the maximum economic benefit, the optimum crop pattern for each branch canal was first determined. Linear programming was adopted in the present study to apply an optimization model to each branch canal separately.

Table 1 Parameters of the north main canal system in Chengai irrigation area

CANAL	Length (m)	Irrigated Area (ha)	Flow Capacity (m^3/s)	Distance to the head of Main Canal (m)
North Main Canal	10100	1018.86	2.50	0
Branch 1	1300	52.00	0.42	870
Branch 2	1279	61.40	0.37	1150
Branch 3	1262	49.40	0.37	1740
Branch 4	1260	67.13	0.37	2410
Branch 5	1307	45.73	0.37	3100
Branch 6	1308	61.67	0.20	3470 (Lined)
Branch 7	1340	66.00	0.42	3990 (Lined)
Branch 8	1389	69.33	0.42	4670
Branch 9	1420	53.33	0.37	5200
Branch 10	600	27.00	0.37	5900
Branch 11	450	20.27	0.37	6250
Branch 12	1420	46.87	0.42	6730
Branch 13	1390	91.73	0.42	7220
Branch 14	1320	82.20	0.67	8050
Branch 15	620	14.27	0.37	8440
Branch 16	620	44.00	0.37	8700
Branch 17	1350	94.67	0.42	9420
Branch 18	790	71.87	0.37	10100

2.1 Selection of decision variables

There are five kinds of crops in Chengai Yellow River Irrigation Area: wheat, maize, beans, cotton and other food grains. In order to determine the optimum crop area irrigated by every branch canal, the areas of different crops irrigated by each branch canal were selected as decision variables (parameters). Therefore, the selected decision variables are as follows:

$A_{i,j}$ = optimum planting area of crop j in the ith branch canal (ha).

i = 1,2 ..... 18.

j=1,2 ..... 5, where 1 stands for wheat, 2 for maize, 3 for beans, 4 for cotton, 5 represents other food grains.

2.2 Design of the objective function

For the purposes of this paper, the objective function is the maximum net benefit, for which the formula is as follows:

$$MaxZ_i = \varepsilon \sum_{j=1}^{N} A_{ij} P_j \Delta d_j - E \sum_{j=1}^{N} A_{ij} \qquad (1)$$

where: ε = irrigation benefit allocation coefficient (0.4 in the study).

P_j = price of the crop j ($ /kg) (Table 2).

Δd_j = increased output of crop j through irrigation (kg/ha).

E = annual operational fee in the gravity irrigated area (13.6 $ /ha).

N = number of the crops (5 in the study).

i = canal reference number 1, 2, ... 18.

j = crop characteristics reference number, 1, 2....5

Table 2 Characteristics of crops in the north main canal system

CROPS	Wheat	Maize	Beans	Cotton	others
Max. crop pattern*	0.90	0.60	0.20	0.25	
Min. crop pattern*	0.80	0.50	0.12	0.11	
Gross duty (m^3/ha)	1275	1125	1050	1125	
Growth period (days)	255	110	120	165	
price ($/kg)	0.171	0.12	0.236	1.091	
Output,1965(kg/ha)	765	1237.5	682.5	165	
Output,2000(kg/ha)	4590	4875	2040	750	
Increment (kg/ha)	3825	3637.5	1357.5	585	
Increment through irrigation ($/ha,)	261.4g	174.6	128.35	255.27	195.57
Irrigation periods	(1)26/11-5/12 (2)10/3-18/3 (3)3/4-17/4 (4)11/5-20/5	(6)21/5-28/5 (3)25/6-30/6	(6)21/5-28/5	(5)3/4-7/4 (7)21/6-24/6	(6)21/5-28/5 (8)25/6-30/6

2.3 Constraints

In the calculation of the optimum crop area, besides the maximum objective function, the relevant constraints must be included. These consist of limitations of total area, maximum and minimum crop areas and water supply. They are as follows:

2.3.1 Constraints of total area

The combined crop area irrigated per branch canal should be equal to or smaller than the total area irrigated by the canal. Considering the inter-plantation of wheat, maize, beans and the other food grains, the sum of the areas planted in wheat and cotton should not be larger than the total area controlled by the canal system. The total planting area of maize, beans and the other food grains should not be larger than the total area either, that is:

$$A_{i,1} + A_{i,4} \leqslant A_i \quad \text{(ha)...} \qquad (2)$$

where: A_i = area irrigated by the ith branch canal

$$\text{and} \quad \sum_{j=2}^{5} A_{i,j} \leq A_i \quad \text{(ha)...} \qquad (3)$$

2.3.2 Constraints of maximum and minimum planting areas

According to local practice and the requirements of contracted farmland, on every branch canal there are maximum and minimum limitations on the planting area of different crops. The maximum and minimum constraint conditions are as follows:

$$0.9A_i \geqslant A_{i,1} \geqslant 0.8\,A_i \quad \text{(ha)} \quad \text{(wheat)} \qquad (4)$$
$$0.6A_i \geqslant A_{i,2} \geqslant 0.5\,A_i \quad \text{(ha)} \quad \text{(maize)} \qquad (5)$$
$$0.2A_i \geqslant A_{i,3} \geqslant 0.12\,A_i \quad \text{(ha)} \quad \text{(beans)} \qquad (6)$$
$$0.25A_i \geqslant A_{i,4} \geqslant 0.11\,A_i \quad \text{(ha)} \quad \text{(cotton)} \qquad (7)$$
$$0.15A_i \geqslant A_{i,5} \geqslant 0.11\,A_i \quad \text{(ha)} \quad \text{(others)} \qquad (8)$$

2.3.3 Constraints of water supply

The irrigation area requires water supply 8 times annually; specific irrigation periods can be seen in Table 2. Every irrigation rotation should be finished within the required time, otherwise the crop yields will be influenced. The volume of water use can be obtained through calculation of crop area and the related irrigation duty (Table 2). The volume of water supply has been obtained from the maximum possible capacity of the North Main Canal. The constraints of water supply are as follow;

$$A_{i,j}M_{k1} \leqslant \eta_m \eta_{bi} \frac{Q_m \times A_i}{F} \times d_k \times 24 \times 3600 \qquad (9)$$

where: M_{k1} = irrigation duty for crop 1 in kth irrigation rotation (m^3/ha),

K = 1,2,3, ...

η_m = water use coefficient in the main canal (0.92.),

η_{bi}= water use coefficient in each branch canal, η_{b6} = 0.99, η_{b7}= 0.9,

η_{bi} =0.71 for other branch canals,

d_k = total days of the kth irrigation rotation,

Q_m= maximum diversion flow in the North Main Canal (2.5 m^3/s),

F =irrigated area controlled by the North Main Canal (1019 ha),

The influence of soil moisture content has not been considered in the above formula for it is very difficult to forecast long-term soil moisture content. Therefore, the present paper selected the average irrigation duty to analyse crop patterns.

Because the first four irrigation rotations are for wheat, the conditions for wheat irrigation determine the water requirements; they can be merged into the one equation (Eq. 4).

The fifth rotation

$$A_{i,4}\ M_{5,4} \leqslant \eta_m \eta_{b,i} \frac{Q_m \times A_i}{F} \times d_5 \times 24 \times 3600 \quad (10)$$

The sixth rotation

$$A_{i,2}\ M_{6,24} + A_{i,3} M_{6,3} + A_{i,5}\ M_{6,5} \leqslant \eta_m \eta_{b,i} \frac{Q_m \times A_i}{F} \times d_6 \times 24 \times 3600 \quad (11)$$

The seventh rotation

$$A_{i,4}\ M_{7,4} \leqslant \eta_m \eta_{b,i} \frac{Q_m \times A_i}{F} \times d_7 \times 24 \times 3600 \quad (12)$$

The eighth rotation

$$A_{i,2}\ M_{8,2} + A_{i,5} M_{8,5} \leqslant \eta_m \eta_{b,i} \frac{Q_m \times A_i}{F} \times d_8 \times 24 \times 3600 \quad (13)$$

The result is shown in Table 3. All the calculations were undertaken on the computer. The optimum crop areas served by the branch canals and the objective function values have been printed out (OBJ.FUNC). Interactive dialogue was used. The following parameters should be input: k (number of branch canal), FK (area controlled by branch canals),G_2 (water use coefficient in branch canals), Q_m(the maximum flow capacity in the main canal).

3 Optimum Water Allocation Based on the Minimum Irrigation Rotation Time

A trial algorithm was used to calculate the minimum irrigation rotation required in the north main canal irrigation systems for the optimum crop areas. The optimum water allocation was calculated for different branch canals under the condition of maximum flow in the north main canal. The irrigation rotation order and water diversion volume of each branch canal were regulated to realize the shortest irrigation rotation and the optimum water allocation scheme.

Table 3 Results of crop optimization (ha)

Canals	CROPS					OBJ.FUNC ($)
	1	2	3	4	5	
1	46.280	31.20	7.280	5.720	7.80	13756.77
2	54.646	36.84	8.596	6.754	9.21	16243.57
3	43.966	29.64	6.916	5.434	7.41	13068.93
4	59.749	40.28	9.399	7.385	10.07	17760.34
5	40.703	27.44	6.403	5.031	6.86	12098.90
6	54.883	37.00	8.633	6.783	9.25	16314.11
7	58.74	39.60	9.24	7.26	9.90	17460.51
8	61.707	41.60	9.707	7.627	10.40	18342.35
9	47.467	32.00	7.467	5.867	8.00	14109.51
10	24.030	16.20	3.780	2.970	4.05	7142.94
11	18.037	12.16	2.837	2.229	3.04	5361.61
12	41.711	28.12	6.561	5.155	7.03	12398.72
13	81.643	55.04	12.843	10.091	13.76	24268.35
14	73.158	49.32	11.508	9.042	12.33	21746.28
15	12.697	8.56	1.997	1.569	2.14	3774.29
16	39.160	26.40	6.160	4.840	6.60	11640.34
17	84.253	56.80	13.253	10.413	14.20	25044.37
18	63.961	43.12	10.061	7.905	10.78	19012.55

3.1 Decision variables

The discharge Q_m in the north main canal for the rotations was selected as the decision variable.

3.2 Objective function

The minimum irrigation duration (TK) related to different irrigation rotations was selected as the objective function, that is:

$$MinTK = \frac{\sum_{i=j}^{M}\sum_{j=1}^{N} A_{ij}(M_j - W_k)}{Q_m \times \eta_m \times \eta_b \times 24 \times 3600} \quad (14)$$

In which, W_k = soil moisture content (m^3/ha).

Q_m = maximum discharge in the North Main Canal (m^3/s).

3.3 Constraints

3.3.1 Constraint of maximum discharge

The flow in the North Main Canal and the branch canals cannot be greater than the maximum canal capacities:

$$Q_{mi} \leqslant Q_m \quad (15)$$

in which: Q_{mi}=the ith discharge diversion in the North Main Canal, i = 1,2 .... (m^3/s).

3.3.2 Constraints of minimum discharge

In order to prevent the main and branch canal systems from silting up, the flow in the main and branch canals should not be less than half of the maximum flow capacity.

$$Q_R \geqslant Q_m/2 \quad (16)$$

$$q_{Ri} \geqslant q_{mi}/2 \quad (17)$$

in which: Q_R = practical flow diversion in the North Main Canal (m^3/s).

q_{Ri} = practical discharge diversion in the branch canal i (m^3/s).

q_{mi} = maximum flow capacity in the branch canal i (m^3/s).

3.3.3 Constraint of irrigation rotation practice

While regulating irrigation order, it is necessary to irrigate from downstream to upstream in order to minimize water loss caused by evaporation and infiltration, that is: i = 18,17,... 1.

In order to minimize the objective function and guarantee irrigation from downstream to upstream, irrigation was ordered by branch canals.

Table 4 Optimum scheme of the minimum irrigation rotation

CANALS	DAYS										
	1	2	3	4	5	6	7	8	9	10	11
1	0.00	0.00	0.00	0.00	0.00	0.00	0.00	0.38	0.42	0.42	0.
2	0.00	0.00	0.00	0.00	0.00	0.19	0.37	0.37	0.37	0.00	0.
3	0.00	0.00	0.00	0.00	0.00	0.00	0.33	0.37	0.37	0.00	0.
4	0.00	0.00	0.00	0.00	0.00	0.00	0.18	0.37	0.37	0.37	0.
5	0.00	0.00	0.00	0.00	0.00	0.00	0.00	0.18	0.37	0.37	0.
6	0.00	0.00	0.00	0.00	0.00	0.09	0.19	0.19	0.19	0.19	0.
7	0.00	0.00	0.00	0.00	0.00	0.42	0.42	0.42	0.00	0.00	0.
8	0.00	0.00	0.00	0.42	0.42	0.42	0.42	0.00	0.00	0.00	0.
9	0.00	0.00	0.00	0.00	0.37	0.37	0.37	0.00	0.00	0.00	0.
10	0.00	0.00	0.00	0.24	0.37	0.00	0.00	0.00	0.00	0.00	0.
11	0.00	0.00	0.00	0.00	0.30	0.37	0.00	0.00	0.00	0.00	0.
12	0.00	0.25	0.25	0.42	0.00	0.00	0.00	0.00	0.00	0.00	0.
13	0.42	0.21	0.21	0.42	0.42	0.42	0.00	0.00	0.00	0.00	0.
14	0.35	0.66	0.66	0.00	0.00	0.00	0.00	0.00	0.00	0.00	0.
15	0.37	0.00	0.00	0.00	0.00	0.00	0.00	0.00	0.00	0.00	0.
16	0.37	0.37	0.37	0.00	0.00	0.00	0.00	0.00	0.00	0.00	0.
17	0.42	0.42	0.42	0.42	0.42	0.00	0.00	0.00	0.00	0.00	0.
18	0.37	0.37	0.37	0.37	0.00	0.00	0.00	0.00	0.00	0.00	0.
Qm	2.50	2.50	2.50	2.50	2.50	2.50	2.50	2.50	2.28	1.48	0.

4 Analysis of Research Results

The results can be seen in Table 4. It shows that the flow in the North Main Canal reaches maximum capacity in the first 8 days, and that flow is greater than half of its capacity in the following 2 days, which can prevent silting up in branch canals as well as control the discharge diversion at the head of branch canals conveniently. One irrigation rotation under the optimum water allocation requires 10 days, which saves about 4 days, compared with 14 days in the traditional irrigation system. Therefore, the purpose of time and water saving has been achieved.

The time unit of the present research is based on days for convenient management. The time unit can be shortened for further water saving purposes; as long as the parameter Ti in the programme is changed, the relevant results will be obtained. When irrigation starts, the measured W and Q_m must be input into the computer and the results will be achieved through calculation. The data input is interactive, which is very convenient for application.

Acknowledge

This research has been supported by IDSS developing for water Resources optimum allocation and management {20025700003}and by Innovatory found in Henan Province.

References

[1] Yellow River Irrigation Bureau. Water Saving Irrigation experiment in Chengai Yellow River Irrigation Area[R]. Zhengzhou, Yellow River Water conservancy Commission, the Ministry of Water Resources, 1992.

[2] Yuan H, Shao D. Water Resources System Analysis [M]. Wuhan, Wuhan University of WRHP. 2000.

[3] Guolter IC. Systems analysis in water distribution network design. Water Resources Planning and Management, ASCE, 1992.

[4] Shamir U. Optimization in water distribution systems engineering, Mathematical Programming Study, North Holland, 1979, 11:65-84.

Nature and Science

Call for Papers

Dear Friends:

Do you have scientific research results, opinions/debates or review papers to be published? The new international academic journal "*Nature and Science*" (ISSN 1545-0740) is inviting you to publish your papers. Please visit http://www.sciencepub.net and send your manuscripts to editor@sciencepub.net.

The *Nature and Science* is an international journal to enhance our natural and scientific knowledge spreading in the world under the free publication principle. Any valuable paper to describe natural phenomena/existence or report scientific researches/pursuits will be acceptable, including both natural and social sciences. Papers submitted could be reviews, objective descriptions, research reports, opinions/debates, news, letters, and all other information nature and science related.

As a formal academic journal, the *Nature and Science* is registered in the United States and published in the both print and Internet online versions from November of 2003. The journal is calling for papers and looking for more co-operators and editors.

To cover the publication expenses of printing and website maintenance, the journal will charge authors limited publication fee (US$20/page for print version, and US$5/page for Internet online version). For the printed version, at least 1 hard copy of printed journal for each author and 20 offprints (reprints) for each article will be provided to authors by free charge.

If you have anything including research reports, review papers or any other related article to be published, it is a good chance. At least it is better than letting your precious achievements sleep in your drawers. If you have some friends for this, let them contribute papers also. Let's work together to promulgate our research results/opinions, to do what we can do.

Papers in all the fields are accepted: including natural science and social science.

Thank you for your support!

Marsland Company
P.O. Box 753
East Lansing, Michigan 48826
The United States
Telephone: 517-862-6881
E-mail: editor@sciencepub.net
Homepage: http://www.sciencepub.net

editor@sciencepub.net

http://www.sciencepub.net

Marsland Company

P.O.Box 753

East Lansing,Michigan 48826

The United States

Tel: (517) 862-6881